2003-09-18

Theory, Design, and Fabrication of Diffractive Grating Coupler for Slab Waveguide

Kevin Randolph Harper
Brigham Young University - Provo

BYU ScholarsArchive Citation

Harper, Kevin Randolph, "Theory, Design, and Fabrication of Diffractive Grating Coupler for Slab Waveguide" (2003). *Theses and Dissertations*. 101.
https://scholarsarchive.byu.edu/etd/101

THEORY, DESIGN, AND FABRICATION OF

DIFFRACTIVE GRATING COUPLER

FOR SLAB WAVEGUIDE

by

Kevin Randolph Harper

A thesis submitted to the faculty of

Brigham Young University

in partial fulfillment of the requirements for the degree of

Master of Science

Department of Electrical and Computer Engineering

Brigham Young University

December 2003

BRIGHAM YOUNG UNIVERSITY

GRADUATE COMMITTEE APPROVAL

Of a thesis submitted by

Kevin Randolph Harper

This thesis has been read by each member of the following graduate committee and by majority vote has been found to be satisfactory.

_____ _____

Date   Stephen M. Schultz, Chair

_____ _____

Date   Richard H. Selfridge

_____ _____

Date   Aaron R. Hawkins

BRIGHAM YOUNG UNIVERSITY

As chair of the candidate's graduate committee, I have read the thesis of Kevin Randolph Harper in its final form and have found that (1) its format, citations, and bibliographical style are consistent and acceptable and fulfill university and department style requirements; (2) its illustrative materials including figures, tables, and charts are in place; and (3) the final manuscript is satisfactory to the graduate committee and is ready for submission to the university library.

_____   _____
Date   Stephen M. Schultz
                                     Chair, Graduate Committee

Accepted for the Department

                                     _____
                                     Michael A. Jensen
                                     Graduate Coordinator

Accepted for the College

                                     _____
                                     Douglas M. Chabries
                                     Dean, College of Engineering and
                                     Technology

ABSTRACT

THEORY, DESIGN, AND FABRICATION OF

DIFFRACTIVE GRATING COUPLER

FOR SLAB WAVEGUIDE

Kevin Randolph Harper

Department of Electrical Engineering

Master of Science

This thesis presents the theory design and fabrication of a diffractive grating coupler. The first part of the design process is to choose the period of the grating coupler based on the desired coupling angle. The second part of the design process is to choose the geometry of the grating that gives maximum coupling efficiency based on rigorous analyses.

The diffraction gratings are fabricated by recording the interference between two waves in photoresist. The waveguide is fabricated from silicon nitride that is deposited by chemical vapor deposition. The diffraction grating recording assembly is described along with the grating coupler fabrication process. A grating coupler is fabricated with an input coupling efficiency of 15% at a coupling angle of 22.9°. The results also show that the light is being coupled into the nitride waveguide indirectly. The light is coupled first into a photoresist slab and then into the nitride waveguide

through modal coupling and scattering. An analysis of the structure explains the coupling, and rigorous analyses are given to show that the measured results are in accordance with theory.

ACKNOWLEDGEMENTS

There are many people that I would like to thank for helping to make this thesis possible. I would first like to acknowledge and thank my wife, Bonnie, for her support of me throughout all of my schooling here at BYU, and especially for her support as I have written this thesis. I am also greatful for my daughter, Maggie, who makes my life fun and interesting.

I am thankful to Dr. Stephen Schultz for his help, advice and patience as we have discussed the many challenges that we have faced in carrying out this research. I have learned much from sitting in his office for hours discussing the intricacies of this research. I would also like to thank Dr. Richard Selfridge for his insight into the details of this research, and Dr. Aaron Hawkins for his advice relating to fabrication processes.

I am thankful to Eli Tamanaha and Chris Marchant for all of their help in performing much of the experimental work given in this thesis. I also am greatful for Kevin Smith for listening to some of the difficulties that I have experienced in this research and offering suggestions and advice. I am also thankful to John Barber for his seemingly encyclopedic knowledge of clean room equipment and procedures.

Contents

List of Figures

xiv

List of Tables

Chapter 1

1   Introduction

For decades diffraction gratings have been used by scientists in many fields to analyze the spectrum of light. The diffraction grating has been a tool of such importance and in so many fields of science that MIT spectroscopist G. M. Harrison said:

> "It is difficult to point to another single device that has brought more
> important experimental information to every field of science than the
> diffraction grating. The physicist, the astronomer, the chemist, the
> biologist, the metallurgist, all use it as a routine tool of unsurpassed
> accuracy and precision, as a detector of atomic species to determine
> the characteristics of heavenly bodies and the presence of atmospheres
> in the planets, to study the structures of molecules and atoms, and to
> obtain a thousand and one items of information without which modern
> science would be greatly handicapped. [1]"

Today the diffraction grating is still used in the application of spectroscopy; however, with the recent advances in computers and communications technology, diffraction gratings have found even more applications. Some of these applications

include optical interconnects for computer systems, integrated optical devices, and optical communications.

1.1   Diffraction Grating Applications

1.1.1   Optical Interconnects

As the complexity and speed of integrated circuits and computer systems increase, there is a trade off between the length of a wire signal path and the bandwidth supported by those paths. Optical interconnects do not exhibit this trade off and in the future will likely replace metal wiring for long interconnects. Researchers have also shown that optical interconnects provide advantages over electrical interconnects in terms of fanout [2], energy conversion [3], latency [4], and electromagnetic interference immunity. Several researchers have implemented diffractive grating couplers as the coupling element for optical interconnect systems [5-13]. Diffraction gratings are desirable because they are more compact than other coupling schemes.

1.1.2   Integrated Optical Devices

Diffraction gratings also find an application in integrated optical devices. Integrated optical devices attempt to accomplish the same task as bulk optics, but on a compact and integrated scale. Some examples of diffractive integrated optical devices are beam expanders [14,15], polarization dependant devices [16-21], and holographic filters for beam intensity profile reshaping [22-26]. Other integrated optical devices with applications to computer systems are optical read/write heads

[27-30], grating coupled surface emitting lasers [31,32], optical sensors [33-35], and printer heads [36].

1.1.3 Fiber Optical Communications

Another area in which diffraction gratings have found application is in fiber optical communications. Optical communications over fiber optic links have potentially large bandwidths and experience low loss for long distances. One advance in the bandwidth of optical communications is wavelength division multiplexing. Wavlength division multiplexing and dense wavelength division multiplexing require devices that are highly sensitive to wavelength for interacting with narrow wavelength communication channels. Diffraction gratings have the potential to play an important role in this arena. Some diffraction grating devices that have been demonstrated by researchers are Bragg gratings for wavelength division multiplexing [37-41] and optical filters [42,43].

1.2 Research Focus

While there are many areas in which diffraction grating based devices can make a significant impact, the focus of our research is diffractive grating couplers. Grating couplers have their uses in many of the applications listed above, especially in optical interconnects and integrated optical devices. Grating couplers can either diffract light into substrate guided modes, meaning that the light propagates in a substrate by total internal reflection, or grating couplers can diffract light into the mode of a single mode waveguide. The research focus for this thesis is the theory, design, and fabrication of diffractive grating couplers to couple light into single mode slab waveguides.

1.3   Thesis Overview

The goals of this thesis are twofold. The first goal is to present the research that has been done in developing the design and fabrication processes for holographically recorded diffraction gratings in general and more specifically, for grating couplers. Other researchers at Brigham Young University have investigated grating coupling into fibers [44], but this is the first thesis at Brigham Young University in the Electrical and Computer Engineering Department to study the topic of grating couplers for broader application in integrated optical devices. Therefore, the second goal of this thesis is to provide future researchers in this area at Brigham Young University all of the background and theory that is necessary for continuing this research.

The background for diffraction by gratings is given in Chapter 2. Different types of diffraction gratings are discussed. The physical description of the behavior of diffraction gratings is derived culminating in the diffraction grating equation. Also, the wavevector diagram is presented as a tool for the analysis of diffraction gratings.

Chapter 3 presents a rigorous analysis technique for determining the efficiency of an arbitrary surface relief grating. This method is known as rigorous coupled-wave analysis. The electromagnetic behavior of the electric fields in the system is derived. The solution method is discussed as well as a numerical implementation. Examples using this analysis technique are given, and a discussion of the numerical accuracy is also presented.

Chapter 4 presents the method of design for grating couplers for slab waveguides. First the design is presented from the perspective of wavevectors. The design is also discussed in terms of the optimal efficiency. A numerical technique for determining the characteristics of grating couplers is presented along with its implementation. Finally, some grating couplers are designed using the methods described. Fabricating these couplers is the goal of the research.

Chapter 5 presents an overview of different diffraction grating fabrication methods. The method of holography is presented as being the best choice for this research.

Chapter 6 explains the fabrication process of the grating couplers. A discussion on the holographic recording assembly is given. The results of some experimentation done to characterize the holographic recording process are also given. Experimental results are presented for finding the optimal exposure dosage for our holographic diffraction gratings. It is shown that we are able to make gratings in the proper range of performance, but that we experience a low yield. Possible causes for our low yield are given.

Chapter 7 presents the results of our attempts to fabricate the grating coupler from the design given in Chapter 4. There is first a discussion of the testing method for qualifying the performance of our grating couplers. The results of our fabricated grating coupler are then given. It is shown that we were successful in fabricating a grating coupler. Although the efficiency of the grating coupler is less than the designed value, the reasons for the degraded performance are accounted for.

Chapter 8 is a summary of the research presented here. A discussion of future research in the area of diffraction gratings and grating couplers is given.

Chapter 2

2   Diffraction Gratings

2.1   Diffraction

If an opaque object is placed between a light source and an observation

screen, the edges of the shadow cast by the object will contain intricate patterns that

cannot be explained by simple geometric ray optics. This phenomenon was first

discussed in a publication in 1665 by Francesco Grimaldi, a professor of physics and

mathematics at the Jesuit college of Bologna, Italy. In Grimaldi's experiments, he

allowed a small pencil of light to come into a dark room. He observed that the

shadow cast by a rod held in the cone of light was wider than the shadow predicted by

geometric optics. He also noted that colored bands bordered the edges of the shadow.

Grimaldi named this phenomenon "diffractio" which literally means "breaking up".

Grimaldi used the results of this experiment to be one of the first to argue for the

wave nature of light. Grimaldi's original name for this phenomenon, "diffraction", is

still used today [45]. Diffraction is a general characteristic of wave phenomena. If a

wavefront encounters a blocking object, the portions of the wave that pass beyond the

object interfere to cause the diffraction pattern [46]. A very important application of

diffraction is if the blocking object is a repetitive array of diffracting elements that

7

produce a periodic alteration of the amplitude or phase of the transmitted wave. Such an object is said to be a diffraction grating.

2.1.1 Diffraction Grating Specifications

Diffraction gratings are so important because they transmit or reflect light only at discrete angles and because the angles of the diffractive orders are highly sensitive to the wavelength content of the incident light, which is why diffraction gratings are used so heavily in the area of spectroscopy. A diffraction grating can be characterized by two important specifications. The first specification is the direction of the diffracted beams or the set of angles that the incident light will be diffracted into for a given wavelength and angle of incidence. This specification depends only on the period of the diffraction grating and the material parameters of the incident and transmitted medium, and is solved by a simple geometric relationship that is discussed in this chapter. The second important specification of a diffraction grating is its efficiency or the ratio of power in each order relative to the total incident power. This specification depends very strongly on the physical shape and structure of the grating and is a more difficult problem to solve. Chapter 3 is dedicated to this analysis.

2.1.2 Types of Diffraction Gratings

Having discussed the important specifications for diffraction gratings, we now examine some common types of diffraction gratings. For a more complete discussion of the types of diffraction gratings, see [47]. The earliest and simplest diffraction gratings were periodic slits. The first diffraction grating was invented by American astronomer David Rittenhouse in about 1785, who reported constructing a half-inch

wide grating with fifty-three apertures.   Joseph von Fraunhoffer independently

created diffraction gratings and studied their uses in spectroscopy. Using his

diffraction gratings, Fraunhoffer was able to measure the spectra of solar radiation

[48]. Over the years, the ability to make quality diffraction gratings has increased,

and the use of diffraction gratings has become very widespread in the scientific

community. Generally diffraction gratings fall into two broad categories: amplitude

gratings and phase gratings.

Amplitude gratings are simply an array of multiple slits, either etched out of

an opaque surface, or consisting of a grid of fine wires. As discussed above, the first

gratings built were amplitude gratings. It was through the study of amplitude gratings

that the theory of how diffraction gratings work was experimentally verified. These

gratings spatially modulate only the amplitude of the transmitted wave by either

periodically blocking the beam, or only attenuating it slightly. Figure 2.1 shows an

example of an amplitude grating.
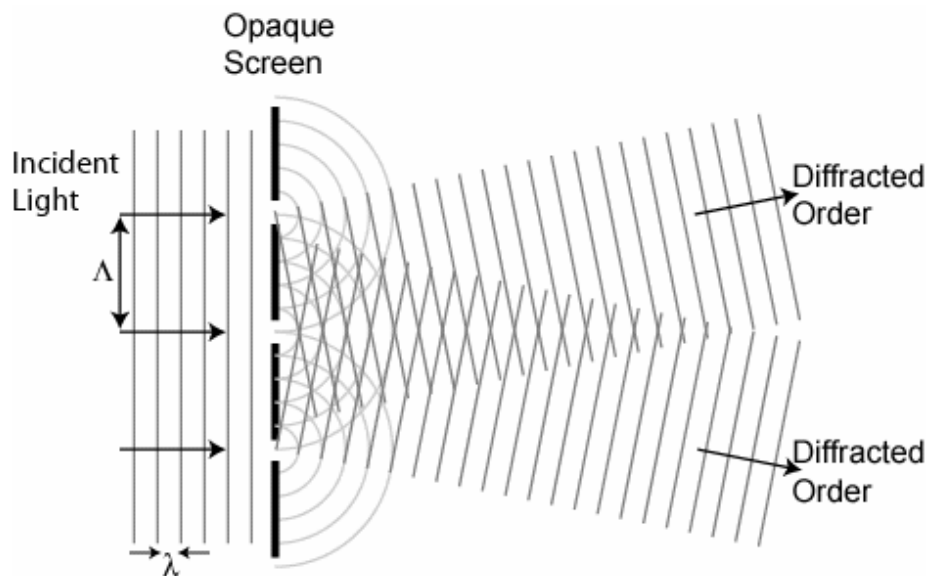
Figure 2.1 Amplitude grating

A second type of diffraction grating is the phase grating. A phase grating is made up of an array of extremely narrow ridges of alternatively repeating indices of refraction. These gratings spatially modulate only the phase of the transmitted wave by periodically adjusting the phase of the portions of the beam that are transmitted through the ridges of alternating refractive index. There are two important classes of phase gratings: surface relief gratings and volume gratings.

For surface relief gratings, the physical topography of the grating changes periodically. The two alternating indices of refraction are the index of the grating substrate and the index of the cover medium, which is usually air. The simplest example of a surface relief grating consists of periodic thin rectangular ridges. This type of grating is known as a binary grating. The binary grating is important because it is easily manufactured by the method of photolithography, however, it is difficult to manufacture binary gratings with small periods. The method of photolithography is discussed in Chapter 5. Binary gratings are also important because, as discussed in Chapter 3, the method to analyze the efficiency of arbitrary grating shapes slices the arbitrary grating into thin binary gratings. Other important surface relief gratings include the sinusoidal grating and the blazed grating. The sinusoidal grating is important because it is fabricated easily by holographic recording or recording the sinusoidal interference between two uniform beams. The method of holographic recording is discussed in Chapter 5. The blazed grating is important in that it can exhibit strong preferential coupling into one of its diffractive orders. A blazed grating would be desirable in an application where efficiency is critical such as an optical interconnect system. Larger period blazed gratings are manufactured by a scribing or

10

mechanical process, which is discussed in Chapter 5. Small period blazed gratings are difficult to manufacture, however, and are thus not as widely used as other types of gratings. Figure 2.2 shows examples of surface relief gratings.
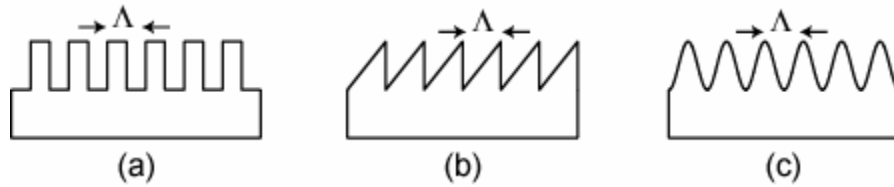
Figure 2.2 Examples of surface relief gratings: (a) binary, (b) blazed, (c) sinusoidal

A volume grating has a flat surface topography. The periodicity of this grating is in the alternating index of refraction between repeating periodic sections. One advantage of volume gratings is that the direction of periodicity can easily be made in a direction other than parallel to the substrate surface. By this property, volume gratings can be made with efficiencies of almost 100% into a desired diffractive order. Volume gratings are attractive for uses in optical interconnect systems because of their high efficiencies. A volume grating can be manufactured easily by a modified holographic recording process. Figure 2.3 shows an example of a volume grating.
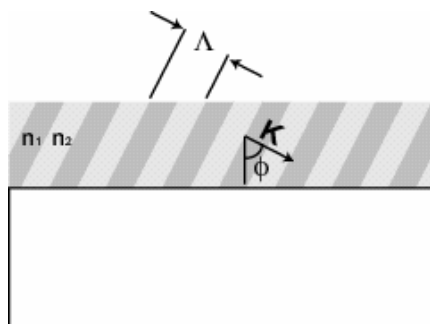
Figure 2.3 Volume grating

2.2   The Diffraction Equation

Now that we have discussed some different types of diffraction gratings, let's take a closer look and examine how they interact with light to redirect incident light into diffractive orders. A diffraction grating is characterized by its grating vector **K,** which is defined as having magnitude $|\mathbf{K}| = 2\pi/\Lambda$, where Λ is the period of the grating, and points in the direction of periodicity. The interaction of the grating in redirecting the incident light is simply the discrete addition of integer multiples of the grating vector to the undiffracted transmitted wavevector.

$$\mathbf{k}_q = \mathbf{k}_u - q\mathbf{K}, \qquad (2.1)$$

where $q = 0, \pm 1, \pm 2, ...$ is the diffracted order number, $\mathbf{k}_u$ is the wavevector of the undiffracted, i.e. $q = 0$, beam, and $\mathbf{k}_q$ is the wavevector of the qth diffracted order. The condition just described, where the grating vector adds to the undiffracted wavevector, is known as the Floquet condition, and the infinite set of resulting wavevectors are known as Floquet waves. Although the set of Floquet waves contains an infinite number of diffracted orders, only certain of those orders can exist physically. To explore further, we rewrite (2.1) by substituting the vector components of the wavevectors into a two-dimensional geometry as shown in Figure 2.4.

$$\frac{2\pi n_t}{\lambda}\left(\sin\theta_q \hat{x} + \cos\theta_q \hat{z}\right) = \frac{2\pi n_t}{\lambda}\left(\sin\theta_u \hat{x} + \cos\theta_u \hat{z}\right) - \frac{2\pi q}{\Lambda}\hat{x}, \qquad (2.2)$$

where n_t is the index of refraction for the transmitted medium, θ_u is the angle of the undiffracted beam, θ_q is the angle of the qth diffracted beam, and λ is the wavelength. We can solve for $\sin\theta_q$ by examining the $\hat{x}$ components of equation (2.2)

$$n_t \sin \theta_q = n_t \sin \theta_u - q\frac{\lambda}{\Lambda}.$$ (2.3)

In order to relate (2.3) to the incident light we need only use Snell's law and substitute $n_t \sin \theta_u$ with $n_i \sin \theta_i$. Finally, we are left with what is known as the diffraction equation.

$$n_t \sin \theta_q = n_i \sin \theta_i - q\frac{\lambda}{\Lambda}$$ (2.4)
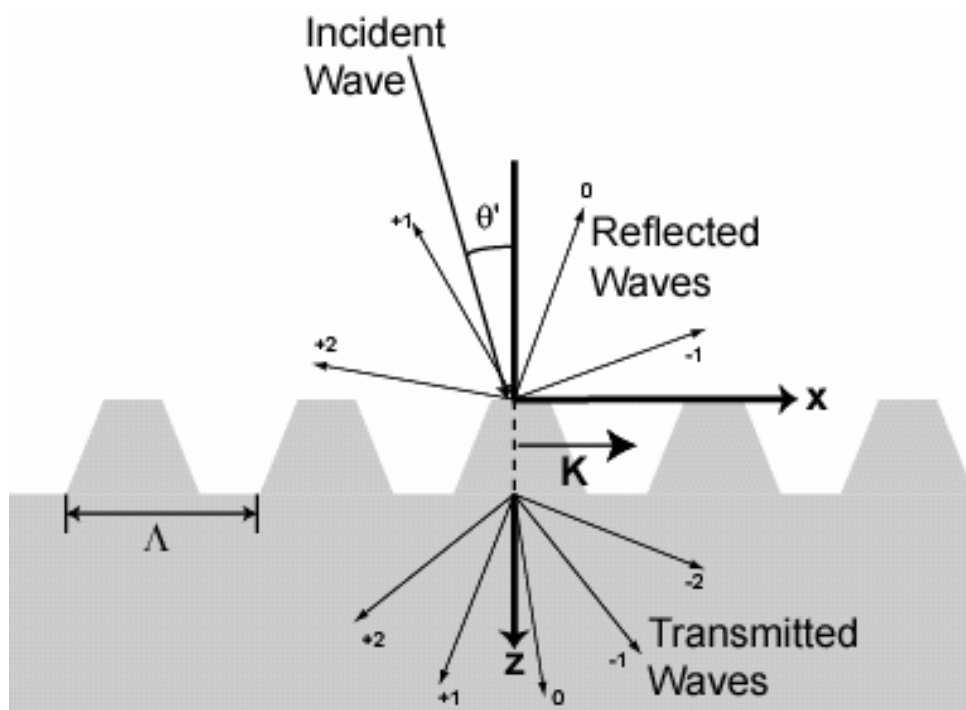
Figure 2.4 Geometry of two dimensional surface relief grating

What we have really done in deriving (2.4) is to apply the electric field boundary condition for tangential components that requires the tangential components at the boundary to be continuous. From the diffraction equation we can see the strong dependence on λ. If the grating period is chosen such that it is small with respect to the wavelength, then small changes in the wavelength affect θ_q significantly. Because

13

gratings are highly dispersive, i.e. sensitive to wavelength, they find a natural and direct application to spectroscopy.

We also can see from equation (2.4) that if the magnitude of the right side is greater than n_t, the angle θ_q is complex, and therefore non-physical. This requirement gives a range for the physical solutions for q.

$$\left\lceil \frac{\Lambda}{\lambda}\left(n_i \sin\theta_i + n_t\right) \right\rceil \le q \le \left\lfloor \frac{\Lambda}{\lambda}\left(n_i \sin\theta_i - n_t\right) \right\rfloor, \qquad (2.5)$$

where the notation $\lceil \; \rceil$, or "ceiling", means to round up to the nearest integer, and the notation $\lfloor \; \rfloor$, or "floor", means to round down to the nearest integer. In general the greater the ratio of the grating period to the incident wavelength, the more diffractive orders exist. Also, higher index incident and transmitted mediums results in more diffractive orders.

2.3   K-Space Diagrams

A handy tool for understanding and analyzing diffraction gratings is the k-space, or wavevector diagram. The k-space diagram models the transmission and reflection of the incident beam due to the effect of the diffraction grating. The diagram uses concentric circles whose radii represent the magnitude of the wavevector k in the medium in question. Rays, with magnitude equal to the magnitude of k, travel towards and away from the center of the circle at angles representing the direction of propagation. The diffraction grating is modeled as existing at the center of all circles.

As discussed earlier, diffraction gratings are characterized by their grating vector **K**. The grating vector is an important graphical tool used to make the

14

wavevector diagram. Recall that the Floquet condition states that each diffractive

order is the result of adding integer multiples of the grating vector to the undiffracted

transmitted wave. Graphically, the Floquet condition can be easily represented by

successively adding multiples of the grating vector to the undiffracted wave vector of

the transmitted field by the head to tail method.

The remaining task is to translate the result of the Floquet addition to actual

reflected and transmitted diffracted waves in the incident and transmitted mediums.

This is done as before by applying the boundary conditions for tangential electric

fields. Applying this boundary condition is also known as phase matching. We can

represent phase matching graphically by drawing sets of lines that pass through the

head of each Floquet wave vector and are perpendicular to the boundary between the

concentric circles representing the incident and transmitted mediums. The reflected

and transmitted diffracted wave vectors start at the center of the circles, and end

where the lines of matched phase intersect with the circles.

2.4   Example

Now that all of the pieces of the K-space diagram have been described, we

can demonstrate how a K-space diagram is created with an example. For this

example, light of wavelength $\lambda = 632.8$ nm is incident on a diffraction grating with

period $\Lambda=1$ µm, periodic in only the x-dimension. The incident material is free space,

and the transmitted material has index of refraction n=1.5. The incoming light has an

angle of incidence of   10°. We start the diagram by drawing semicircles with radii

representing the magnitude of the wave vector, $|k| = \dfrac{2\pi n}{\lambda}$, in the incident and

15

transmitted mediums. The top semicircle represents the incident medium, and the bottom semicircle represents the transmitted medium. The next step is to plot the incident vector and the undiffracted reflected and transmitted vectors. For this step, we are ignoring the diffraction grating and are simply looking at the reflection of the incident wave due to Snell's law. The incident vector is drawn pointed toward the center of the circles with angle of incidence measured with respect to the normal. The undiffracted reflected beam is drawn pointing away from the center of the circles at an angle opposite the angle of incidence. The undiffracted transmitted beam is phase matched to the undiffracted reflected beam. Figure 2.5 shows the k-space diagram at this point, as well as a physical picture representing an air-glass interface. The angles of the reflected and transmitted beams in the k-space diagram are the same as the angles shown in the physical picture on the right.
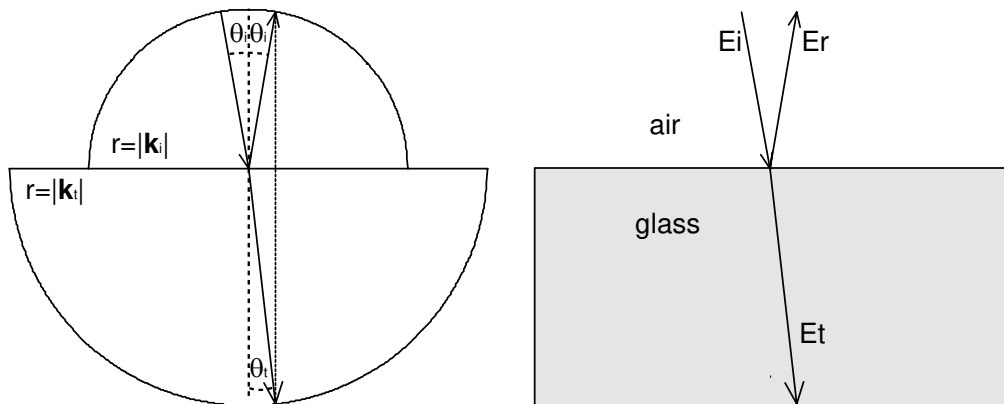
Figure 2.5 k-space diagram illustrating Snell's law

The next step is to apply the Floquet condition and draw the lines of matched phase. We first draw the set of grating vectors pointed away from the head of the undiffracted transmitted beam. Each grating vector that is added corresponds to a different diffractive order. The Floquet waves are drawn from the center of the circle

16

to the head of each added grating vector. Recall that the Floquet waves are an infinite

set of waves that exist only in the grating, and determine the interaction of the grating

with the incident wave. The lines of matched phase are drawn from the head of each

Floquet wave perpendicular to the interface of the two circles. These lines of

matched phase represent the tangential components of the Floquet waves, which must

be matched to the waves outside of the grating according to electromagnetic boundary

conditions. Figure 2.6 shows the k-space diagram at this point. The dashed lines are

the Floquet waves, and the dotted vertical lines are the lines of matched phase

corresponding to the tangential component of each Floquet wave.
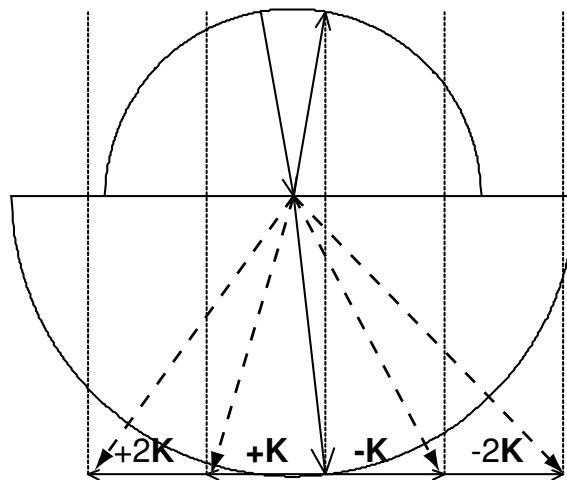
Figure 2.6 k-space diagram showing Floquet waves

The final step is to match boundaries with the Floquet waves, and obtain the

vectors for the transmitted and reflected diffractive orders. The diffracted rays start at

the center of the circles, and end at the intersections of the lines of matched phase

with the k-space circles. This set of vectors represents the transmitted and reflected

waves from the diffraction grating. The angles of these vectors in the diagram are the

same as the angles of the transmitted and reflected waves. Figure 2.7 shows the final

diagram, where the Floquet vectors have been removed, but the lines of matched phase remain. Figure 2.7 also shows the physical picture that the k-space diagram represents.
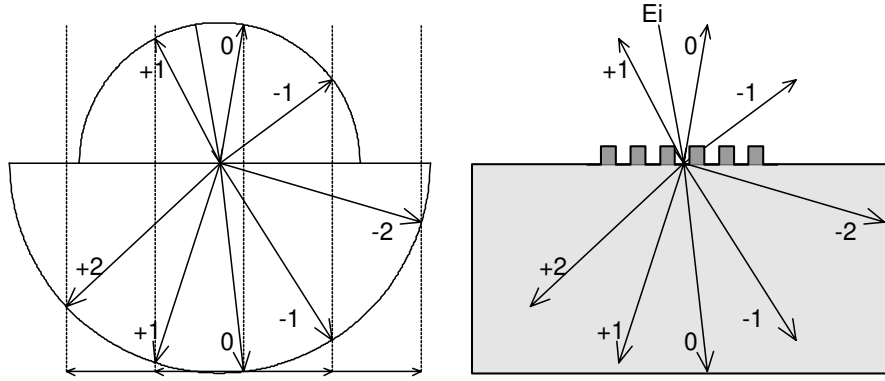
Figure 2.7 Final k-space diagram showing diffractive orders.

For this example we can see that there are three reflected orders and five transmitted orders. If we use equation (2.5), we can calculate how many orders there should be in the reflected region and in the transmitted region. For the transmitted region we have $-2 \leq q \leq 2$, and for the incident region we have $-1 \leq q \leq 1$. These are the same results obtained graphically. Also for this example, the angles of the transmitted and reflected diffractive orders calculated from equation (2.4) are given in Table 2.1 below. Positive angles are defined as counterclockwise from normal.

Table 2.1 Angles of diffractive orders for a 1 μm period diffraction grating illuminated by 632.8 nm light

Diffractive Order	-2	-1	0	1	2
Reflected	--	-53.7503°	-10.0°	27.3324°	--
Transmitted	73.6375°	32.5226°	6.6478°	-17.8244°	-46.7163°

The values of these calculated angles are the same as those that could be found by measuring the angles, with respect to the normal, of each ray in the k-space diagram in Figure 2.7 with a protractor. While this example only shows the angles of the diffractive orders, in the following chapter, we explore how to analyze the structure of a grating to determine the efficiencies of each diffractive order. We revisit this example in the next chapter, and see what the efficiencies of these orders are for different shaped diffraction gratings.

Chapter 3

3   Diffraction Grating Analysis

In the previous chapter, the behavior of diffraction gratings in redirecting light

into various diffractive orders was discussed. The number of diffractive orders that a

grating produces and the angles of these orders was explained. Another important

characteristic of a diffraction grating is the efficiency, meaning the ratio of power in

each of the orders to the total incident power. The angles of the diffractive orders are

independent of the shape of the periodic structure of the grating; however, the

efficiency is strongly dependant on the shape of the grating. The topic of this chapter

is to explain a formulation for calculating the efficiency of surface relief gratings.

3.1   Theory of Rigorous Coupled Wave Analysis

Rigorous analyses, which provide "exact" numerical solutions to the

diffraction problem, have been and continue to be the subject of extensive research

[49-79] The method explained here is known as rigorous coupled-wave analysis.

This method was developed by researchers at Georgia Tech in the 1980s, and is

important because it computes the efficiencies of the diffraction grating directly with

no approximations in the analysis, and up to an arbitrary degree of accuracy. The

computational method is easy to implement numerically, and can achieve results
quickly [55,58-61,78,79].

3.1.1 Geometry of Problem

Before we begin, we should first define the geometry of the problem that we
are investigating. The development presented here of this solution follows the
formulation in [58]. The general surface-relief diffraction grating for this problem is
shown below in Figure 3.1.
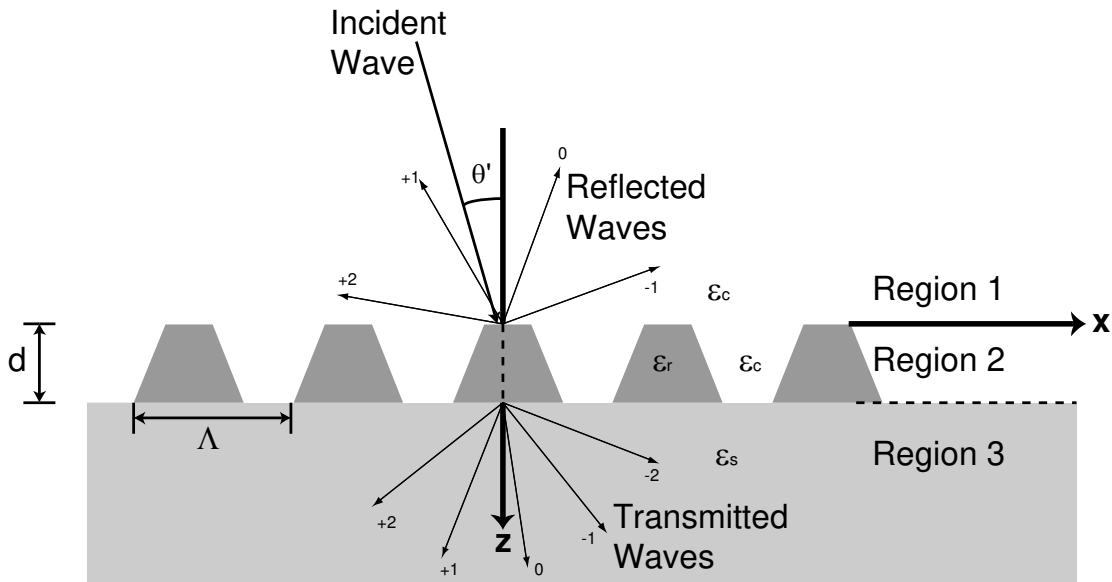
Figure 3.1 Geometry for surface relief grating

This structure consists of a surface relief grating between a cover region with
relative permittivity ε_c and a semi-infinite substrate region with relative permittivity
ε_s. The ridges of the grating have a relative permittivity ε_r. The structure is divided
into three regions with Region 1 being the region of the cover, Region 2 being the
region of the diffraction grating, an Region 3 being the region of the substrate. The $\hat{\mathbf{x}}$

22

($\hat{\mathbf{x}}$ and $\hat{\mathbf{z}}$ are the unit vectors in the x and z directions) direction is tangential to the boundaries between the different regions. The $\hat{\mathbf{z}}$ direction is normal to the boundary and points toward the substrate region. The diffraction grating has height d and grating period Λ. The grating vector $\mathbf{K}$ is defined which has magnitude $|\mathbf{K}| = 2\pi/\Lambda$ and points in the $\hat{\mathbf{x}}$ direction. The grating is illuminated by a plane wave of free space wavelength λ at an angle of incidence θ'. The wavevector for this incident plane wave in the cover region, region 1, is defined to be $\mathbf{k}_1 = k_{x,1}\hat{\mathbf{x}} + k_{z,1}\hat{\mathbf{z}}$, where $k_{x,1} = k_0 \varepsilon_c^{1/2} \sin\theta'$, $k_{z,1} = k_0 \varepsilon_c^{1/2} \cos\theta'$, and $k_0 = 2\pi/\lambda$ is the free space wavevector magnitude. The polarization is defined with respect to the plane of incidence, so that for the TE polarization considered here, the electric field $\mathbf{E}$ is perpendicular to the plane of incidence.

3.1.2 Electric Fields in Different Regions

We begin by defining the total electric fields in the different regions. In the cover region, region 1, the total electric field is the sum of the incident and all of the backward traveling waves. The normalized total electric field in this region may be expressed as

$$E_1 = e^{j\mathbf{k}_1 \cdot \mathbf{r}} + \sum_{i=-\infty}^{\infty} R_i e^{-j\mathbf{k}_{1,i} \cdot \mathbf{r}} , \tag{3.1}$$

where $\mathbf{k}_1$ is the wavevector of the incident field as defined above, and $\mathbf{r} = x\hat{\mathbf{x}} + y\hat{\mathbf{y}} + z\hat{\mathbf{z}}$. R_i is the normalized amplitude of the ith reflected wave in region 1 with wavevector $\mathbf{k}_{1,i}$. We can also define the total electric field in the substrate region, region 3, as consisting of the sum of all transmitted waves. The normalized total electric field in region 3 may be expressed as

23

$$E_3 = \sum_{i=-\infty}^{\infty} T_i e^{-j\mathbf{k}_{3,i}\cdot(\mathbf{r}-d\hat{\mathbf{z}})} \ , \tag{3.2}$$

where T_i is the normalized amplitude of the ith transmitted wave into region 3 with wave vector $\mathbf{k_{3,i}}$ and d is the grating depth. The quantities $\mathbf{k_{1,i}}$ and $\mathbf{k_{3,i}}$ are determined later by the phase matching requirement.

3.1.3 Fourier Expansion of Permittivity of Grating Region

Having defined all of the field quantities in region 1 and region 3, we now look at the fields in the grating region, region 2. For this analysis we divide the grating region into N thin planar strips perpendicular to the z axis. Each strip represents a thin planar binary grating. The rigorous coupled wave analysis for binary gratings is applied to each of the N strips, and the result of the total analysis gives the behavior of the entire structure. If each strip is thin enough than the analysis is accurate to an arbitrary level. Figure 3.2 shows the nth slab within region 2. Each slab consists of a periodic distribution of the relative permittivity of the ridge, and the relative permittivity of the cover region.
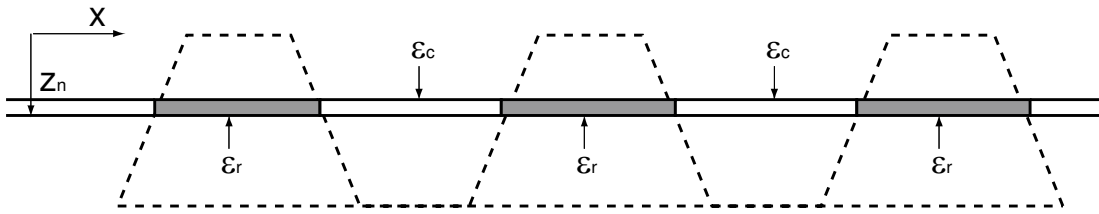
Figure 3.2 The nth planar grating resulting from splitting the surface-relief grating into n thin slices

Because the relative permittivity distribution for the nth slab is periodic, i.e. $\varepsilon_n(x, z_n) = \varepsilon_n(x + \Lambda, z_n)$, this distribution can be expanded in a Fourier series which is written

$$\varepsilon_n(x, z_n) = \varepsilon_c + (\varepsilon_r - \varepsilon_c) \sum_{h=-\infty}^{\infty} \widetilde{\varepsilon}_{h,n} e^{jhKx} , \qquad (3.3)$$

where z_n is the z coordinate of the nth slab, h is the harmonic index, K is the

magnitude of the grating vector ($K = 2\pi / \Lambda$), and $\widetilde{\varepsilon}_{h,n}$ are the normalized Fourier

coefficients of the nth slab given by

$$\widetilde{\varepsilon}_{h,n} = (1/\Lambda) \int_0^{\Lambda} f(x, z_n) \exp(-jhKx) dx , \qquad (3.4)$$

where the function $f(x, z_n)$ has a value of one or zero depending on if for a particular

value of x, the relative permittivity of the nth slab grating is ε_r or ε_c, respectively.

3.1.4   Coupled Wave Expression of Fields inside Grating

Now we express the electric fields inside the grating region with a coupled-

wave representation. In the coupled-wave representation, the fields in each of the N

slabs are expanded in terms of the space harmonics of the fields in the periodic

structure. Each of these space harmonics inside the grating correspond to different

diffractive orders outside of the grating. The partial fields inside the grating can be

visualized as diffracted waves that progress through the grating and couple energy

between each other as they propagate. In this coupled-wave formulation, the total

electric field in the nth slab grating can be expressed

$$E_{2,n} = \sum_{i=-\infty}^{\infty} S_i(z) e^{-j\boldsymbol{\sigma}_{i,n} \cdot \mathbf{r}} , \qquad (3.5)$$

where i is an integer representing the space-harmonic index, or the diffracted order.

$S_{i,n}(z)$ are the amplitudes of the space-harmonic fields. The vectors $\boldsymbol{\sigma}_{i,n}$ are the wave

vectors for the diffracted waves, and are given from the Floquet theorem as

$$\boldsymbol{\sigma}_{i,n} = \mathbf{k}_{2,n} - i\mathbf{K}, \tag{3.6}$$

where for this geometry $\mathbf{K} = K\hat{x}$ and $\mathbf{k}_{2,n}$ is the wave vector for the zero order, i.e. $i = 0$, diffracted wave with magnitude $k = 2\pi\varepsilon_{0,n}^{1/2}/\lambda$, where $\varepsilon_{0,n}$ is the average relative permittivity of the nth slab grating.

3.1.5   Application of Boundary Conditions

Now we are ready to discuss the phase matching requirement. Each of the ith diffracted waves in regions 1 and 3 must be phase matched to the ith space harmonic fields inside each nth slab grating. Therefore the equalities $\mathbf{k}_{1,i} \cdot \hat{x} = (\mathbf{k}_{2,n} - i\mathbf{K}) \cdot \hat{x} = \mathbf{k}_{3,i} \cdot \hat{x}$ must hold true for any i and n. We know the magnitudes of the wavevectors in regions 1 and 3, and the x components from the phase matching boundary condition. Knowing these quantities, the z components are determined to be

$$\mathbf{k}_{1,i} \cdot \hat{z} = \sqrt{\left(2\pi\varepsilon_c^{1/2}/\lambda\right)^2 + \left(\mathbf{k}_{1,i} \cdot \hat{x}\right)^2} \text{ and } \mathbf{k}_{3,i} \cdot \hat{z} = \sqrt{\left(2\pi\varepsilon_s^{1/2}/\lambda\right)^2 + \left(\mathbf{k}_{3,i} \cdot \hat{x}\right)^2}. \tag{3.7}$$

3.1.6   Total Electric Field in Each Region

Now we are ready to express the total electric fields for each of the three regions. Using the vector quantities defined above, these fields can be rewritten

$$E_1 = e^{jk_1(\sin\theta x + \cos\theta z)} + \sum_{i=-\infty}^{\infty} R_i e^{-j\left[(k_1\sin\theta' - iK)x - \sqrt{k_1^2 - (k_1\sin\theta' - iK)^2}\,z\right]}, \tag{3.8}$$

$$E_{2,n} = \sum_{i=-\infty}^{\infty} S_{i,n}(z) e^{-j\left[(k_1\sin\theta' - iK)x - \sqrt{k_{2,n}^2 - k_1^2\sin^2\theta'}\,z\right]}, \tag{3.9}$$

26

and

$$E_3 = \sum_{i=-\infty}^{\infty} T_i e^{-j\left[(k_1 \sin\theta' - iK)x - \sqrt{k_3^2 - (k_1 \sin\theta' - iK)^2} z\right]}.$$ (3.10)

3.1.7 Coupled Wave Equations

We have three unknown quantities in equations (3.8-10). We begin by solving for $S_{i,n}(z)$, the amplitudes of the space-harmonic fields in the grating. The electric fields in the grating region must satisfy Maxwell's equations. The wave equation for the TE polarization in region 2 is

$$\nabla^2 E_{2,n} + k^2 \varepsilon_n(x, z_n) E_{2,n} = 0.$$ (3.11)

Substituting the expressions for $E_{2,n}$ and $\varepsilon_n(x,z_n)$ given in (3.9) and (3.3) into this wave equation, and performing all of the derivations and setting the coefficient of each exponential term equal to zero for nontrivial solutions yields the rigorous coupled wave equations for the nth slab grating:

$$\begin{aligned}
&\frac{d^2 S_{i,n}(z)}{dz^2} - j2(k_{2,n}^2 - k_1^2 \sin^2\theta')^{1/2} \frac{dS_{i,n}(z)}{dz} + K^2 i(m-i) S_{i,n}(z) \\
&+ k^2 (\varepsilon_s - \varepsilon_c) \sum_{h=1}^{\infty} \left[\tilde{\varepsilon}_{h,n} S_{i-h,n}(z) + \tilde{\varepsilon}_{h,n}^* S_{i+h,n}(z) \right].
\end{aligned}$$ (3.12)

These coupled wave equations are an infinite set of second-order coupled difference-differential equations. Each diffracted wave (i) is coupled to other diffracted waves through the harmonics of the grating ($i - h$ and $i + h$). The quantity m has been defined as

$$m = 2\Lambda(\varepsilon_c)^{1/2} \sin\theta' / \lambda.$$ (3.13)

When m is equal to an integer, this represents a Bragg condition, which simply means that one of the diffractive orders is retro-reflected onto the incident beam.

3.2   Solution Method for Rigorous Coupled Wave Equations

The dielectric surface-relief grating diffraction problem described above is solved in a sequence of steps. First, the rigorous coupled wave equations are solved for the nth slab grating using a state-variables method. Second, the electromagnetic boundary conditions (continuous tangential E and tangential H) are applied between the cover region and the first slab grating, then between the first slab grating and the second slab grating and so forth, and finally between the Nth slab grating and region 3. Third, the resulting matrix of boundary condition equations is solved for the amplitudes of the reflected and transmitted diffracted orders, R_i and T_i. From these amplitudes, the efficiencies of each diffractive order is determined directly.

3.2.1   State Space Description for nth Slab Grating

First, we use the methods of linear systems analysis to transform the coupled-wave differential equation description in (3.12) to a state-space description. By defining the state variables for the nth slab grating as

$$S_{1,i,n}(z) = S_{i,n}(z),\tag{3.14}$$

and

$$S_{2,i,n}(z) = \frac{dS_{i,n}(z)}{dz},\tag{3.15}$$

we can transform the infinite set of second order differential equations into two sets of first order state equations

$$\frac{dS_{1,i,n}(z)}{dz} = S_{i,n}(z),\tag{3.16}$$

and

$$\frac{dS_{2,i,n}(z)}{dz} = -k^2(\varepsilon_s - \varepsilon_c)\sum_{h=1}^{\infty}\widetilde{\varepsilon}_{h,n}S_{1,i-h,n}(z) - K^2 i(m-i)S_{1,i,n}(z) -$$

$$k^2(\varepsilon_s - \varepsilon_c)\sum_{h=1}^{\infty}\widetilde{\varepsilon}_{h,n}^* S_{1,i+h,n}(z) + j2(k_{2,n}^2 - k_1^2\sin^2\theta')S_{2,i,n}(z).$$

(3.17)

These state equations for the nth slab grating can be written in matrix form as

$$
\begin{bmatrix}
\vdots \\
\dot{S}_{1,-2,n} \\
\dot{S}_{1,-1,n} \\
\dot{S}_{1,0,n} \\
\dot{S}_{1,1,n} \\
\dot{S}_{1,2,n} \\
\vdots \\
\dot{S}_{2,-2,n} \\
\dot{S}_{2,-1,n} \\
\dot{S}_{2,0,n} \\
\dot{S}_{2,1,n} \\
\dot{S}_{2,2,n} \\
\vdots
\end{bmatrix}
=
\begin{bmatrix}
 & & \vdots & & & & & \vdots & & & \\
\cdots & 0 & 0 & 0 & 0 & 0 & \cdots & 1 & 0 & 0 & 0 & 0 & \cdots \\
 & 0 & 0 & 0 & 0 & 0 & & 0 & 1 & 0 & 0 & 0 & \\
 & 0 & 0 & 0 & 0 & 0 & & 0 & 0 & 1 & 0 & 0 & \\
 & 0 & 0 & 0 & 0 & 0 & & 0 & 0 & 0 & 1 & 0 & \\
 & 0 & 0 & 0 & 0 & 0 & & 0 & 0 & 0 & 0 & 1 & \\
 & & \vdots & & & & & \vdots & & & \\
\cdots & b_{-2,n} & c_{1,n} & c_{2,n} & c_{3,n} & c_{4,n} & \cdots & d_n & 0 & 0 & 0 & 0 & \cdots \\
 & a_{1,n} & b_{-1,n} & c_{1,n} & c_{2,n} & c_{3,n} & & 0 & d_n & 0 & 0 & 0 & \\
 & a_{2,n} & a_{1,n} & b_{0,n} & c_{1,n} & c_{2,n} & & 0 & 0 & d_n & 0 & 0 & \\
 & a_{3,n} & a_{2,n} & a_{1,n} & b_{1,n} & c_{1,n} & & 0 & 0 & 0 & d_n & 0 & \\
 & a_{4,n} & a_{3,n} & a_{2,n} & a_{1,n} & b_{2,n} & & 0 & 0 & 0 & 0 & d_n & \\
 & & \vdots & & & & & \vdots & & & \\
\end{bmatrix}
\begin{bmatrix}
\vdots \\
S_{1,-2,n} \\
S_{1,-1,n} \\
S_{1,0,n} \\
S_{1,1,n} \\
S_{1,2,n} \\
\vdots \\
S_{2,-2,n} \\
S_{2,-1,n} \\
S_{2,0,n} \\
S_{2,1,n} \\
S_{2,2,n} \\
\vdots
\end{bmatrix}
$$
, (3.18)

where $\dot{S} = dS/dz$, $a_{i,n} = -k^2(\varepsilon_s - \varepsilon_c)\widetilde{\varepsilon}_{i,n}$, $b_{i,n} = -K^2 i(m-i)$, $c_{i,n} = -k^2(\varepsilon_s - \varepsilon_c)\widetilde{\varepsilon}_{i,n}^*$,

and $d_n = j2(k_{2,n}^2 - k_1^2\sin^2\theta')$. The elements of the four submatrices have local

indices p and q. The value of the size of the four submatrices, s, is the number of

diffracted orders retained in this analysis. The value $p = 1$ corresponds to the most

negative diffracted order retained, and the value $p = s$ corresponds to the most

positive order retained. The matrix equation above can be written concisely as

$\dot{S} = AS$, where $\dot{S}$ and S are the column vectors, and A is the total coefficient matrix.

Although the dimensions are infinite, results may be obtained to an arbitrary level of

accuracy by truncating the matrices. Each of the four submatrices is truncated to size

29

s x s. As s increases, the solution converges rapidly. The solution to this matrix

equation is written

$$S_{p',n}(z) = \sum_{q'=1}^{2s} C_{q',n} w_{p',q',n} \exp(\lambda_{q',n} z), \qquad (3.19)$$

where p' and q' are new index variables corresponding to the entire matrix-vector

indices of the (3.18) with p' = 1 to $2s$ and q' = 1 to $2s$, whereas p and q only

correspond to the indices of the submatrices of **A** with size s x s. $S_{l,p,n}$ has been

rewritten as $S_{p',n}$ with p' = p + (l - 1)s. The quantities $\lambda_{q',n}$ and $w_{p',q',n}$ are the

eigenvalues and eigenvectors of the matrix **A**. These values are easily determined by

standard computational routines. The quantities C $_{q',n}$ are unknown coefficients that

are determined from the boundary conditions. Finally, the desired diffracted wave

amplitudes for the nth slab grating are given by

$$S_{i,n}(z) = S_{p',n}(z), \qquad (3.20)$$

where p' corresponds to the ith diffracted wave.

3.2.2   Application of Boundary Conditions

We have just covered the solution method for the nth slab grating. Now the

task remains to connect the solutions of all slab gratings to the incident region and the

transmitted region. The way that this connection is to be made is through application

of the electromagnetic boundary conditions, which require that the tangential electric

and magnetic fields are continuous across all boundaries. We start by defining the

boundary condition between region 1 and the first slab grating with, then define the

boundary condition between slab the first slab grating and the second slab grating and

so forth until we define the boundary condition between the Nth slab grating and region 3.

For the TE polarization shown here, the electric field only has a tangential component in the y direction. The tangential component of the magnetic field is in the x direction and from Maxwell's equations is given by $H_x = (-j/\omega\mu)\partial E_y/\partial z$. Therefore, for the boundary between the incident region and the first slab, $z = 0$, the boundary condition for tangential E is

$$\delta_{i0} + R_i = \sum_{q'=1}^{2s} C_{q',1} w_{p',q',1},\qquad(3.21)$$

and the boundary condition for tangential H is

$$j(\mathbf{k}_{1i}\cdot\hat{z})(R_i - \delta_{i0}) = \sum_{q'=1}^{2s} C_{q',1} w_{p',q',1}\left[\lambda_{q',1} - j(\boldsymbol{\sigma}_{i,1}\cdot\hat{z})\right],\qquad(3.22)$$

where δ_{i0} is the Kronecker delta function and the value of p' is chosen to correspond to the ith wave. For the boundary between the nth and $n+1$th slab gratings, $z = nd/N$, the boundary condition for tangential E is

$$\sum_{q'=1}^{2s} C_{q',n} w_{p',q',n} \exp\left\{\left[\lambda_{q',n} - j(\boldsymbol{\sigma}_{i,n}\cdot\hat{z})\right]nd/N\right\}$$
$$= \sum_{q'=1}^{2s} C_{q',n+1} w_{p',q',n+1} \exp\left\{\left[\lambda_{q',n+1} - j(\boldsymbol{\sigma}_{i,n+1}\cdot\hat{z})\right]nd/N\right\},\qquad(3.23)$$

and the boundary condition for tangential H is

$$\sum_{q'=1}^{2s} C_{q',n} w_{p',q',n}\left[\lambda_{q',n} - j(\boldsymbol{\sigma}_{i,n}\cdot\hat{z})\right]\exp\left\{\left[\lambda_{q',n} - j(\boldsymbol{\sigma}_{i,n}\cdot\hat{z})\right]nd/N\right\}$$
$$= \sum_{q'=1}^{2s} C_{q',n+1} w_{p',q',n+1}\left[\lambda_{q',n+1} - j(\boldsymbol{\sigma}_{i,n+1}\cdot\hat{z})\right]\exp\left\{\left[\lambda_{q',n+1} - j(\boldsymbol{\sigma}_{i,n+1}\cdot\hat{z})\right]nd/N\right\}.\qquad(3.24)$$

For the boundary condition between the Nth slab grating and region 3, z = d, the boundary condition for tangential E is

$$\sum_{q'=1}^{2s} C_{q',N} w_{p',q',N} \exp\left\{ \left[\lambda_{q',N} - j(\boldsymbol{\sigma}_{i,N} \cdot \hat{z}) \right] d \right\} = T_i, \qquad (3.25)$$

And the boundary condition for tangential H is

$$\sum_{q'=1}^{2s} C_{q',N} w_{p',q',N} \left[\lambda_{q',N} - j(\boldsymbol{\sigma}_{i,N} \cdot \hat{z}) \right] \exp\left\{ \left[\lambda_{q',N} - j(\boldsymbol{\sigma}_{i,N} \cdot \hat{z}) \right] d \right\} = -j(k_{3i} \cdot \hat{z}) T_i . (3.26)$$

Equations (3.21-26) represent a total of $2(N+1)s$ equations. There are s unknown values each of R_i and T_i and $2s$ unknown values of $C_{q',n}$ for each slab grating. Thus the total number of unknowns is $2(N+1)s$, which is the same as the number of boundary condition equations. If s values of i are retained in the analysis, then the calculations yield s transmitted wave amplitudes (T_i), and s reflected wave amplitudes (R_i).

3.2.3   Matrix Solution for System of Equations

This system of equations can be solved by writing the boundary equations in matrix form. Figure 3.3 depicts the matrix form resulting from the boundary condition equations. The matrix is $2(N+1)s$ by $2(N+1)s$ and consists of the coefficients of $C_{q',n}$ (for $q' = 1$ to $2s$) and $n = 1$ to N), R_i (s values) and T_i (s values). There are many well-known ways to solve this matrix equation. The simplest way is multiply **b** by $\mathbf{A}^{-1}$. To achieve accurate results, N would be in the range of 50-100, while s could also be in the same range. Under these conditions **A** might be as large as 20,000 by 20,000. A matrix of this size represented with 32-bit floating point complex numbers would require over 3 GB of storage space. Even with today's computing power, this requirement is high for a typical PC.
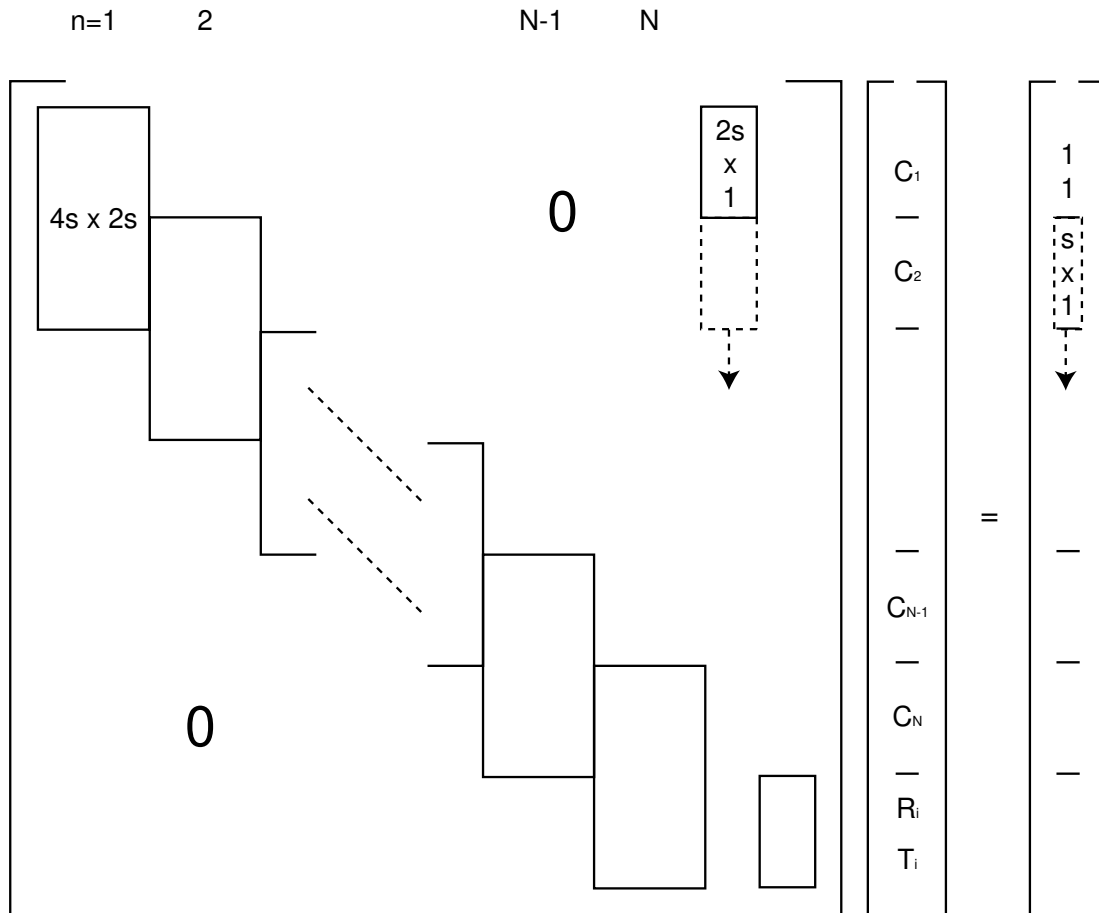
Figure 3.3 Matrix-equation representation of boundary condition equations

An alternative approach to attempting to invert the entire boundary condition matrix is to use a technique like Gauss elimination applied successively to each boundary starting at the $z = 0$ input surface. By using this technique $N + 1$ times, the s values of R_i and T_i may be obtained on the last step. For each slab grating, the boundary condition equations produce a $4s$ by $2s$ submatrix. Starting with the first slab grating, represented by the upper-left-hand submatrix, a technique like Gauss elimination is applied to make all the elements of the lower half of the submatrix equal to zero. In so doing, the system is reduced to $2Ns$ equations. Repeating this process on the next submatrix also reduces the number of equations in the system by

33

one. For each step in this process, a new 2*s* by *s* submatrix of coefficients for R_i is generated and is passed down, as shown by the dashed box in Figure 3.3. After *N* steps, these coefficients have reached the bottom of the matrix, and the remaining 2*s* equations are solved for R_i and T_i. This sequential process greatly reduces the storage and computational requirements for this problem, as only one 4*s* by 2*s* matrix is treated at each step. In fact, the data-storage requirement is reduced by a factor of $(N+1)^2/3$ and reduces the execution time by a factor of N^2, where *N* is the number of layers [58].

Having determined the complex amplitudes R_i and T_i, the diffraction efficiencies, or ratio of diffracted intensity to input intensity, can be directly determined. The diffraction efficiencies in regions 1 and 3 are respectively

$$DE_{1i} = \text{Re}\{(k_{1i} \cdot \hat{z})/(k_{10} \cdot \hat{z})\}|R_i|^2 \tag{3.27}$$

and

$$DE_{3i} = \text{Re}\{(k_{3i} \cdot \hat{z})/(k_{10} \cdot \hat{z})\}|T_i|^2 . \tag{3.28}$$

For a lossless grating, the output power is conserved, and the sum of all efficiencies of all diffracted transmitted and reflected waves sum to unity. The above computational process has been implemented as a MATLAB script. The script and instructions on how it is used is found in Appendix 8.2B.2.

3.3   Example Efficiency Calculations

Having discussed the formulation of this computational method, we now look back to the example grating from Chapter 2. This grating had a period of 1 μm and was periodic only in the *x* dimension. The incident medium was free space, and the

transmitted medium had a refractive index n_t of 1.5. The light illuminating the

grating had wavelength $\lambda = 632.8$ nm at an angle of incidence of -10º. In Chapter 2

we determined the angles of each diffracted order. We can now use rigorous

coupled-wave analysis to determine the efficiencies of those orders for different

grating shapes.

3.3.1   Binary Grating

First we examine the binary grating. As stated in Chapter 2, binary gratings

are made easily by photolithography. We assume that the grating height is .5 µm, and

that the grating material is a photoresist with an index of refraction of 1.6. This

grating geometry is chosen because it is realistic of the type of binary grating that

could be made by photolithography. Figure 3.4 below shows this grating.
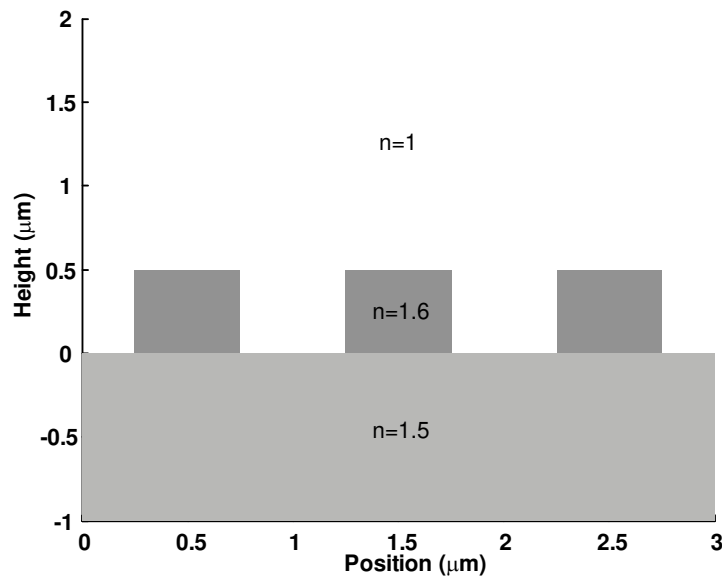
Figure 3.4 Binary grating with grating height .5 µm

For this shape of diffraction grating, the efficiencies of the reflected and transmitted orders are given in Table 3.1 below. As seen from these calculations almost half of the power goes into the -1 order.

Table 3.1 Efficiency for binary diffraction grating with 1 µm period

Diffractive Order	-2	-1	0	1	2
Reflected	--	1.28%	1.50%	1.19%	--
Transmitted	4.14%	45.62%	9.754%	25.79%	10.69%

3.3.2   Blazed Grating

Now we look at an example with a blazed grating. We assume that this grating was mechanically scribed into a glass substrate. This means that the grating index of refraction isbe 1.5. First, we choose the total blaze height to be 2.24 µm. This height is chosen because it maximizes the efficiency into the first diffractive order. For this blazed grating, we use 50 slices in the analysis. Figure 3.5 below shows the model of the grating that we analyze.
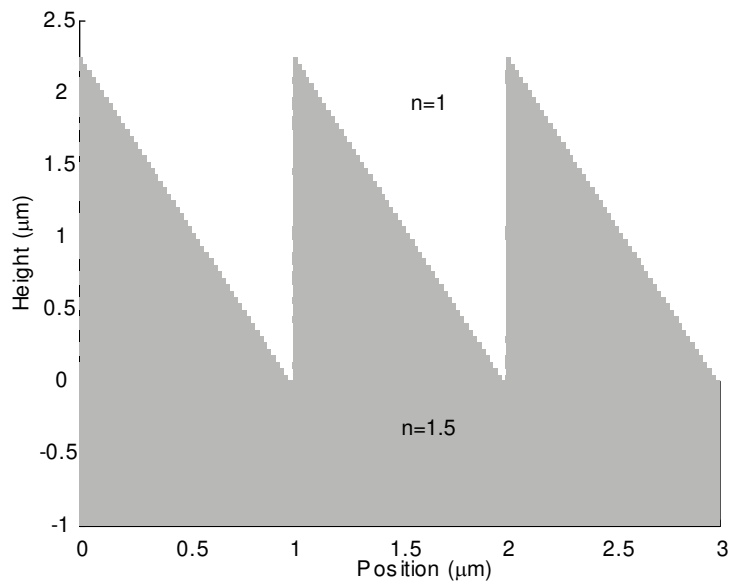
Figure 3.5 Blazed grating with grating height 2.24 µm

36

For this shape of diffraction grating, the efficiencies of the different diffractive

orders calculated from rigorous coupled-wave analysis are shown in Table 3.2 below.

Table 3.2 Efficiency of blazed grating with 1 μm period

Diffractive Order	-2	-1	0	1	2
Reflected	--	.015%	.006%	.008%	--
Transmitted	.028%	12.37%	16.21%	64.3%	7.08%

As seen from the table, there is strong coupling into the +1 Transmitted order.

In Chapter 2, blazed gratings were discussed as having this property of placing higher

efficiencies into single diffractive orders. In designing the blaze grating, the angle of

the blaze is chosen such that if the incident beam were to encounter a surface at that

angle, the angle of the refracted beam matches an angle of one of the diffractive

orders.

3.3.3   Sinusoidal Grating

Finally, we look at a sinusoidal grating. In Chapter 2, it was said that

sinusoidal gratings are easily recorded holographically. We assume that the

sinusoidal grating has been holographically recorded in photoresist with refractive

index 1.6, and that the substrate is glass. We choose grating heights of .5 μm and

compare these results with the binary grating. We use 100 slices for this analysis.

Figure 3.6 below shows the model of the grating that is analyzed.
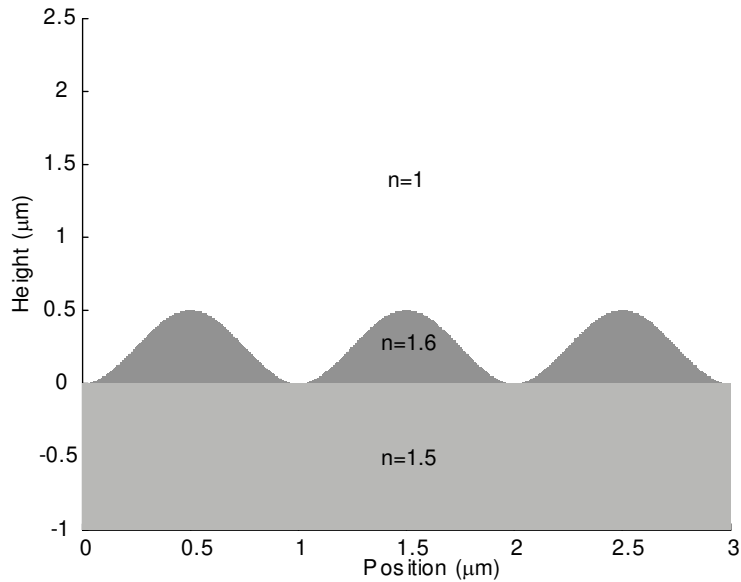
Figure 3.6 Sinusoidal grating profile

For this shape of diffraction grating, the efficiencies of the different diffractive

orders calculated from rigorous coupled-wave analysis are shown in Table 3.3 below.

Table 3.3 Efficiency of sinusoidal grating with 1 μm period

Diffractive Order	-2	-1	0	1	2
Reflected	--	.33%	1.15%	.01%	--
Transmitted	5.97%	32.45%	15.27%	42.70%	2.12%

As shown in Table 3.3, the +1 transmitted order has the most power. The

efficiency of the sinusoidal grating is different than the efficiency of the binary

grating, even though their heights are the same. From all of these examples, it is

easily seen how the shape of a diffraction grating impacts its efficiency.

3.4 Numerical Accuracy

To complete this discussion on the implementation of the rigorous coupled-

wave analysis for surface relief gratings, we address the issue of numerical

convergence. There are two factors in the implementation that affect the accuracy of the results. One factor is the number of diffractive orders retained in the analysis. The second factor is the number of grating slices used in the analysis. For a more formal discussion of the numerical accuracy of this method see [58,75].

3.4.1   Number of Orders Retained in Analysis

First, we explore the issue of how many orders must be retained in the analysis. A common mistake is to assume that the numbers of orders retained should be the number of orders that the grating produces. For instance, in the examples shown earlier, there were five diffractive orders. If in the analysis only five orders were retained, the result would not be accurate. Although only a finite number of diffractive orders exist outside the grating, the fields inside the grating contain an infinite number of Floquet waves. The efficiency of the orders outside the grating depends on the coupling between the infinite set of Floquet waves inside the grating. Truncating the number of Floquet waves considered in the analysis too far results in an inaccurate solution, therefore a sufficient number of orders must be retained in the analysis beyond the number of physical diffractive orders.

To illustrate this convergence, we use the example of the binary grating above. We calculate the efficiency of the first order transmitted while at each step increasing the number of orders retained in the analysis. As the number of orders retained increases, the efficiency value converges to the actual solution. The result of this calculation is shown below in Figure 3.7.
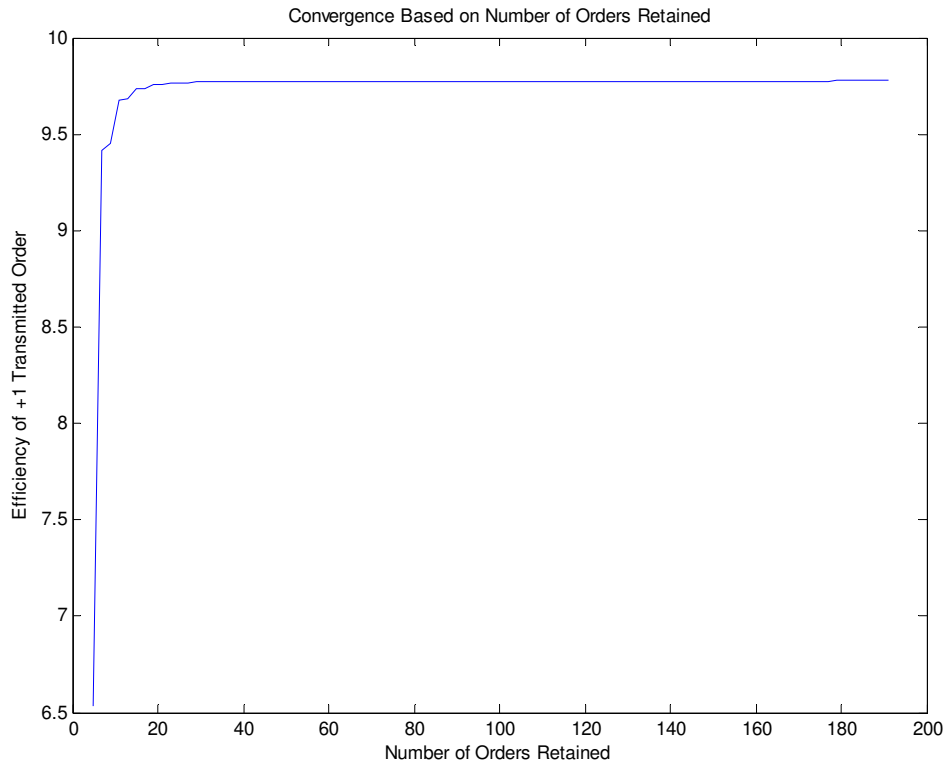
Figure 3.7 Effect of number of orders retained in rigorous coupled wave analysis on accuracy of solution

From Figure 3.7, we see that there is a knee in the value at about 10 orders. After 40 orders, the calculated value is converging very slowly. Any additional orders retained does not improve the accuracy by a substantial amount. When this implementation of rigorous coupled-wave analysis is used, it is important to calibrate the number of orders retained to be sure that the solution is accurate.

3.4.2   Number of Slices in Grating Representation

The second issue of accuracy is how many grating slab slices are needed to converge to within a reasonable tolerance. The more slabs are used, the more the modeled grating resembles the actual grating that is to be analyzed. To explore this

issue, we use the sinusoidal grating example from above and calculate the efficiency of the first order transmitted beam. At each step we increase the number of slab gratings. For this analysis we retain 101 diffractive orders. As the number of slab gratings used increases, the solution converges to the actual value. The result of this analysis is shown below in Figure 3.8.
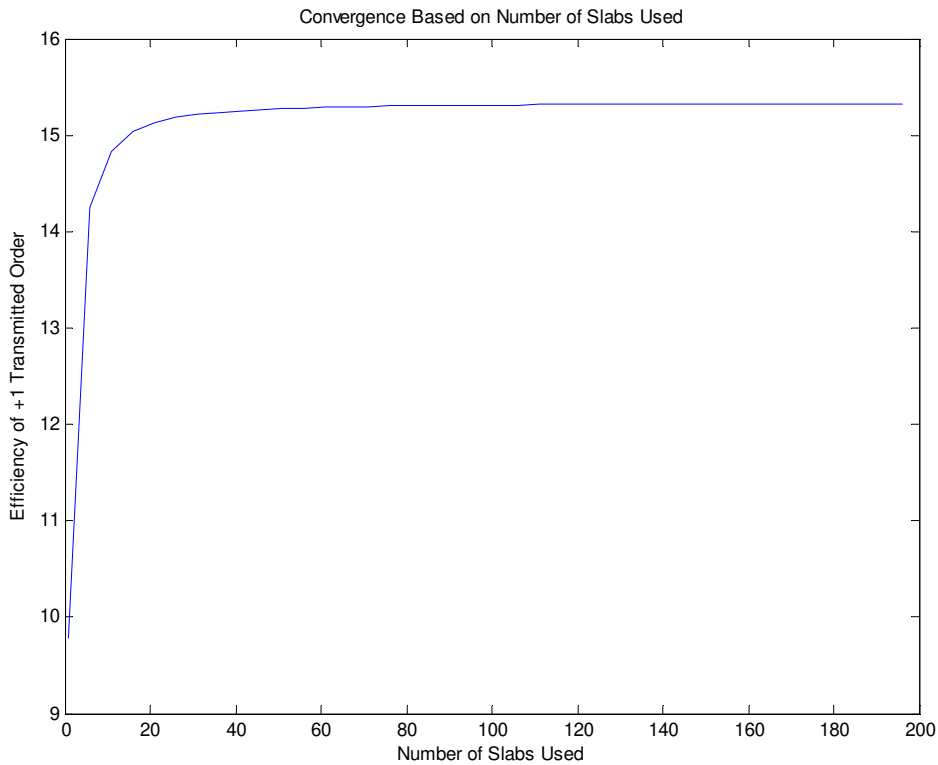
Figure 3.8 Effect of number slabs used in grating representation on accuracy of solution

From Figure 3.8, we can see that the convergence due to increasing the number of slabs is a little slower than the convergence due to the number of orders retained. However, there is a knee in the curve at about 20 slabs. After 60 slabs, the calculated value is converging slowly, and increasing the number of slabs beyond this point provides little increased accuracy. In order to make sure that the results are

41

accurate, it is important to calibrate the number of slabs used in representing the grating.

   With the methods discussed in this chapter, the efficiencies of any surface relief grating can be calculated to an arbitrary degree of accuracy, with no approximations used in the analysis. This tool is very useful in the design of diffraction grating applications, especially the design of grating couplers to couple light into waveguides, which is the topic of Chapter 4.

Chapter 4

4   Grating Coupler Design

In Chapter 2, the method of wavevector analysis was presented as a tool for

analyzing the behavior of diffraction gratings in terms of the direction that the light is

diffracted. In Chapter 3, the method of rigorous coupled wave analysis was presented

as a tool for analyzing the efficiencies of the diffraction grating based on the physical

geometry of the diffraction grating. This chapter applies these tools to the design of

grating couplers. The grating couplers that are of interest to us are those that diffract

light into a guided mode of an optical waveguide. First we show the basic structure

for the design. We then look at grating couplers from a wavevector standpoint.

Following the wavevector analysis, we characterize the efficiency of a grating coupler

based on a mathematical model. We then discuss a method for finding the

efficiencies of the grating coupler that involves the use of rigorous coupled wave

analysis. A discussion of the design variables and strategy is then be presented, and

finally we display some calculations of the coupler parameters based on design

variables.

4.1 Basic Structure

The basic structure of the grating coupler is shown in Figure 4.1. As seen in Figure 4.1, the basic structure consists of a cover region, a waveguide region, and a substrate region. There are two diffraction gratings. One grating is for input coupling and the other is for output coupling. The light is incident on the input grating which diffracts the light into the waveguide. The output grating diffracts the propagating light out of the waveguide.

cover

input   output

waveguide
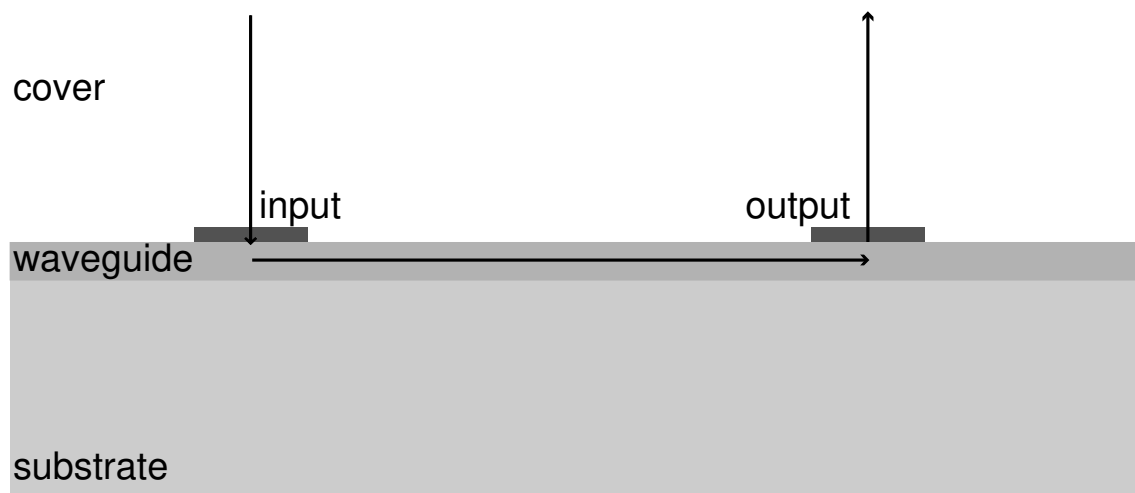
substrate

Figure 4.1 Basic structure of grating coupler

For our research purposes, we use light from a HeNe laser to test the grating couplers that are built. Therefore, the incident light has a wavelength of 632.8 nm. The substrate we use is a glass slide with an index of refraction of about 1.46. The waveguide region is a silicon nitride layer deposited by PECVD. The index of refraction of our waveguide is 2.1 as measured by ellipsometry. The cover region is free space. The input and output gratings are recorded in photoresist and eventually etched into the SiN waveguide layer. The design parameters are the period of the input and output grating, the etch depth of the grating into the waveguide, the

thickness of the waveguide, and the angle of incidence. From the parameters above, the waveguide thickness is chosen such that the waveguide supports a single mode. Using electromagnetic theory, the range of waveguide thicknesses is found to be from .0379 μm to .245 μm. The thickness of the waveguide determines the effective index of refraction of the single mode. The effective index of refraction for a guided wave is defined as the ratio of the propagation constant of the guided wave to the propagation constant of free space. Based on the range of waveguide thicknesses above, Figure 4.2 shows a plot of the effective index of refraction of the mode in the slab waveguide as a function of waveguide thickness.
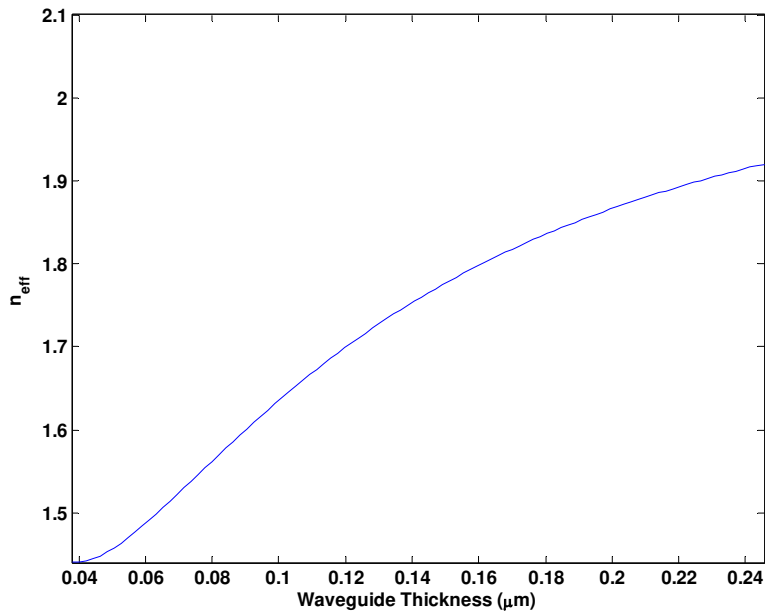
Figure 4.2 Plot of effective index of refraction for single mode waveguide vs. thickness of waveguide

In order for the diffraction gratings to couple light into the single mode waveguide, the diffraction gratings have to diffract the incident light in such a way that the effective index of the diffracted wave matches the effective index of the mode

in the waveguide. The effective index of a diffracted wave is the ratio of the tangential component of the diffracted wavevector to the wavevector of free space. This quantity is very important in the design of the grating coupler, and its effect is discussed in greater detail later. The remaining design parameters are the grating period, angle of incidence, grating depth, and waveguide thickness. The effect of each of these are discussed in the following sections.

4.2   Wavevector Analysis

We begin our discussion of grating coupler design with the wavevector analysis method. This analysis method allows us to determine the period of the input and output grating, and the angle of incidence that allows coupling into the waveguide. This analysis first addresses input coupling, and the effect of grating period and angle of incidence are discussed. We then explore the effect of the grating in terms of the effective index of refraction for the diffractive orders. The analysis then addresses output coupling, where the effect of grating period is discussed, along with the effective index of refraction. Following the analysis of input and output coupling, the design method is discussed in more detail and actual parameters are be chosen for the period and angle of incidence.

4.2.1   Input Coupling

We begin our wavevector analysis with input coupling. First, we examine the effects of varying the grating period, and second, we examine the effects of varying the angle of incidence.

4.2.1.1   Effect of Grating Period

In general, as grating period decreases, eventually all diffractive orders other than the zero order are cutoff, meaning that the tangential component of the wavevector of the diffracted order is greater than the magnitude of the wavevector of that medium and therefore the field is evanescent in that medium. The point at which the diffractive orders are cutoff depends on the refractive index of the transmitted medium. The higher the refractive index of the transmitted medium, the smaller the grating period must be before the diffractive orders in that medium are cutoff. Figure 4.3 shows the diffraction from a .8 μm period grating at normal incidence with other parameters as defined above.
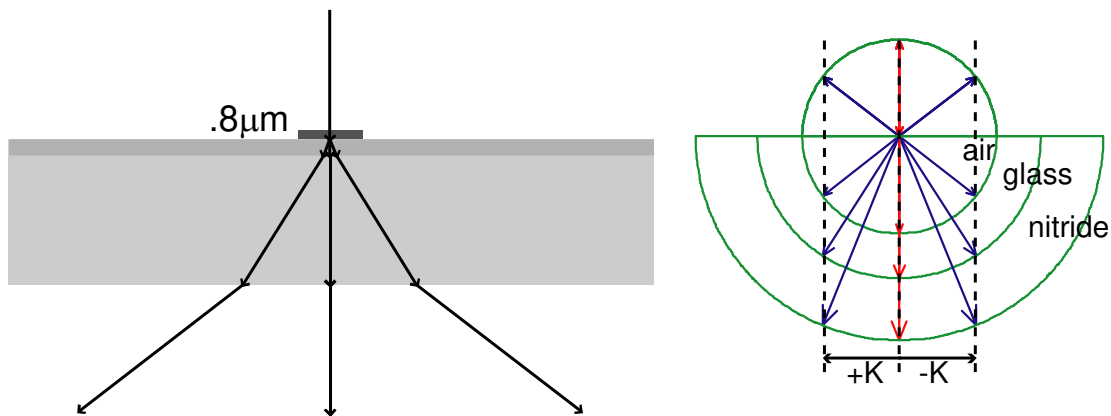
Figure 4.3 Diagram of .8 μm grating at normal incidence

Figure 4.3 shows that with this size period, the diffractive orders exist in all three regions, and have not yet been cutoff. This type of coupling is simply free space coupling. Figure 4.4 shows the diffraction from a .5 μm period grating at normal incidence.
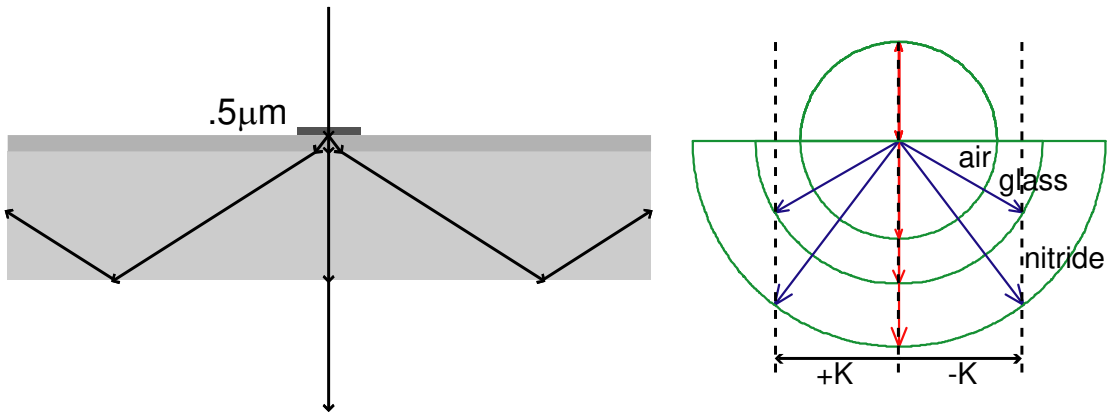
Figure 4.4 Diagram of .5 µm grating at normal incidence

Figure 4.4 shows that the with this size period, the diffractive orders in air have been cutoff. The transmitted orders in the substrate stay in the glass by total internal reflection. This type of coupling is known as substrate coupling. If the period of the diffraction grating is decreased further, the diffractive orders in glass also are cutoff, and only orders in the waveguide layer can exist. Figure 4.5 shows the diffraction from a .35 µm period grating at normal incidence.
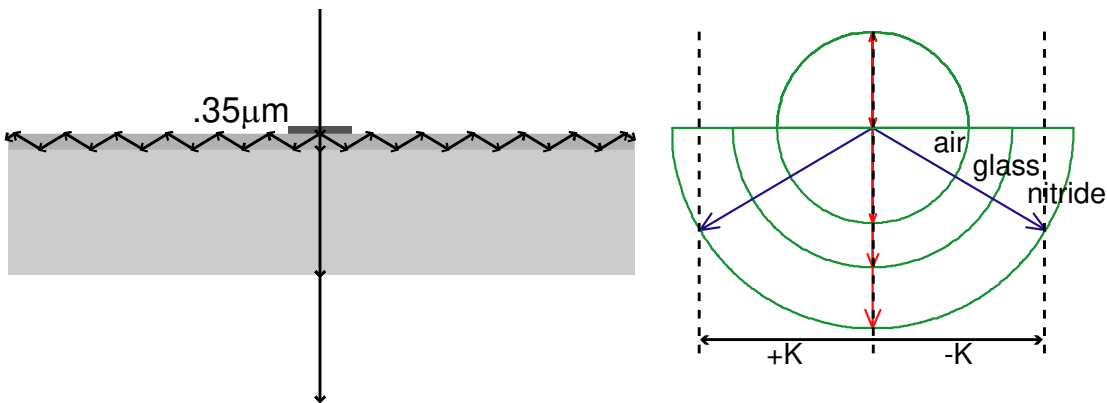
Figure 4.5 Diagram of .35 µm grating at normal incidence

Figure 4.5 shows that the light isonly be transmitted into the nitride region. While Figure 4.5 depicts the light in the waveguide region as rays, the light actually

couples into the mode supported by the waveguide. This type of coupling is known as guided mode coupling, and is the type of grating coupler that we wish to design. However, it is important to note that the coupling depicted in Figure 4.5 only happens if the effective indices of the +1 and -1 diffractive orders match the effective index of the mode supported by the nitride waveguide, which is only the case if the diffracted beam into the nitride is within a very small range of angles.

It is important now to look at the effect of grating period on grating coupling in terms of effective index of refraction. The dependence on grating period depicted in Figure 4.3-Figure 4.5 can all be explained in terms of effective index. As mentioned earlier, the effective index of refraction is the ratio of the tangential component of the diffracted wavevector to the wavevector of free space. The tangential component of the diffracted wavevector, k_{qx} can be written

$$k_{qx} = \frac{2\pi n_t}{\lambda}\left(\sin\theta_q \hat{x} + \cos\theta_q \hat{z}\right)\cdot\hat{x} = \frac{2\pi n_t}{\lambda}\sin\theta_q .$$ (4.1)

The ratio of this quantity to the wavevector of free space is simply $n_t\sin\theta_q$, which happens to be the left side of the diffraction equation (2.4). In terms of the effective index of refraction, n_{eff}, the diffraction equation is

$$n_{eff}^q = n_i\sin\theta_i - q\frac{\lambda}{\Lambda} ,$$ (4.2)

where n_{eff}^q is the effective index of refraction for the qth diffracted order. Figure 4.6 shows a plot of n_{eff}^1 for normal incidence.
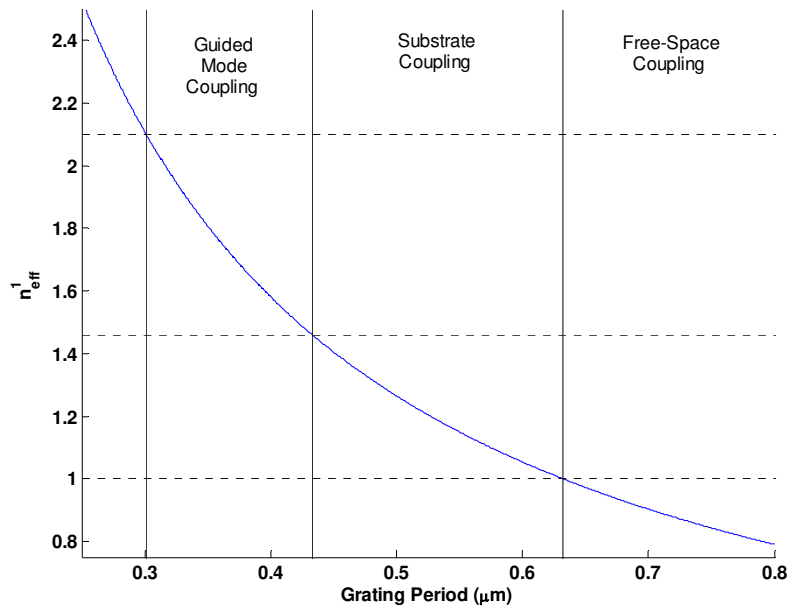
Figure 4.6 Plot of n_{eff} for first diffractive order.

Figure 4.6 also shows the ranges over which different types of coupling occur. Free-space coupling occurs if the effective index is less than the effective index of free-space, which in this example corresponds to the grating period being greater than .6328 μm, or the wavelength of the incident light in free space. Free space coupling was demonstrated in Figure 4.3. Substrate coupling occurs if the effective index is between the index of the substrate and the index of the cover region, which in this example corresponds to a grating period between .4334 μm and .6328 μm. Substrate coupling was demonstrated in Figure 4.4. Guided mode coupling occurs if the effective index is between the index of the waveguide and the index of the substrate, which for this example corresponds to a grating period between .3013 μm and .4334 μm. Guided mode coupling was demonstrated in Figure 4.5. An effective index higher than the index of the waveguide means that the diffracted order is cutoff. The

50

effective index of refraction is a powerful design tool that allows for intuitive choices in design parameters.

4.2.1.2   Effect of Angle of Incidence

In the previous section, we studied the effect of varying the grating period, assuming normal incidence. We now study the effects of varying the angle of incidence while holding the grating period constant. In general if the angle of incidence increases, the effective index of refraction for the diffractive orders changes. This means that as the angle of incidence increases, diffractive orders that were once cutoff in a certain region rise above cutoff. To illustrate this dependence, we begin with the example in Figure 4.5, and increase the angle. Recall that in this thesis, positive angles are measured counterclockwise from the normal. Figure 4.7 shows the diffraction from a .35 μm period grating at an angle of incidence of 30º.
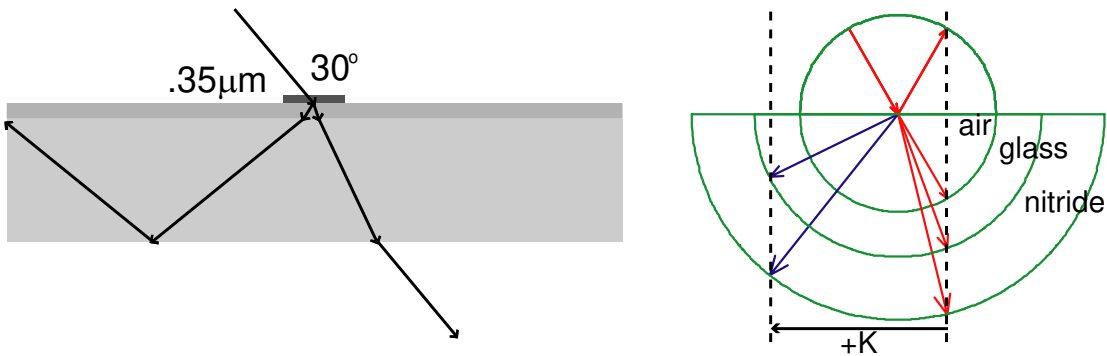
Figure 4.7 Diagram of .35 μm grating at incidence of 30º

Figure 4.7 shows that by changing the angle of incidence to 30º, the +1 order has risen above cutoff in the glass substrate, but not in air. By changing the angle, we have moved from a guided mode coupling to a substrate coupling. If we continue to

increase the angle of incidence, we are able to move to a free space coupling. Figure 4.8 shows the diffraction of a .35 µm period grating at an angle of incidence of 60º.
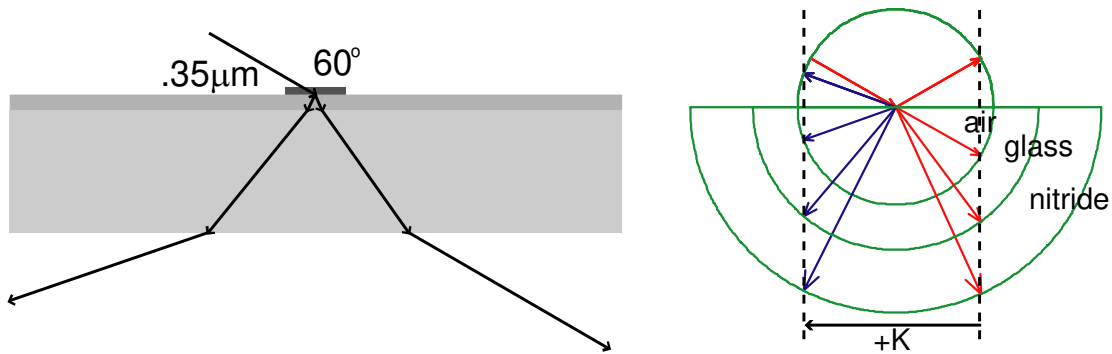
Figure 4.8 Diagram of .35 µm grating at incidence of 60º

Figure 4.8 shows that by changing the angle of incidence to 60º, the +1 order has risen above cutoff in air. While increasing the angle of incidence has decreased the effective index of the +1 order, the effective index of the -1 order has increased such that in both Figure 4.7 and Figure 4.8, the -1 order is cutoff in all regions.

As we did when we were investigating the effect of grating period, we now look at the effect of angle of incidence on grating coupling in terms of effective index of refraction. If we hold the grating period at .35 µm, we can change incidence and see how n_{eff} varies with angle of incidence. Figure 4.9 shows a plot of n_{eff}^{1} with respect to incidence angle.
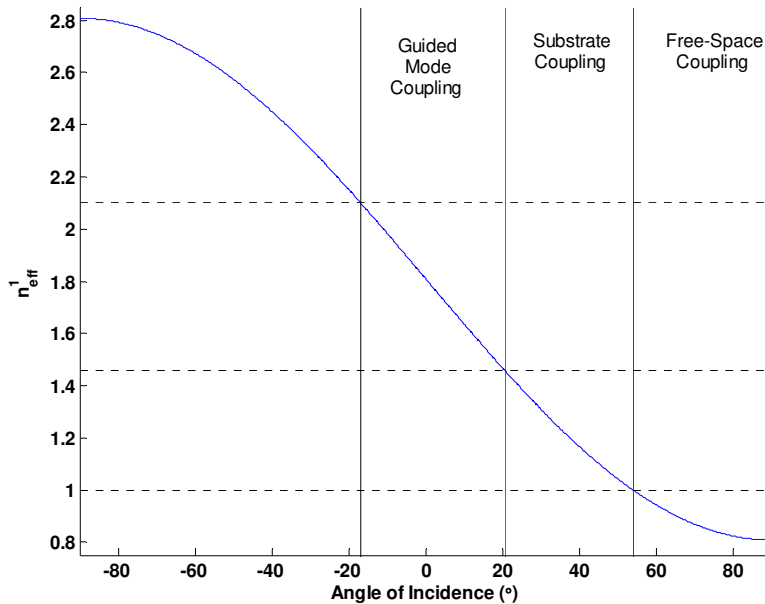
Figure 4.9 Plot of n_eff for +1 diffracted order

Figure 4.9 shows that for the +1 diffractive order, increasing the angle of

incidence decreases the effective index, and allows coupling into lower index

mediums. As before, free space coupling occurs if the effective index is less than the

effective index of free space, which in this example corresponds to the incidence

angle being greater than 53.9º. Free space coupling was demonstrated in Figure 4.8.

Substrate coupling occurs if the effective index is between the index of the substrate

and the index of the cover region, which in this example corresponds to the incidence

angle being between 20.36º and 53.9º. Substrate coupling was demonstrated in

Figure 4.7. Guided mode coupling occurs if the effective index is between the index

of the waveguide and the index of the substrate, which for this example corresponds

to the incidence angle being between -16.98º and 20.36º. Guided mode coupling was

demonstrated in Figure 4.5. An effective index higher than the index of the

waveguide, or in this example, an angle of incidence below -16.98º, means that the diffracted order is cutoff. From the above discussion we have shown that it is possible to adjust the effective index of a diffractive order by adjusting the angle of incidence. However, the change in effective index due to changing the angle of incidence is limited. Solving equation (4.2) for $\sin\theta_i$, we obtain

$$\sin\theta_i = \frac{n_{eff}^q \Lambda + q\lambda}{\Lambda n_i} .$$

(4.3)

The sine function is bounded from its maximum of +1 to its minimum of -1. Therefore the maximum value for n_{eff} is

$$\max(n_{eff}) = \frac{\Lambda n_i - q\lambda}{\Lambda} ,$$

(4.4)

and the minimum value for n_{eff} is

$$\min(n_{eff}) = \frac{-\Lambda n_i - q\lambda}{\Lambda} .$$

(4.5)

The maximum change in effective index due to adjusting the angle of incidence is

$$\Delta n_{eff}^q = \max(n_{eff}) - \min(n_{eff}) = \frac{\Lambda n_i - q\lambda}{\Lambda} - \frac{-\Lambda n_i - q\lambda}{\Lambda} = 2n_i$$

(4.6)

Therefore, adjusting the angle of incidence can change the effective index of the diffractive order no more than twice the value of the index of refraction of the cover medium. Choosing the right combination of angle of incidence and grating period allows us to design a grating coupler that couples light into a single mode slab waveguide.

4.2.2   Output Coupling

Having discussed the effect of grating period and angle of incidence on input coupling to a waveguide, we now look at how these parameters affect the output coupling from a waveguide. First we discuss the reciprocal duality of input and output coupling. Then we look at the effect of grating period on output coupling.

4.2.2.1   Reciprocity with Input Coupling

A grating coupler is a reciprocal system [80,81]. Meaning that if the output beam becomes the input beam and is turned around such that it encounters the grating coupler in the same manner in which it left, the resulting output beam would be the same as the original input beam traveling in the opposite direction. In other words, the output and input are interchangeable. However, output coupling is a little simpler than input coupling, because instead of the incident beam coming into the grating at an arbitrary angle, the incident wave is the single mode of the waveguide. Thus, given a waveguide, the only variable in the design is the period of the output grating coupler. This period determines the angle at which the light is coupled out. If the same grating is used as the input coupler, the output coupling angle is the same as the input coupling angle such that the incident beam is matched to the effective index of the waveguide.

4.2.2.2   Effect of Grating Period

Having discussed the dual nature of input and output coupling, we now examine the effects of grating period on output coupling. This discussion follows the same structure as the discussions in previous sections. For this analysis, we assume

that the thickness of the SiN waveguide is .2 μm, and the index of refraction is 2.1. The single mode for this waveguide has an effective refractive index of 1.8663.

Before we get into the examples, we need to choose a range for the grating period. Ideally, we would like only one diffracted order coupled out of the waveguide. This request places a maximum on the grating period for the coupler. For output coupling, the diffraction equation is:

$$n_t \sin\theta_t = n_{eff}^m - q\frac{\lambda}{\Lambda},$$ (4.7)

where n_{eff}^m is the effective index of refraction of the mode in the waveguide. We want orders higher than $q = 1$ to be cutoff. Substituting this condition into (4.7) and solving for the grating period gives the following inequality for maximum grating period.

$$\Lambda < \frac{2\lambda}{n_{eff}^m + n_s},$$ (4.8)

where n_s is the index of refraction of the substrate. Using the same reasoning, we can derive an expression for the minimum value of the grating period. The requirement is that the first order diffracted beam be above cutoff. Substituting this condition into (4.7) and solving for the grating period gives the following inequality for minimum grating period.

$$\Lambda > \frac{\lambda}{n_{eff}^m + n_t},$$ (4.9)

where n_t is the index of refraction of either the cover or substrate region depending on which region we want the first order beam to be above cutoff. Thus for the example we have chosen, Λ must be between .2208 μm and .3805 μm for diffraction into air, and Λ must be between .1902 μm and .3805 μm for diffraction into the glass.

To illustrate the effect of the grating period on output coupling, let's first look at an example where the grating period is equal to .37 μm. Figure 4.10 shows the diffraction from this output coupler

Figure 4.10 Output coupling from .37 μm period grating coupler

Figure 4.10 shows that in this configuration the grating coupler produces free space coupling. Note that, in the k-space diagram, the horizontal ray that is higher in magnitude than the wavevector of glass is the undiffracted wavevector corresponding to the guided mode in the waveguide.

As before, we can decrease the period even more until the diffracted order is cutoff in air. Figure 4.11 shows the diffraction from a grating coupler with a period of .2 μm.

Figure 4.11 Output coupling from .2 µm period grating coupler

Figure 4.11 shows that the diffracted beam only is transmitted into the substrate medium. Thus, this grating provides substrate coupling. If the grating period is decreased further, the diffracted order in the substrate is also cutoff, and the grating does not have any interaction with the light in the waveguide as far as being able to couple light out. In general as the grating period decreases, the angles of the outcoupled beams increase until they are cutoff.

There are two other special conditions that need to be considered in this discussion. What if the grating diffracts light back down the waveguide in the opposite direction? This type of grating is known as a Bragg grating. Figure 4.12 illustrates a Bragg coupler.

Figure 4.12 Second order Bragg grating coupler

The type of grating coupler shown in Figure 4.12 is known as a second order Bragg grating coupler, because the second order diffracted beam matches the effective index of the guided mode and is reflected back down the waveguide. Therefore, second order Bragg gratings achieve guided mode coupling between a forward traveling wave and a backwards traveling wave. The grating vector **K** that results in the second order Bragg condition is equal to the wavevector of the guided mode. Therefore the grating period is equal to the free space wavelength of the light divided by the effective index of the guided mode. Another example of a Bragg coupler is the first order Bragg coupler. Figure 4.13 shows the interaction of a first order Bragg grating coupler.

Figure 4.13 First order Bragg grating coupler

Figure 4.13 shows that the first order diffracted beam is reflected back down the waveguide with no coupling of the light out of the waveguide. For the first order Bragg grating coupler the grating vector **K** is equal to two times the wavevector of the guided mode. Therefore the period is equal to the free space wavelength divided by two times the effective index of the guided mode. This discussion has shown that free space coupling, substrate coupling, and guided mode coupling are achievable with output grating couplers by adjusting the period.

To finish this discussion, we address the concept of effective index of refraction, and output coupling angle. Figure 4.14 shows the effective index of refraction of the diffracted orders from the output grating vs. grating period.
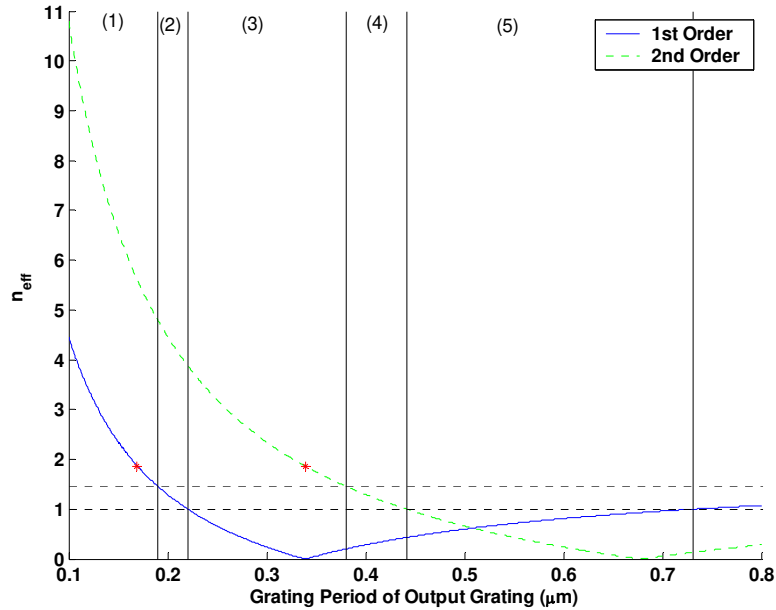
Figure 4.14 Plot of effective index vs. grating period for output coupler

In Figure 4.14, the solid line is the effective index of the first diffracted order, and the dotted line is the effective index of the second diffracted order. The points where these lines have the value of the effective index of the guided mode are each labeled with an asterisk. The asterisk on the solid curve is the point at which first order Bragg coupling occurs. Coupling at this point is illustrated in Figure 4.13. The asterisk on the dotted curve is the point at which second order Bragg coupling occurs. Coupling at this point is illustrated in Figure 4.12. The plot is divided into five regions. In region one, both the first and second order are cutoff in the cover and substrate layers. In region two, the first order is cutoff in the air cover region, but is

60

not cutoff in the glass substrate region and the second order is still cutoff for both air and glass. This region corresponds to the coupling illustrated in Figure 4.11. In region three, the first order is below cutoff for both the air cover region and the glass substrate region, and the second order is still cutoff in both air and glass. Coupling in this region is illustrated in Figure 4.10. In region four, the second order is below cutoff for the substrate layer, and in region five the second order is below cutoff for both the cover and substrate layers.

Not only can we analyze the effect of grating period in terms of effective index. We can also analyze the effect of grating period in terms of output coupling angle. For a given guided wavevector, the effect of decreasing the grating period is an increase in output coupling angle. Figure 4.15 shows the relationship between grating period and output coupling angle in the air cover region.
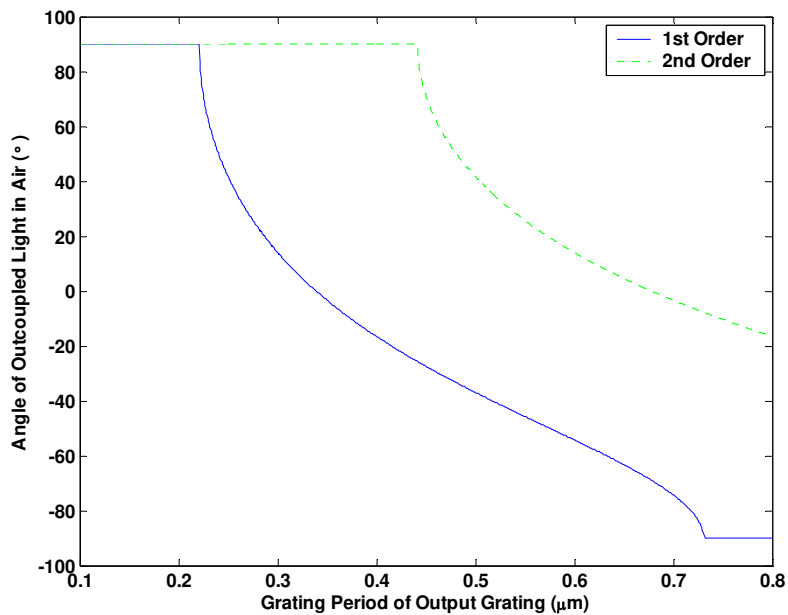
Figure 4.15 Plot of angle of outcoupled light vs. grating period

In Figure 4.15, the solid line is the first order diffracted wave, and the dotted line is the second order diffracted wave. Positive angles are measured as being countercloskwise from normal. Therefore, a beam with an outcoupled angle of 0° would be coupled out perpendicular to the waveguide. The portions on the plot where the curve is flat at 90° are the regions where the diffracted order is in cutoff. The curve shows that output angles between +10° and –10° can be obtained for grating periods in the range of .3μm to .4μm. For optical interconnect systems small angles with respect to the normal are desirable.

4.2.3   Wavevector Design Method

Now that we have discussed both input and output coupling, and analyzed the effects of grating period and angle of incidence, we are ready to make some design decisions. For a single mode waveguide with a given effective index of the guided mode, the method for designing a grating coupler starts with determining the desired output coupling angle. Once the output coupling angle is chosen, the grating period is determined accordingly based on the effective index of the guided mode that we desire to couple into. Because of the reciprocity of grating couplers, the input coupling angle is the same as the output coupling angle.

For our design, we choose an output coupling angle of 10° into air. Based on the parameters of the system given earlier and from equation (4.7), we can calculate that the period of the grating coupler needs to be about 0.374 μm. Figure 4.16 shows the wavevector diagrams for input and output coupling.
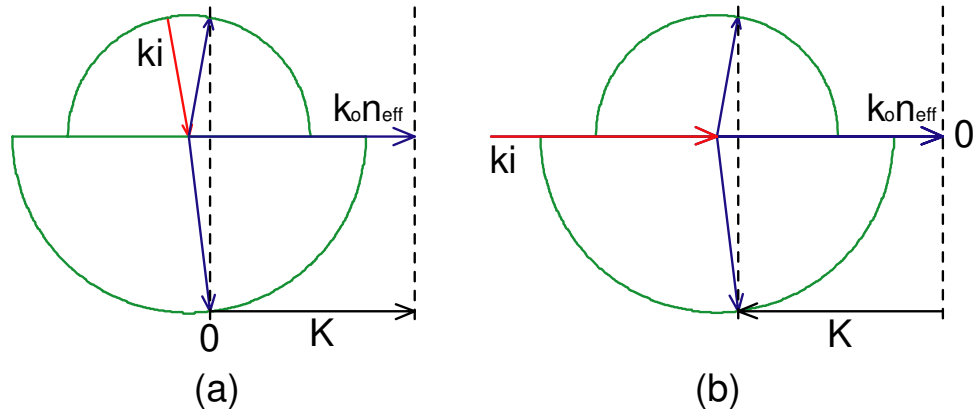
Figure 4.16 Wavevector diagrams for (a) input coupling and (b) output coupling for grating coupler with period of .374 µm.

Perhaps it may be difficult to actually fabricate this grating coupler with its 0.374 µm period. A grating coupler that is easier to manufacture is one with a slightly larger period.

As a second design for a grating coupler, we choose a period of 0.517 µm. This grating is less desirable because it gives more than one outcoupled order. This grating coupler has output angles of 35.57º and -39.96º. Therefore we can couple in to the waveguide with the -1 order diffracted beam if the input beam is at 35.57º, or we can couple into the waveguide with the -2 order diffracted beam if the input beam comes at -39.96º. Figure 4.17 shows wavevector diagrams for input and output coupling for this design.
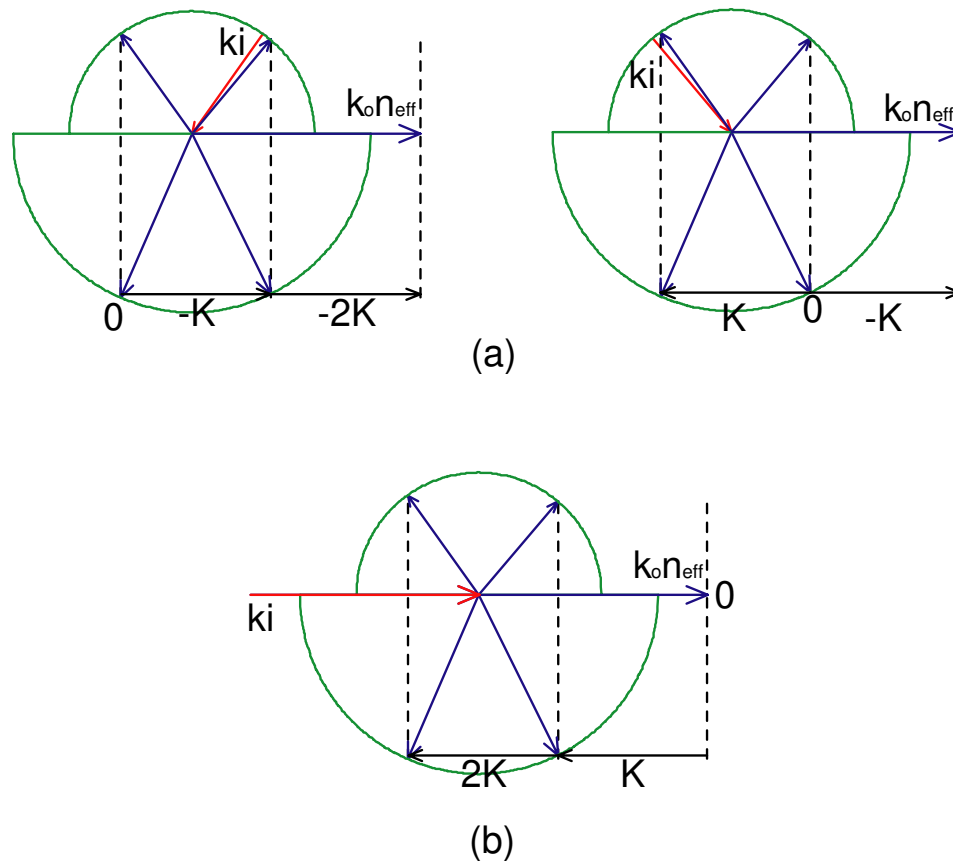
Figure 4.17 Wavevector diagrams for (a) input coupling and (b) output coupling for grating coupler with period of .517 μm.

For this research, we first attempt to build the 0.517 μm period grating coupler, and, if possible, attempt to build the 0.374 μm period grating coupler. If the grating vector or effective index of the guided mode in the waveguide is slightly different than the design values after the coupler is fabricated, we can tune the coupling angle to compensate. Having designed the periods and coupling angles of these two couplers, this concludes this section on wavevector analysis.

4.3 Efficiency Analysis for Grating Coupler

Now that we have a design in terms of the period of the grating coupler and the coupling angle, let's look closer at the grating coupler in terms of its efficiency in

coupling light out of the waveguide. In this mathematical analysis we first address

output coupling. We derive expressions for the intensity profile of the light coupled

out of the waveguide by the grating coupler. We use the results of the output coupling

analysis to derive expressions for the input coupling efficiency. The design variable

of interest in this analysis is the height of the grating. For this analysis we assume

that the grating is binary. Following the mathematical derivations, we outline how

the problem is implemented and solved numerically using rigorous coupled-wave

analysis.

4.3.1 Power Coupled Out of Waveguide

If light traveling in a single mode waveguide encounters a diffraction grating,

the waveguide becomes lossy, and light in the waveguide is be coupled out. This

type of waveguide is known as a leaky waveguide. A leaky waveguide is

characterized by a decay factor α_r. By definition for a leaky waveguide, the change in

electric field in the direction of propagation is

$$\frac{dE(x)}{dx} = -\alpha_r E(x) .$$
(4.9)

This equation is a linear first order ordinary differential equation that is easily solved

by rearranging the terms and integrating.

$$\int_0^{x_0} \frac{1}{E(x)} \frac{dE(x)}{dx} dx = \int_0^{x_0} -\alpha_r dx$$
(4.10)

$$\ln(E(x))\Big|_0^{x_0} = -\int_0^{x_0} \alpha_r dx$$
(4.11)

$$\ln(E(x_0)) - \ln(E(0)) = -\int_0^{x_0} \alpha_r dx \qquad (4.12)$$

$$E(x_0) = E_0 \exp\left[-\int_0^{x_0} \alpha_r dx \right] \qquad (4.13)$$

Equation (4.13) is an expression for the total electric field remaining in the waveguide at the point x_0. In terms of power, the power flowing in the waveguide is

$$P(x) \propto \iint |E(x)|^2 \, dy\, dz . \qquad (4.14)$$

Therefore, the power remaining in the waveguide at $x = x_0$ is

$$P_{in}(x_0) = P_0 \exp\left[-2\int_0^{x_0} \alpha_r dx \right], \qquad (4.15)$$

and, because power is conserved, the total power coupled out of the waveguide at $x = x_0$ is

$$P_{out}(x_0) = P_0\left(1 - \exp\left[-2\int_0^{x_0} \alpha_r dx \right] \right), \qquad (4.16)$$

where P_0 is the initial power in the waveguide just after encountering the grating. In this analysis, we assume that the guided field profile in the coupler region is the same as the guided field profile in the waveguide before the coupler region. In other words, scattering of the wave due to mode mismatch is neglected. The total outcoupled power is split between diffractive orders in the substrate and cover regions. The efficiency of each order is the ratio of the power coupled into that order to the total power coupled out of the waveguide. Therefore, the efficiencies of the diffracted orders in the cover region are

$$R_q = \frac{P_q^c}{P_{out}}, \qquad (4.17)$$

and the efficiencies of the diffracted orders in the substrate region are

$$T_q = \frac{P_q^s}{P_{out}},$$ (4.18)

where q is the diffracted order, and the superscripts c and s correspond to cover region and substrate region respectively. The coupling of light out of the waveguide is illustrated in Figure 4.18.
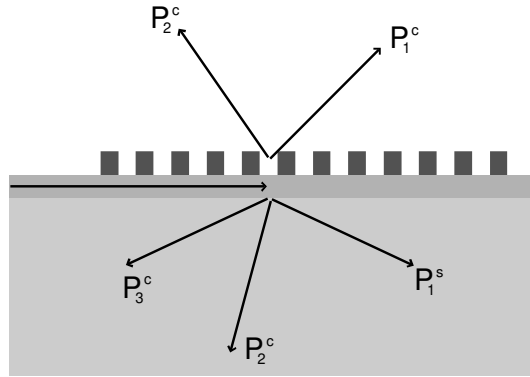
Figure 4.18 Illustration of power coupled out of waveguide into various diffractive orders

Usually, the diffractive order that we want to have the highest efficiency is the first order in the cover region. If the diffraction grating is of length L, then the total power coupled out of the grating in the desired diffractive order is

$$P_1^c = R_1 P_0 \left(1 - \exp\left[-2\int_0^L \alpha_r dx \right] \right).$$ (4.19)

From equation (4.19), we see that the performance of a grating coupler in placing light into the desired diffractive order is determined by the parameters R_1, L, and α_r. The parameters R_1 and α_r depend on the physical characteristics of the grating and the waveguide. For our binary analysis, these parameters depend on the height of the grating and the height of the waveguide.

4.3.2   Intensity Profile of Light Coupled Out of Waveguide

Now we examine the intensity of the outcoupled light. In order to find the intensity we need to find the ratio of power to distance. In order to derive the intensity, we first find the power at a point $x = x_0$, which we call P_1, and then at a point $x = x_0 + \Delta x$, which we call P_2, as shown in Figure 4.19.
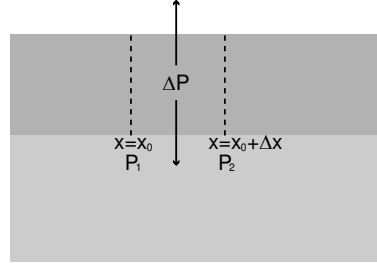
Figure 4.19 Power coupled out of small section of waveguide

The power in coupled out of the waveguide at point $x = x_0$, P_1, can be expressed

$$P_1 = P_0\left(1 - \exp\left[-2\int_0^{x_0} \alpha_r dx\right]\right),$$ (4.20)

and the power coupled out at the point $x = x_0 + \Delta x$, P_2, can be expressed

$$P_2 = P_0\left(1 - \exp\left[-2\int_0^{x_0+\Delta x} \alpha_r dx\right]\right).$$ (4.21)

The difference between P_1 and P_2 is

$$\Delta P = P_1 - P_2 = P_0\left(\exp\left[-2\int_0^{x_0} \alpha_r dx\right] - \exp\left[-2\int_0^{x_0+\Delta x} \alpha_r dx\right]\right).$$ (4.22)

The power in ΔP is split between diffracted orders, therefore

$$\Delta P_q^c = R_q P_0\left(\exp\left[-2\int_0^{x_0} \alpha_r dx\right] - \exp\left[-2\int_0^{x_0+\Delta x} \alpha_r dx\right]\right),$$ (4.23)

68

$$\Delta P_q^c = R_q P_0 \left(\exp\left[-2\int_0^{x_0} \alpha_r dx \right] - \exp\left[-2\int_0^{x_0} \alpha_r dx - 2\int_{x_0}^{x_0 + \Delta x} \alpha_r dx \right] \right), \qquad (4.24)$$

$$\Delta P_q^c = R_q P_0 \exp\left[-2\int_0^{x_0} \alpha_r dx \right] \left(1 - \exp\left[-2\int_{x_0}^{x_0 + \Delta x} \alpha_r dx \right] \right). \qquad (4.25)$$

To find the intensity of the light exiting the coupler at the point $x = x_0$, we allow Δx to decrease, and take the ratio of ΔP to Δx.

$$I(x_0) = \lim_{\Delta x \to 0} \frac{\Delta P_q^c}{\Delta x} = R_q P_0 \exp\left[-2\int_0^{x_0} \alpha_r dx \right] \lim_{\Delta x \to 0} \frac{1 - \exp\left[-2\int_{x_0}^{x_0 + \Delta x} \alpha_r dx \right]}{\Delta x} = \frac{0}{0} \quad (4.26)$$

In order to take this limit, we need to use L'Hôpital's rule and take the limit of the derivatives of the numerator and denominator.

$$I(x_0) = \lim_{\Delta x \to 0} \frac{\frac{d\Delta P_q^c}{d\Delta x}}{\frac{d\Delta x}{d\Delta x}} = R_q P_0 \exp\left[-2\int_0^{x_0} \alpha_r dx \right] \lim_{\Delta x \to 0} \frac{d}{d\Delta x} \left(-\exp\left[-2\int_{x_0}^{x_0 + \Delta x} \alpha_r dx \right] \right) \quad (4.27)$$

First, we concentrate on taking the derivative in 4.27. By the chain rule

$$\frac{d}{d\Delta x}\left(-\exp\left[-2\int_{x_0}^{x_0 + \Delta x} \alpha_r dx \right] \right) = -\exp\left[-2\int_{x_0}^{x_0 + \Delta x} \alpha_r dx \right] \frac{d}{d\Delta x}\left(-2\int_{x_0}^{x_0 + \Delta x} \alpha_r dx \right) (4.28)$$

$$= -\exp\left[-2\int_{x_0}^{x_0 + \Delta x} \alpha_r dx \right] \frac{d}{d\Delta x}\left(-2\left[A_r(x_0 + \Delta x) - A_r(x_0) \right] \right), \qquad (4.29)$$

where A_r is the antiderivative of α_r. Using the chain rule once again, the derivative of the term in parentheses can be taken easily and is given by

$$= -\exp\left[-2\int_{x_0}^{x_0 + \Delta x} \alpha_r dx \right] \left(-2\left[\alpha_r(x_0 + \Delta x) \cdot 1 - 0 \right] \right). \qquad (4.30)$$

Using this result in (4.27), we now have

$$I(x_0) = R_q P_0 \exp\left[-2\int_0^{x_0} \alpha_r dx \right] \lim_{\Delta x \to 0} \exp\left[-2\int_{x_0}^{x_0 + \Delta x} \alpha_r dx \right] \left(2\alpha_r(x_0 + \Delta x) \right). \quad (4.31)$$

Taking the limit gives

$$I(x_0) = R_q P_0 (2\alpha_r(x_0)) \exp\left[-2\int_0^{x_0} \alpha_r dx\right].$$ (4.32)

Equation (4.32) is the intensity profile for a beam coupled out of the waveguide by the grating coupler. If the diffraction grating is uniform over its length, α_r is a constant value. In this case (4.32) may be rewritten

$$I(x_0) = R_q P_0 2\alpha_r \exp\left[-2\alpha_r x\right]$$ (4.33)

For this thesis, the gratings couplers that are of interest are built with the attempt that the gratings are uniform over the length of the coupling region. Therefore, equation (4.33) describes the behavior that we attempt to observe in the light that is coupled out of our grating couplers.

4.3.3 Input Coupling Efficiency

Now that we have derived an expression for the intensity profile of the outcoupled beam of a grating coupler, we are now ready to discuss input coupling efficiency. We use the reciprocity theorem to analyze the input coupling. From the reciprocity theorem, the maximum input coupling efficiency would be when the intensity profile of the input beam matches the intensity profile of the output beam, and the maximum input efficiency is the same as the output coupling efficiency of that order. If the intensity profile does not match the output intensity profile, the input efficiency, or the ratio of the incident light to the amount of light that is actually coupled into the waveguide, is determined by an overlap integral of the intensity profiles given by

$$\eta_q^{(i)} = P_q^{(i)} \frac{\left[\int I_{in}^{1/2}(x) I_{out}^{1/2}(x) \, dx\right]^2}{\int I_{in}(x) \, dx \int I_{out}(x) \, dx}, \qquad (4.34)$$

where i is either c or s depending on if the input coupling is coming from the cover or

substrate medium, q is the diffractive order, I_{in} is the intensity profile of the input

beam, and I_{out} is the intensity profile of the outcoupled beam given by (4.33). Input

coupling and output coupling and the quantities in (4.34) are demonstrated in Figure

4.20 below.
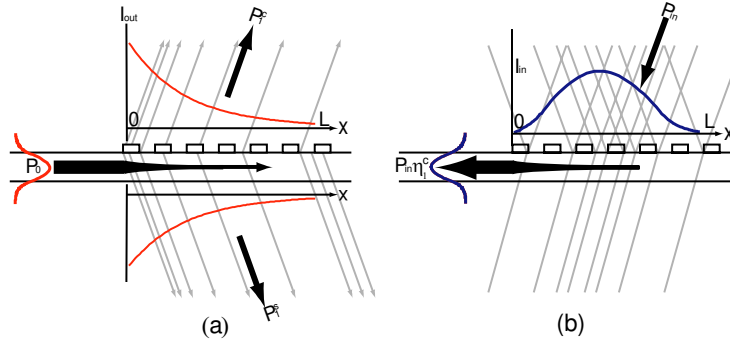
Figure 4.20 Illustration of (a) output coupling and (b) input coupling

From (4.34) we see that the input coupling efficiency is decreased if there is a

mismatch between the input and output beams, or if the output coupling efficiency is

low. Both of these two factors are dependant on the decay parameter α_r. Higher

values of α_r mean higher amounts of output coupling, but can also mean a poor

overlap integral. To illustrate this point, we give an example. A common input

intensity profile is a Gaussian beam from a laser. Suppose the input beam to a grating

coupler is a Gaussian beam with a diameter of 1mm. The intensity profile for this

beam is given by

$$I_{in}(x) = e^{-\left(\frac{x-x_0}{d/2}\right)^2}, \qquad (4.35)$$

where x_0 is an offset parameter, and d is the diameter of the beam. For this beam, given a grating length L, there is an optimal value for α_r and x_0 that maximizes the input coupling efficiency, which from (4.34) and (4.19) is given by

$$\frac{\eta_1^c}{R_1} = (1 - \exp[-2\alpha_r L]) \frac{\left[\int I_{in}^{1/2}(x) I_{out}^{1/2}(x)\, dx\right]^2}{\int I_{in}(x)\, dx \int I_{out}(x)\, dx}. \qquad (4.36)$$

The values that maximize the efficiency can be found by optimization routines. Figure 4.21 shows a contour plot of the right side of (4.36) for a coupler length of 5 mm.
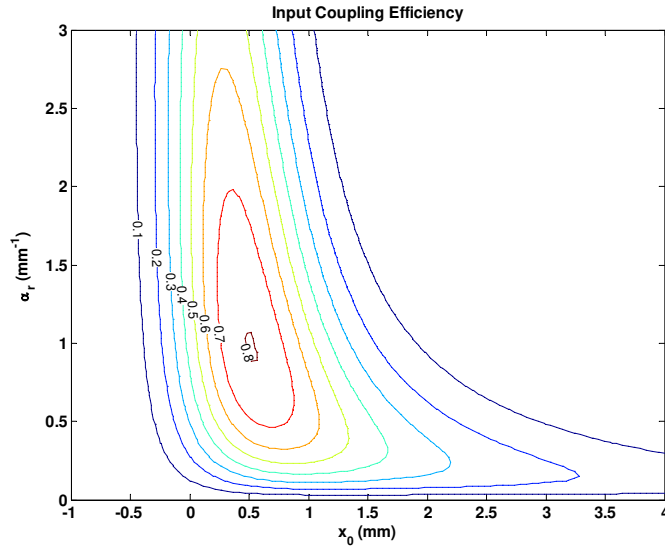
Figure 4.21 Contour plot of the input coupling efficiency of a Gaussian beam

As Figure 4.21 shows, there is a small rage of values of x_0 and α_r that can provide efficiencies of over 80%. However, the true input efficiency into the waveguide would be this value multiplied by the efficiency of the diffracted order, R_1. Figure 4.22 shows the normalized intensity profiles of a Gaussian beam, and the

output intensity profile as a function of position for $x_0 = 0.5152$ mm and $\alpha_r = 0.9697$ cm^{-1}.
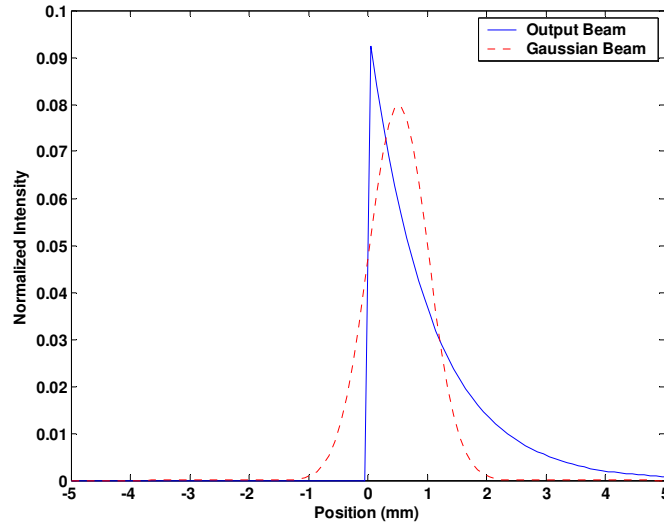
Figure 4.22 Normalized intensity of input and output beams

The example shown in Figure 4.22 has an input efficiency of .803 R_1. Because the total outcoupled power is split into a cover beam and a substrate beam and the value of R_1 could typically be in the range of .5, the maximum total efficiency would be in the range of 40%. This problem of low efficiency can be improved slightly by adjusting the input Gaussian beam radius and lowering the decay factor; however, the underlying problem is in the mismatch between a Gaussian shape and a decaying exponential shape. Better efficiencies can be obtained by designing more complex grating structures that have varying grating heights or fill factors. By varying the decay parameter α_r, a grating can be designed to have an output intensity profile to match any arbitrary input beam profile. Such gratings are difficult to build in practice, and this thesis is only concerned with the design of uniform grating couplers with constant decay parameters. A second and perhaps more significant way

that the efficiency can be increased is by increasing the efficiency of the grating in diffracting power into the desired order. Preferential coupling also requires more complex schemes than those investigated in this thesis. Some ways to improve the preferential coupling efficiency are given in [82-90].

4.4   Numerical Method for Determining Radiation Decay Factor

So far in this analysis, we have not addressed how the radiation decay factor relates to the physical structure of the grating coupler. The purpose of this section is to explain how, given a grating coupler, to calculate the radiation decay factor and the efficiencies of each diffractive order using rigorous coupled wave analysis. Before we begin, it is important to note that the radiation decay factor, α_r, is simply the imaginary part of the propagation constant of the guided mode in the grating coupler region. The real part of the propagation constant is $k_0 n_{eff}$. Therefore, the propagation constant of the mode in the waveguide is

$$\gamma = \beta + j\alpha_r. \tag{4.37}$$

If we can calculate the propagation constant, we are able to determine the effective index, and the decay parameter of the leaky mode in the grating coupler. This calculation can be done using rigorous coupled wave analysis.

4.4.1   Solution Method

Let's first examine the system that we are analyzing [91]. Figure 4.23 shows the structure of the problem and the fields in the different regions of the problem.
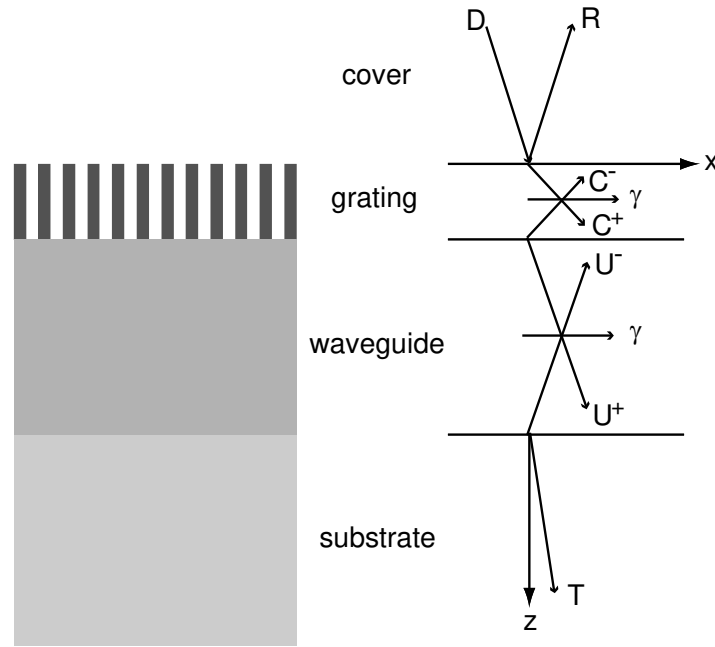
Figure 4.23 Fields in the regions of the grating coupler

Figure 4.23 shows a TE polarized plane wave incident from the cover region

on the grating coupler. This wave excites scattering waves in the cover and substrate,

with amplitudes R and T respectively. Forward and backward propagating waves are

also excited inside the grating and waveguide layers, with amplitudes C^+, C^-, U^+, and

U^- respectively. Phase matching at the boundaries between the different layers

requires each wave to have the same x wavevector component, denoted γ. The z

components of the wavevectors depend on γ via the dispersion relationships for the

materials in each region, i.e. $k_z^p = [k_0^2 n_p^2 - \gamma^2]^{1/2}$, where p is c, g, w, or s depending on

if the region is the cover, grating, waveguide, or substrate respectively. Matching the

tangential components results in a linear system that can be expressed in matrix form

as

$$\begin{bmatrix} \overline{\overline{\mathbf{M}}} \end{bmatrix} \begin{bmatrix} C^+ \\ C^- \\ U^+ \\ U^- \\ R \\ T \end{bmatrix} = \begin{bmatrix} D \\ jk_z^c D \\ 0 \\ 0 \\ 0 \\ 0 \end{bmatrix}, \tag{4.38}$$

where $\overline{\overline{\mathbf{M}}}$ is a matrix describing the coupling between all of the fields in the different

regions. The matrix $\overline{\overline{\mathbf{M}}}$ for this problem is the same as the matrix equation developed

in Chapter 3 by rigorous coupled wave analysis, with the addition of the waveguide

layer. This matrix depends on the shape of the grating and the physical constants of

the materials in the system as well as the tangential component of the wavevectors in

all regions, which in this chapter we have called γ. Equation (4.38) can be written

compactly as

$$\overline{\overline{\mathbf{M}}}\mathbf{Y} = \mathbf{A} \tag{4.39}$$

where $\mathbf{Y}$ is a column vector of the field amplitudes for the fields of the different

regions, and $\mathbf{A}$ is a column vector describing the input to the system. If the system

described by $\overline{\overline{\mathbf{M}}}$ supports a guided mode, then the vector $\mathbf{A}$ is zero and we have

$$\overline{\overline{\mathbf{M}}}\mathbf{Y} = 0.$$

Because $\overline{\overline{\mathbf{M}}}$ and $\mathbf{Y}$ are nonzero, this requires that $\overline{\overline{\mathbf{M}}}$ be a singular matrix, meaning its

determinant is zero. This fact can be used to find the propagation constants of a

waveguide and is known as the transverse resonance method. If $\overline{\overline{\mathbf{M}}}$ is a singular

matrix and a nonzero input $\mathbf{A}$ is applied, then the coefficient values of the vector $\mathbf{Y}$

becomes infinite. Therefore, one way to find the complex propagation constant of the

leaky waveguide would be to search for values of γ that cause the determinant of $\overline{\overline{\mathbf{M}}}$

to go to zero. As discussed in Chapter 3, the matrix $\overline{\overline{\mathbf{M}}}$ can be very large. Storing

such a large matrix, and finding its determinant is not a numerically attractive

implementation. An alternative method is to find the value of γ that causes R in

equation (4.38) to grow to infinity, or alternatively for $1/|R(\gamma)| \to 0$. In this manner,

the optimizations for solving the matrix equation discussed in Chapter 3 can be

implemented. Therefore, our solution strategy is to repeatedly solve the scattering

problem of equation (4.39) using rigorous coupled wave analysis while varying γ,

until a value of γ is found that minimizes $1/|R(\gamma)|$. This problem and its solution

method are also addressed in [82,92-94]. Once we have found the complex value of

γ, the real portion is the propagation constant of the guided mode, β, and the

imaginary portion is the radiation decay parameter, α_r.

The procedure described above for determining γ is a sensitive numerical

problem, and requires a good starting value to succeed. There are a discrete number

of solutions corresponding to the modes guided by the structure. The number of

modes depends on the indices of refraction of the various layers and on the

thicknesses of the grating and waveguide layers. The structure is first analyzed to

find the propagation constant of the waveguide without the diffraction grating. This

propagation constant is used as the starting guess for γ for the grating coupler

structure. Also it is often necessary to start the analysis with a weak grating, i.e. very

small grating height, and gradually adjust to the desired level. The computational

process described above has been implemented in a series of MATLAB scripts that are described in Appendix B.3.

4.5 Optimal Grating Efficiency Design Method

Now that we have a method for determining the radiation decay parameter for a given grating coupler, we are ready to discuss further the design method. We have already designed two grating couplers with periods of .374 µm and .517 µm. What we do not know is what these gratings should look like physically. For this analysis, there are two possibilities as far as the fabrication of these grating couplers goes. The first possibility is that the gratings are fabricated in photoresist and sit on top of the waveguide. The second possibility is that the gratings are actually etched into the nitride waveguide. Both of these possible grating couplers are shown in Figure 4.24.

(a)   (b)
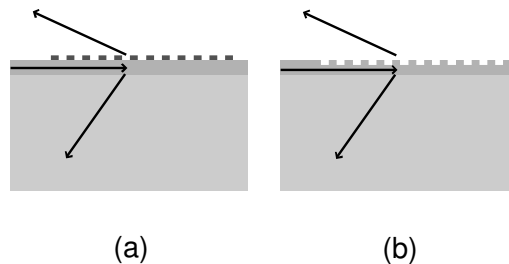
Figure 4.24 (a) Grating coupler fabricated with photoresist gratings; (b) Grating coupler fabricated by etching gratings into the nitride waveguide

As indicated by Figure 4.24, for this analysis, we assume that the grating couplers are made with binary diffraction gratings; therefore, the design variable available to us is the height of the gratings. The first step in this design method is to determine the optimal value for the radiation decay parameter, α_r. The second step is to determine the grating height to give the optimal value of α_r.

4.5.1   Determine Optimal Radiation Decay Parameter

As described above, the optimal value for the radiation decay parameter depends greatly on the intensity profile of the input coupling beam. Figure 4.25 shows the intensity profile of the HeNe laser beam we use to test the grating couplers. This intensity profile was measured by scanning the beam with an optical fiber.
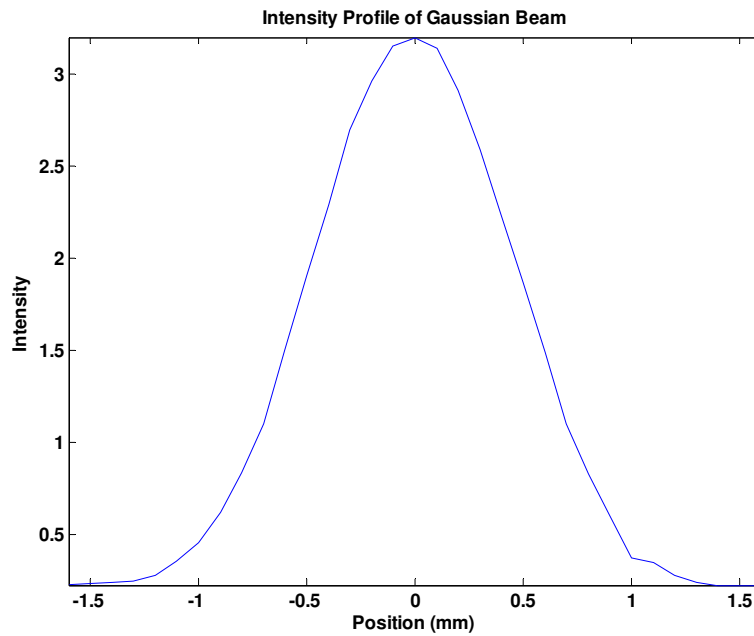
Figure 4.25 Intensity profile of Gaussian Laser beam

Figure 4.25 shows that the source laser Gaussian beam radius of about 0.57 mm. Using the same procedure from above, we can determine the optimal offset amount of the Gaussian beam, and the optimal decay parameter to give the best overlap integral. These quantities are independent of the period of the grating coupler. Therefore, the optimal value of α_r that we find is the same for both of our designs; however the grating heights that achieve the optimal α_r varies between

designs. Figure 4.26 shows the contour for the input coupling efficiency for a 0.57

mm radius Gaussian beam for different offset values and radiation decay parameters.
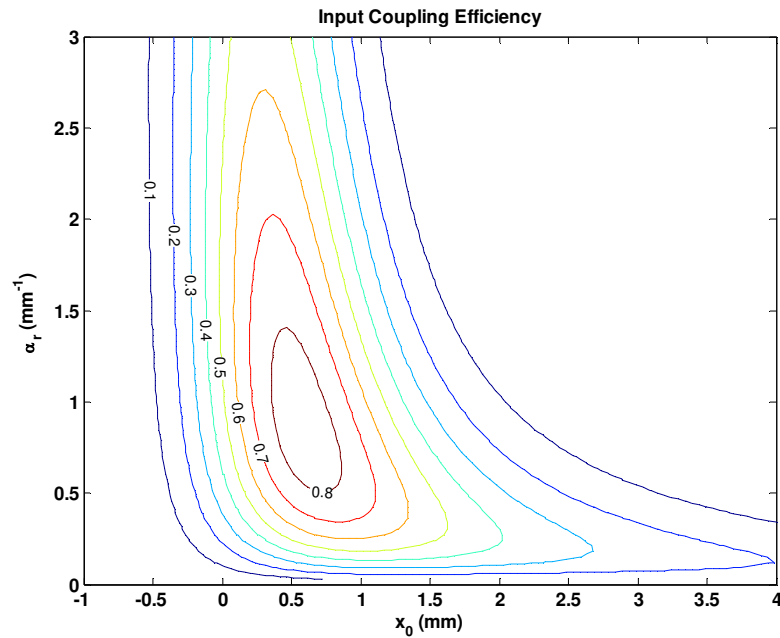
Figure 4.26 Input coupling efficiency for 0.57 radius Gaussian beam and exponential decaying grating coupler

From this analysis, the optimal values for x_0 and α_r are 0.5657 mm and 0.8788

mm^{-1} respectively. With these values the optimal input coupling efficiency is 85.6%

multiplied by the efficiency of the diffractive order which is determined later.

4.5.2   Determine Optimal Grating Characteristics

Now we need to look for the grating characteristics that give us the optimal

decay parameter determined before. After we determine the grating height that gives

the desired value of α_r, we can determine the efficiency of each order coming out of

the grating coupler. We can then determine input coupling efficiency by multiplying

the efficiencies of the orders coupled out of the grating by the value obtained from the

overlap integral. For the first case, we assume that the gratings are binary photoresist gratings on top of the waveguide layer as shown in Figure 4.24(a). The design process follows the rigorous coupled wave analysis method described above. First we present results for the 0.374 μm grating, and then we present results for the 0.517 μm grating.

Figure 4.27 shows the calculations for a 0.374 μm period binary photoresist grating coupler.
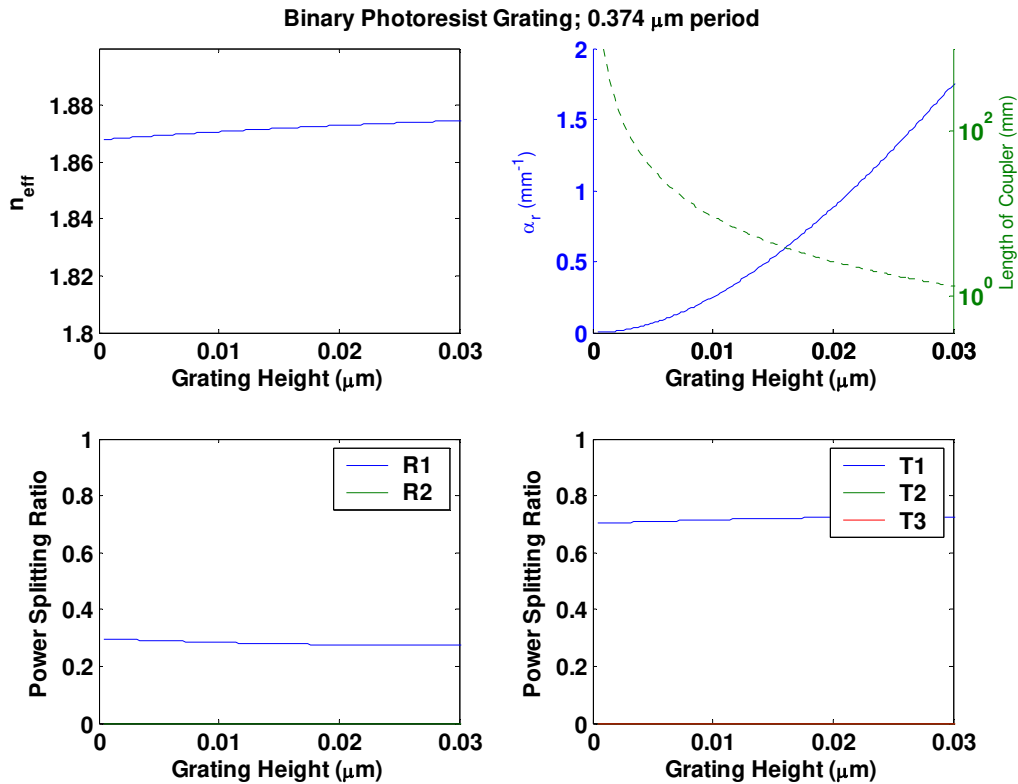
Figure 4.27 Grating coupler characteristics for binary photoresist grating with 0.374 μm period as a function of grating height

From Figure 4.27, the grating height that gives the desired value for the decay parameter is 20 nm. The dotted curve is the length of the coupler to couple out 99.9% of the power, which for this case is about 2.6 mm. Also note from Figure 4.27, that

the effective index in the grating coupler region increases slightly with grating height. With a coupler length greater than 2.6 mm, the efficiency of the output beam in the cover region, R_1, is about 27.62%, while the efficiency of the output beam in the substrate, T_1, is about 72.38%. Therefore if we input couple from the cover, our efficiency into the waveguide is about 23.64%, and if we input couple from the substrate side, our efficiency is about 61.96%.

Figure 4.28 shows the calculations for a 0.517 μm period binary photoresist grating coupler.
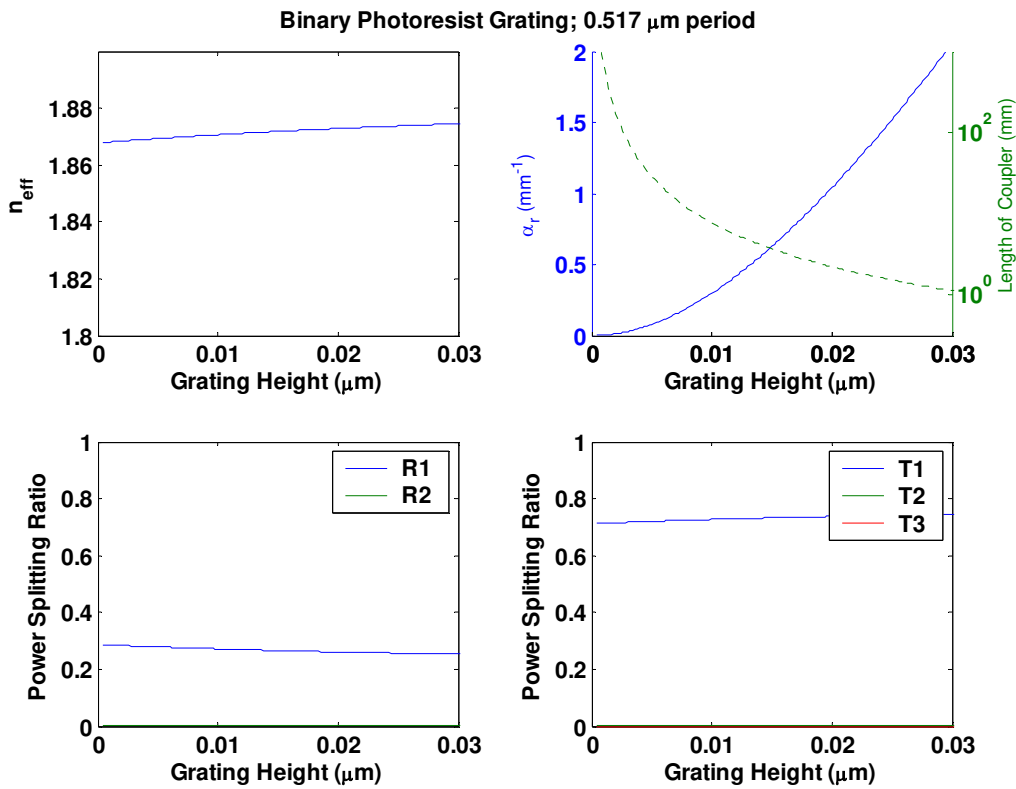
Figure 4.28 Grating coupler characteristics for binary photoresist grating with 0.517 μm period as a function of grating height

The results in Figure 4.28 are close to the results in Figure 4.27. This means that most of these parameters are not very sensitive to the period of the grating

coupler. From Figure 4.28, the grating height that gives the desired value for the

decay parameter is 18.2 nm and the coupler length to couple out 99.9% of the power

is about 2.6 mm. Also note from Figure 4.28, that the effective index in the grating

coupler region increases slightly with grating height. Also note that while there are

two diffracted orders in the cover and substrate regions, the efficiency of the second

order beams is very low. With a coupler length greater than 2.6 mm, the efficiency of

the output beam in the cover region, R_1, is about 27.62%, while the efficiency of the

output beam in the substrate, T_1, is about 73.62%. Therefore if we input couple from

the cover, our efficiency is about 22.5%, and if we input couple from the substrate

side, our efficiency is about 63.02%.

We now analyze the structure for the second possibility for the grating coupler

fabrication where the gratings are etched into the nitride waveguide as shown in

Figure 4.24(b). First we present results for the 0.374 μm period grating, and then for

the 0.517 μm period grating.

Figure 4.29 shows the calculations for a 0.374 μm period grating etched into

the SiN waveguide.
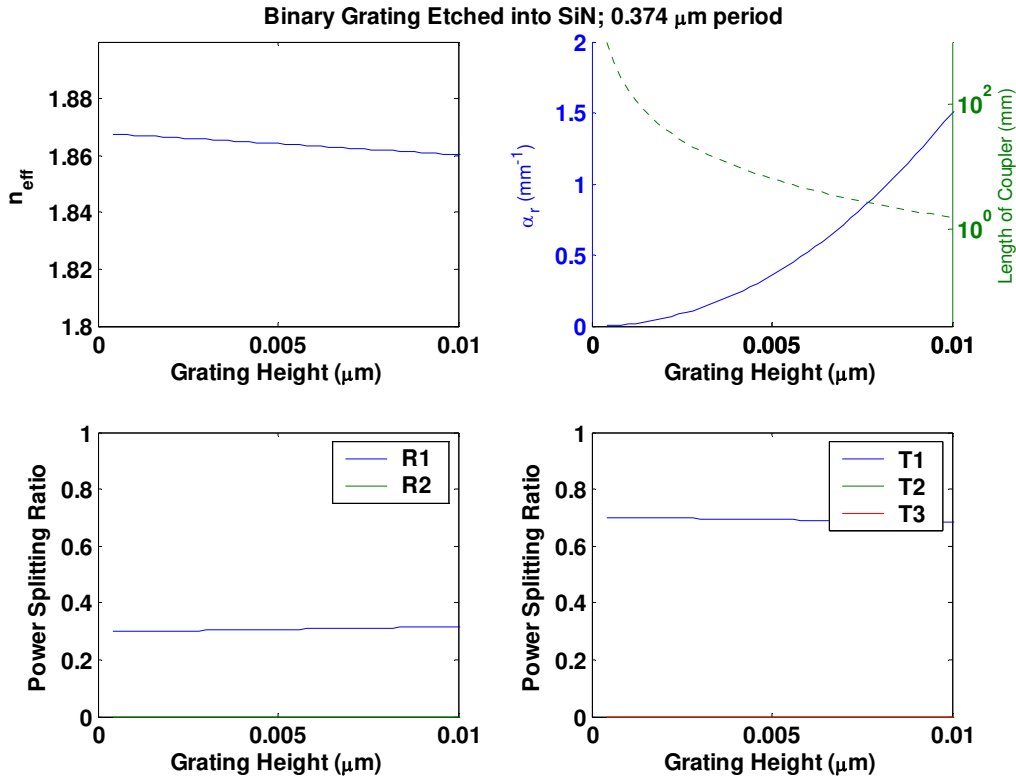
Figure 4.29 Grating coupler characteristics for binary etched grating with 0.374 μm period as a function of grating height

From Figure 4.29, note that the decay parameters increase more rapidly with grating height than the previous two cases. This is to be expected because the gratings are being etched into the waveguide, and should cause higher loss because not only is the grating height increasing, but the waveguide height is decreasing. From Figure 4.29, the grating height that gives the desired value for the decay parameter is 7 nm, and the coupler length to couple out 99.9% of the power is about 2.6 mm. Also note from Figure 4.29, that the effective index in the grating coupler region decreases slightly with grating height. With a coupler longer than 2.6 mm, the efficiency of the output beam in the cover region, R_1, is about 30.02%, while the efficiency of the output beam in the substrate, T_1, is about 69.91%. Therefore if we

input couple from the cover, our efficiency is about 25.69%, and if we input couple from the substrate side, our efficiency is about 59.85%.

Figure 4.30 shows the calculation for a 0.517 µm period grating etched into the SiN waveguide.
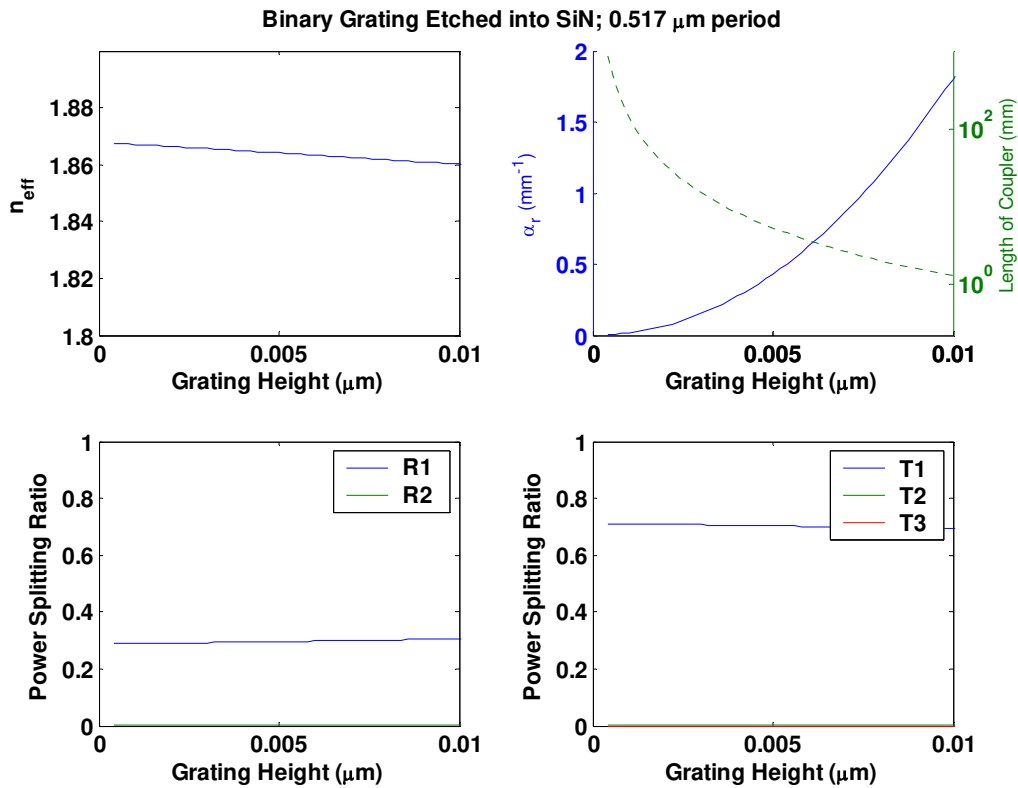
Figure 4.30 Grating coupler characteristics for binary etched grating with 0.517 µm period as a function of grating height

From Figure 4.30, we see that as with the 0.374 µm grating, the loss parameters increase very rapidly with grating height, and that the effective index of the guided mode decreases slightly as the grating height increases. While for this grating coupler, there is more than one diffracted order, the efficiencies of the second order beams are very small. From Figure 4.30, the grating height that gives the desired value for the decay parameter is 7.8 nm, and the coupler length required to

couple out 99.9% of the power is 2.6 mm. For a coupler length greater than 3 mm, the efficiency of the output beam in the cover region, R_1, is about 31.22%, while the efficiency of the output beam in the substrate, T_1, is about 68.78%. Therefore if we input couple from the cover, our efficiency is about 26.73%, and if we input couple from the substrate side, our efficiency is about 58.87%.

4.5.3   Validation of Numerical Results

All of the above calculations were done retaining 21 diffractive orders in the analysis. To validate this choice, I calculated the decay parameter for a binary photoresist grating with a grating period of 0.517 μm and a grating height of 18.2 nm. Figure 4.31 below shows α_r as a function of number of orders retained in the analysis.
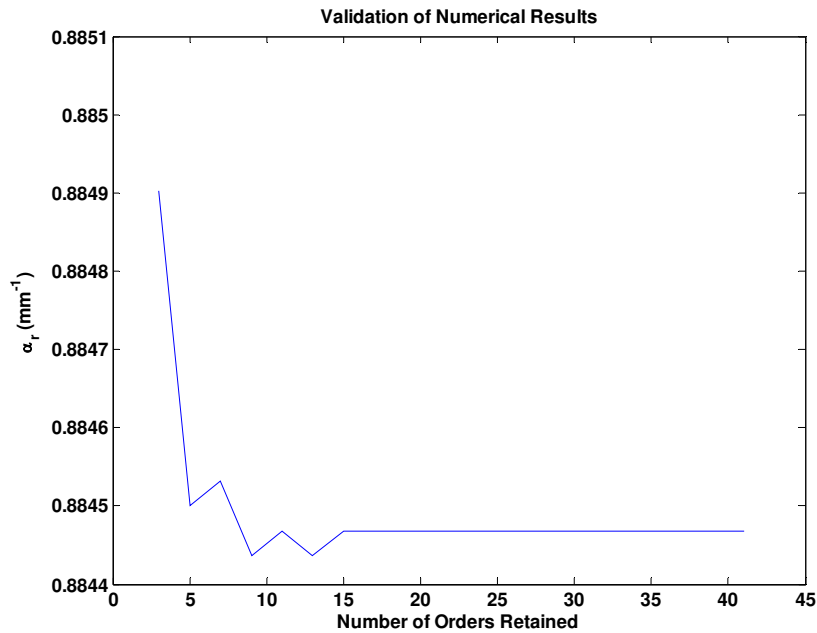
Figure 4.31 Computation of the radiation decay factor as a function of diffractive orders retained in the analysis

From Figure 4.31, we see that after only 15 orders are retained, that the calculated value settles down. With 21 orders, we can be confident that our calculations are accurate.

4.6 Summary of Grating Coupler Designs

The results of these designs are given in Table 4.1 below.

Table 4.1 Design for grating couplers where Λ is the grating period, t_g is the thickness of the grating, t_w is the thickness of the waveguide, η_c^i is the input coupling efficiency from the cover, η_s^i is the input coupling efficiency from the substrate, n_g is the refractive index of the grating, n_w is the refractive index of the waveguide, and θ_c is the coupling angle.

Λ	t_g	t_w	η_c^i	η_s^i	n_g	n_w	θ_c
Binary Photoresist Gratings on top of SiN Waveguide							
374 nm	20 nm	200 nm	23.64%	61.96%	1.6	2.1	10°
517 nm	18.2 nm	200 nm	22.50%	63.02%	1.6	2.1	35.57°
Binary Grating Etched into SiN Waveguide							
374 nm	7 nm	193 nm	25.69%	59.85%	2.1	2.1	10°
517 nm	7.8 nm	192.2 nm	26.73%	58.87%	2.1	2.1	35.57°

As a discussion on the results of the design as shown in the table above, we notice that the grating heights are rather small. Achieving the desired heights requires tight control in the fabrication process. The reason that the decay parameter increases rapidly with grating depth is because of the high contrast in refractive indices of the waveguide, the grating, and the cover region. Also, it is interesting to note that there is little difference between the grating couplers designed with a 0.517 μm period and a 0.374 μm period. Although the larger period grating coupler supports more diffractive orders, the efficiencies of the second order beams are small. However, the efficiencies are also low, which could make testing the gratings difficult.

Chapter 5

5   Grating Fabrication Methods

Now that we can analyze and understand the behavior any surface relief grating, the next topic of discussion is how to make a diffraction grating. The subject of this chapter is the fabrication of diffraction gratings. We examine several methods of grating fabrication and discuss their advantages and disadvantages, and the types of gratings that each method is able to produce effectively. While the list of methods discussed in this chapter is not exhaustive, the methods that are treated include photolithography, electron-beam writing, scribing, phase masks, and holography.

5.1   Photolithography

The electronics industry has used photolithography to fabricate integrated electronic circuits for many years. The principles of photolithography all rely on the use of photoresist. Photoresists are polymers whose chemical properties changes based on exposure to light. Photolithography is the process of patterning selective areas of a substrate with photoresist and etching away these areas to build up an electronic circuit. These techniques are well developed, and are the basis of an entire industry. The method of photolithography can also be used to create diffraction

gratings. Figure 5.1 shows the photolithographic process for fabricating a diffraction grating.

1. Coat Substrate with Resist

Resist
Substrate

2. Expose Resest with Light

Mask

3. Develop Resist

Grating

4. Etch Grating into Substrate
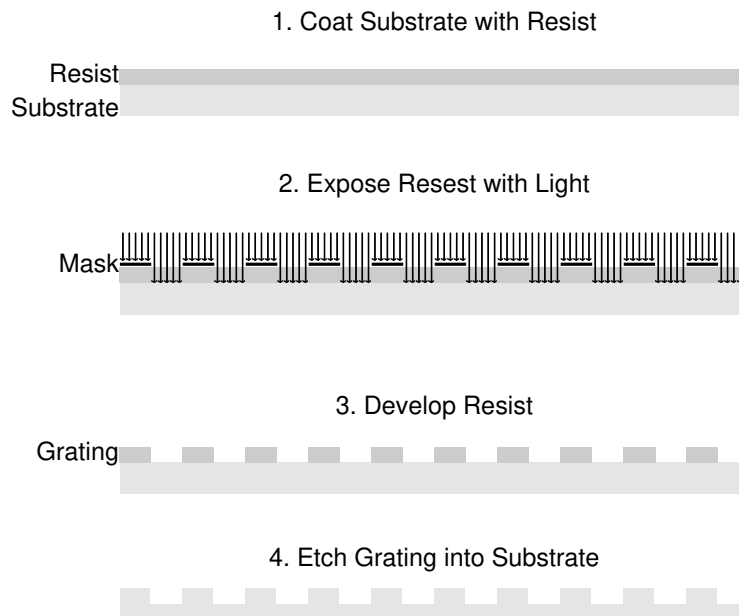
Figure 5.1 Diagram of the photolithographic process for grating fabrication

As Figure 5.1 suggests, this fabrication method works very well for making binary gratings. With multiple expose and develop stages, other types of gratings can also be fabricated, but the difficulty and expense increases. The main advantage of this process is that it uses standard and well developed procedures widely used in industry, and it is well suited for mass-production. The main problem with this process is that the mask used to make the grating is an amplitude diffraction grating, and unlike the lines shown in Figure 5.1, when the light passes through the mask it gets diffracted. This problem of diffraction from the mask as well as resolution limitations, prevent this method from being used to make gratings with very small feature sizes. In the BYU cleanroom, a grating was fabricated using this method that had a period of 1 μm. Figure 5.2 shows an SEM image of this diffraction grating.

90
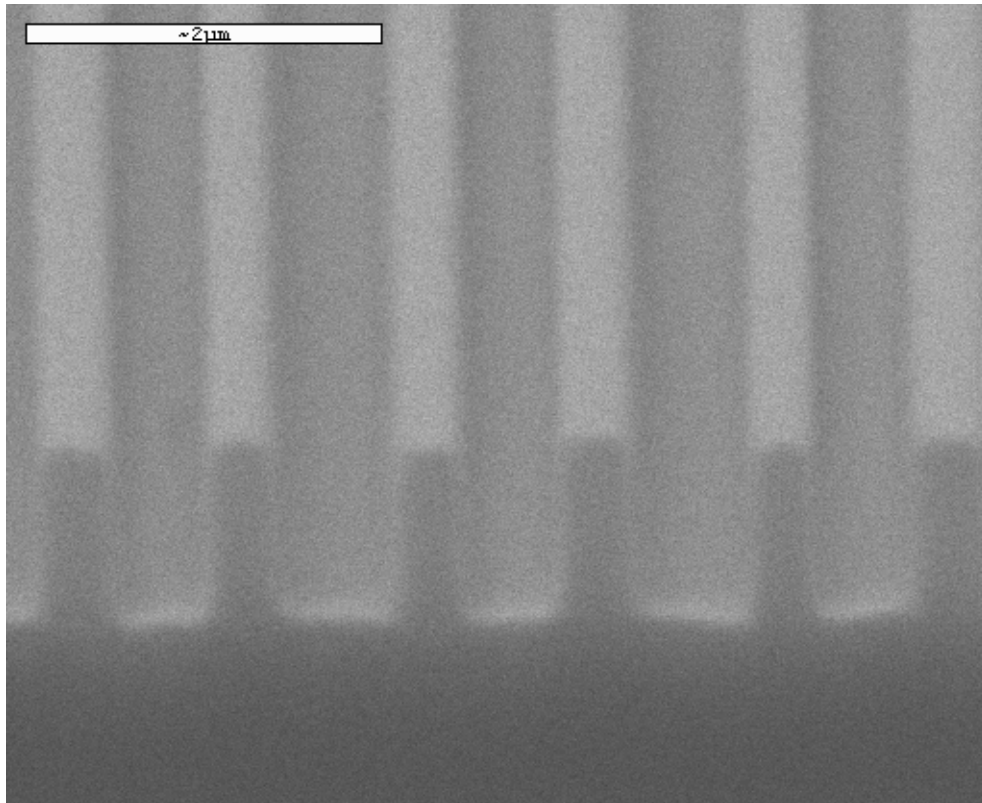
Figure 5.2 Binary grating with 1 μm period

Another reason that photolithography is not good for research is it is not a flexible method. There is a high cost to making a mask, and once that mask is made it can only be used to create one type of grating. For our research, we want a fabrication method that is more flexible, and can obtain smaller feature sizes.

5.2   E-Beam Lithography

A method similar to photolithography, but that can produce very small feature sizes is e-beam lithography [95-99]. Like photolithography, this method involves a photoresist material, but instead of using a mask to block sections of the photoresist from being exposed, an electron beam writes the pattern directly in the photoresist. With this method, extremely small feature sizes can be obtained. Also, variable

dosages in the photoresist are easily obtained as the pattern is written. This method can produce binary gratings, as well as blazed gratings through variable dosage. However, unlike photolithography this method is not suited well for mass production because every sample must be patterned by the e-beam. Therefore, this method is slow and very costly. A method like this does not fit within the budget or time frame of our research.

5.3   Mechanical

Perhaps one of the oldest methods for fabricating gratings is through the mechanical method known as scribing or ruling [100-102]. Ruled gratings are made by a mechanical process where the surface of the substrate is carved away. This method produces wonderful blazed gratings with the blaze angle determined by the shape of the tip of the scribing tool. Once a master grating is made, it can be replicated by stamping, thus this method is suited for mass production. However, it is difficult with this method to make small period gratings due to mechanical limitations. Recent advanced ruling engines have been developed that can produce grating periods as small as .8 μm, but these engines are very costly and are very slow [103, 104]. Like photolithography, this method is not very flexible in terms of cost and time.

5.4   Phase Masks

A further method of grating fabrication is to use phase masks [105-111]. A phase mask is a diffraction grating that is optimized for usually the +1 and -1 transmitted orders. The phase mask is illuminated with light, and the sinusoidal

interference pattern created from the +1 and -1 diffractive orders of the phase mask is

recorded in photoresist. Figure 5.3 shows the operation of a phase mask.
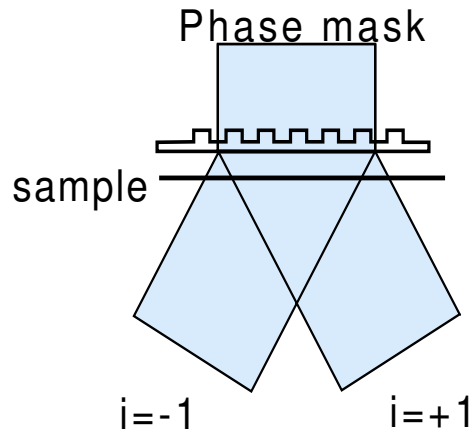
Figure 5.3 Operation of a phase mask

One advantage of phase masks is that they can be used on standard

photolithography equipment, and can be designed to record gratings with small

periods. However, like all of the other methods discussed above, they are not flexible

for research purposes, and having a phase mask made is very expensive.

5.5   Holography

All of the methods discussed above are too slow, too expensive, or not

flexible enough for use in researching diffraction grating applications. For research

purposes we want to adjust the period of the fabricated diffraction gratings. We also

want to have the potential of recording very small periods. We would also like to be

able to make gratings quickly, and we are not concerned at this point with mass

production. The method that provides us with all of these requirements is holography

[112-121].

In the holographic recording of diffraction gratings records the interference of two plane waves traveling at an angle with the z-axis. One wave is at an angle θ with the z-axis, and the other wave is at an angle $-\theta$ with the z-axis, so that the total angle between the object and reference wave is 2θ. Figure 5.4 shows the geometry of this holographic recording. The first wave is given by

$$E_1 = I_o^{1/2} \exp\left(-jk(x\sin(\theta) + z\cos(\theta))\right), \tag{5.1}$$

and the second wave is given by

$$E_2 = I_r^{1/2} \exp\left(jk(x\sin(\theta) - z\cos(\theta))\right). \tag{5.2}$$

The photosensitive material records the intensity of the sum of these two waves. The intensity profile, C, of the sum of (5.1) and (5.2) evaluated at the $z = 0$ plane is

$$C \propto I_o + I_r + E_r^* E_o + E_r E_o^*,$$

$$= I_o + I_r + (I_o I_r)^{1/2} \exp(2jkx\sin\theta) + (I_o I_r)^{1/2} \exp(-2jkx\sin\theta),$$

$$= I_o + I_r + 2(I_o I_r)^{1/2} \cos(2kx\sin\theta). \tag{5.3}$$

It is clear that the recorded holographic code has sinusoidal variation in x. By setting the argument of the cosine term equal to 2π and using $k = 2\pi/\lambda$, the period of this sinusoidal intensity variation can be expressed as

$$\Lambda = \frac{\lambda}{2\sin\theta}. \tag{5.4}$$

When the intensity profile described above is recorded in a photosensitive material, the resulting hologram is a sinusoidal diffraction grating with period Λ. Figure 5.4 below illustrates the holographic recording method for this diffraction grating.

94
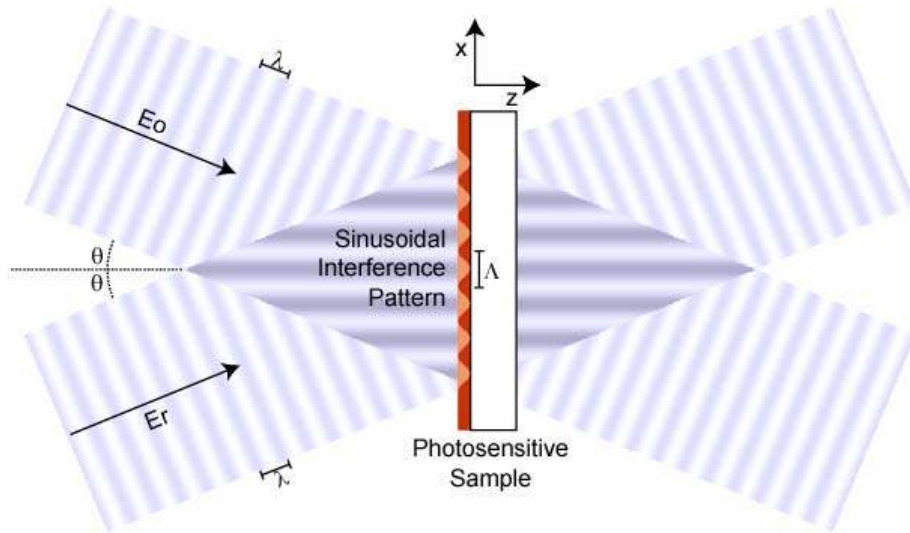
Figure 5.4 Holographic recording of sinusoidal diffraction grating

The ability to record diffraction gratings having any arbitrary period is crucial to this research. The holographic recording method, described above, allows us to record diffraction gratings of a given period simply by adjusting the angle between the two interfering waves.

Chapter 6

6   Grating Coupler Fabrication

This chapter deals with the fabrication of the diffractive grating coupler. The formation of the waveguide is discussed, along with the process of actually recording the sinusoidal interference patterns generated by the holographic recording assembly into photosensitive materials. This chapter first gives an overview of the fabrication scheme. The method of fabricating the waveguide is then given and then the grating fabrication processes are discussed. The holographic recording assembly is also described. As part of the diffraction grating fabrication optimization, an experiment is presented to characterize the recording process with the accompanying experimental results. Then a discussion is provided on the results and the merits of our fabrication scheme.

6.1   Grating Coupler Fabrication Process

6.1.1   Waveguide Formation

Our waveguides are formed by using a Plasma Enhanced Chemical Vapor Deposition (PECVD). The silicon nitride film is deposited with Ammonia and Silane based plasma. The recipe that we use grows the nitride layer at a rate of

approximately 70 Å/min. Our desired waveguide thickness is 200 nm. When the

nitride layer is being deposited, we place a piece of silicon wafer in the chamber with

our glass substrates. The purpose of the silicon wafer is to measure approximate

values for the thickness of the nitride film and the index of refraction by ellipsometry.

For our waveguides the measured thickness is about 200 nm and the measured index

of refraction is about 2.1.

6.1.2   Photoresist Application

    After the waveguide has been formed, we apply the photoresist that will be

used to record our diffraction gratings. The photoresist that we use is AZ® 3312

Photoresist manufactured by Clariant. This photoresist is spin coated on our sample

surface. Figure 6.1 shows the spin speed curve for this photoresist supplied by the

manufacturer.
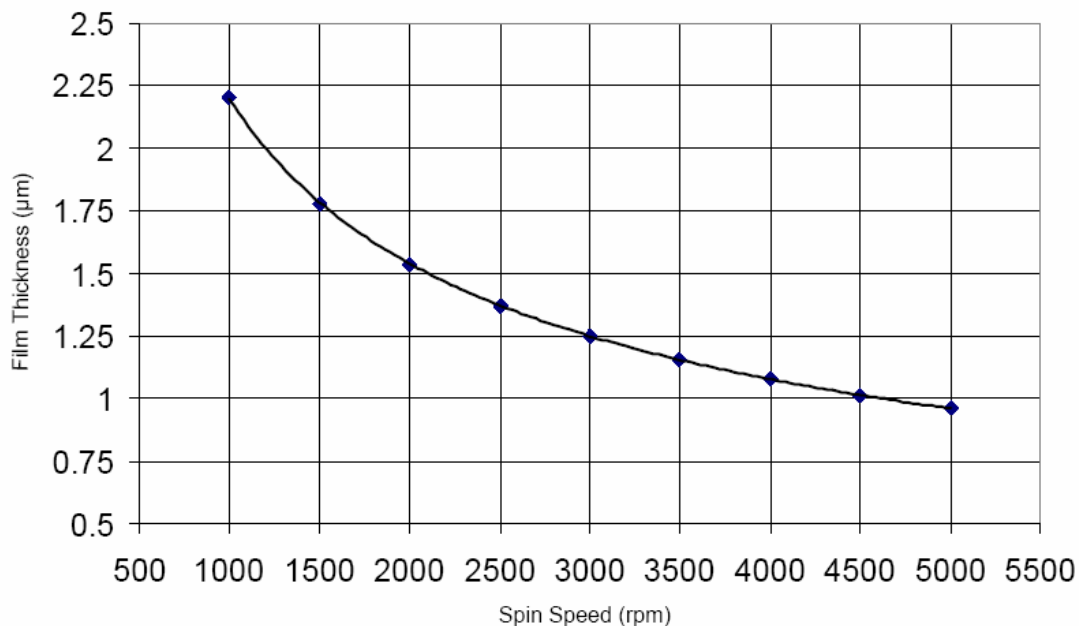
Figure 6.1 Spin speed curve for AZ® 3312 photoresist

We spin coat the photoresist at a spin speed of 5000 rpm, which, as Figure 6.1 shows, corresponds to a photoresist thickness of a little under 1 μm.

6.1.3 Grating Formation

After the photoresist is applied, it is then exposed using our holographic recording assembly. The exposure records a large circular shaped diffraction grating in the middle of the sample. The next step is to form the input grating and the output grating. This is done by masking off two strips close to the center of the circular shaped grating and exposing the rest with a flood UV exposure. After the second exposure, the samples are developed. Once the samples are developed, there are two strips of diffraction gratings sitting on top of the nitride waveguide, and the sample is ready for testing.

6.2 Holographic Recording Assembly

6.2.1 Requirements of Assembly

In Chapter 5, the theory behind holographic recording of diffraction gratings was explained. The conclusion was that by interfering two identical plane waves at a certain angle, the resulting sinusoidal interference pattern could be recorded as a diffraction grating. Therefore, the most important requirement for our recording assembly is the delivery of two collimated beams of equal intensity. The second requirement for the recording assembly is that the angle between the two beams must be adjustable to provide control of the period that we record. We also need to have control of the exposure time because the gratings are recorded in photoresist. Also, in order to record small periods, we would like the wavelength of the exposing light to

be small. Because we are recording such small features, we must isolate the recording assembly from mechanical vibrations as much as possible. Additionally, we would like to have large area gratings; therefore, other requirements are that the interfering beams be large and have a uniform intensity cross-section.

The uniformity of the intensity profile of our recording beams is affected by two factors. The first factor is the source laser, which has a Gaussian beam profile and the second factor is diffraction either from clipping the beam, or from dust particles. The result of the Gaussian intensity profile of the incident beam is a reduction of usable grating area as Figure 6.2 depicts. From Figure 6.2 we can observe the results of recording a grating with a non-uniform intensity profile. The grating area is the dark black crescent. In the central white area, all of the photoresist was exposed because the beam had higher intensity in this center region.
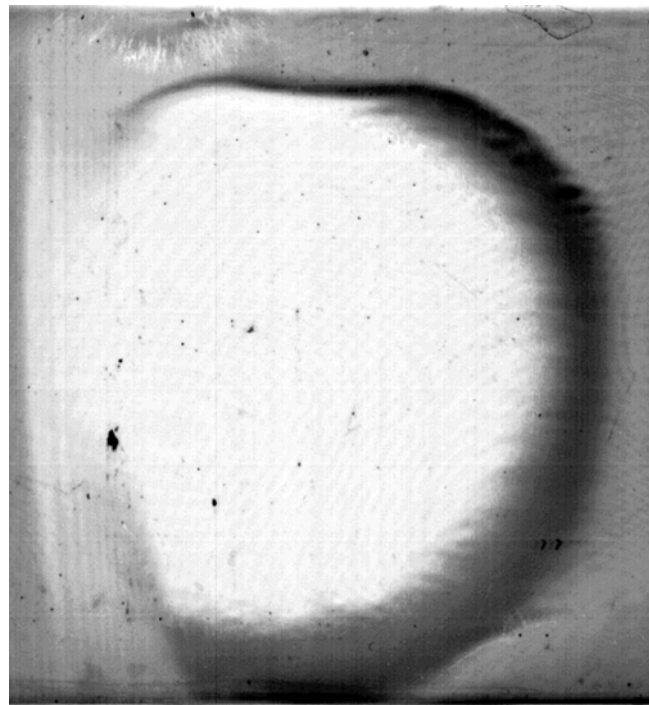
Figure 6.2 Example grating displaying problem of nonuniform intensity profile of recording beam

We can solve this problem of the nonuniform Gaussian intensity profile by expanding the beam out and collimating only the center section of the beam. This uniformity is obtained at the expense of power. Instead of using the full Gaussian beam profile, we use the middle section where the intensity profile is flatter, throwing out the excess power on the sides.

The second factor in grating uniformity is diffraction rings that result from clipping the beam, or from dust particles. If there are apertures that clip the beam after it is collimated, than Fresnel rings will show up in the recording beams. These Fresnel rings are recorded along with the sinusoidal interference pattern. Their effect is an extreme reduction in the usable grating area. Figure 6.3 shows a grating that was recorded with clipped beams. In Figure 6.3, the ring patterns are easily seen, even in the center of the grating.
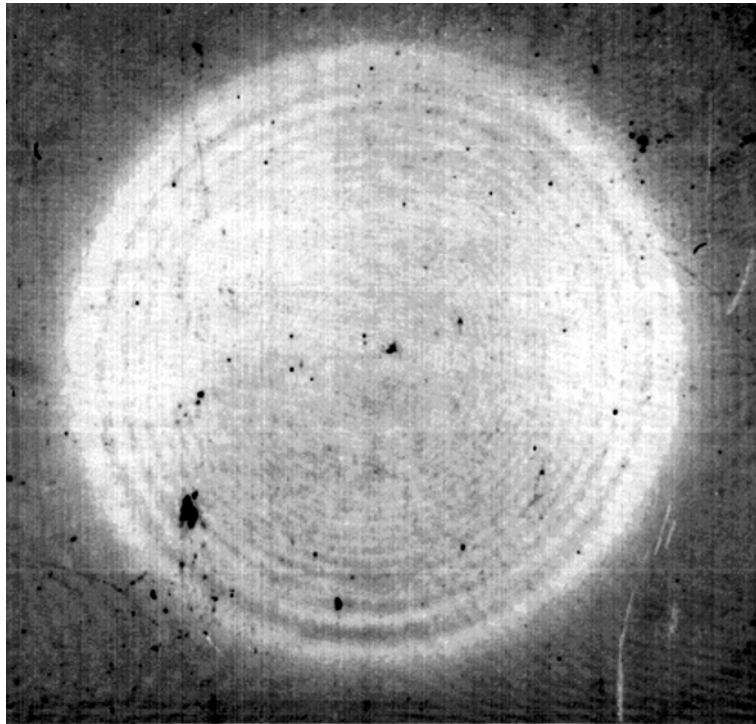
Figure 6.3 Example grating displaying problem of diffraction rings

Dust particles in the recording assembly will also produce diffraction patterns that will be recorded in the grating. Spatial filtering, which is discussed in greater detail in the next section, will smooth out the intensity profile of the beam and remove the effects of diffraction from dust particles. In addition to spatial filtering, we must make sure that beams are not clipped by apertures in our recording assembly after collimating the beams, and that components are kept as clean as possible.

6.2.2   Description of Parts of Recording Assembly

Having defined the requirements of this recording assembly, I now discuss some of the pieces that are used to fulfill these requirements. For a detailed list of the specifications of each part, see Appendix C.

The laser source is a Coherent® INNOVA 306C Argon Laser. This laser has lines in the ultra-violet range, and we use the line at 363.8 nm. Additionally, this laser has a long coherence length which is important when we split the laser beam into two beams and then interfere them. The coherence length of the laser is the maximum path length difference between the two beams, such that when they are combined, they produce an interference pattern.

To control the amount of exposure time, we use an electronic controlled shutter system. The shutter system that we are using can be set for exposure times from 10 milliseconds up to 990 seconds.

The laser splitting is accomplished using a polarizing beamsplitter cube. The beamsplitter cube passes through the *p* polarization and reflects the *s* polarization. In order to adjust the power of both beams, we use a half wave plate to control the amounts of power into each polarization state. Finally, because both beams need to

102

have the same polarization, a second fixed half wave plate is added to the *p*

polarization branch after the beamsplitter cube to rotate it back to *s* polarization. This

arrangement allows for precise adjustment of the power split into the two beams.

Another important piece of the assembly is the spatial filter. Spatial filtering

removes spatial nonuniformities in the intensity profile of the laser beam, as well as

diffraction from dust particles. Spatial filtering is accomplished by focusing the beam

through a small pinhole. At the focus of the beam, the pinhole acts as a spatial low-

pass filter, and the result is a smoothed, approximately spherical beam. Spatial

filtering increases the quality and uniformity of the gratings we record.

The other pieces in the assembly are the necessary mirrors to move the beams

around, and necessary collimating optics to collimate the beam after it has been

through the spatial filter. To control the angle between the two beams, we use two

large mirrors on precision gimbal mounts. These mirrors are the last component that

the beams encounter before they converge on the sample.

To isolate the recording process from mechanical vibrations, the recording

assembly is mounted on a heavy floating tabletop. Vibrations in our recording

assembly will prevent us from recording the interference pattern in photoresist.

Because the grating periods that we are recording are on a micron scale, even tiny

fluctuations will move the interference pattern with respect to the photoresist, and

wash out the grating.

6.2.3   Holographic Assembly

Figure 6.4 shows the layout of our holographic recording assembly.
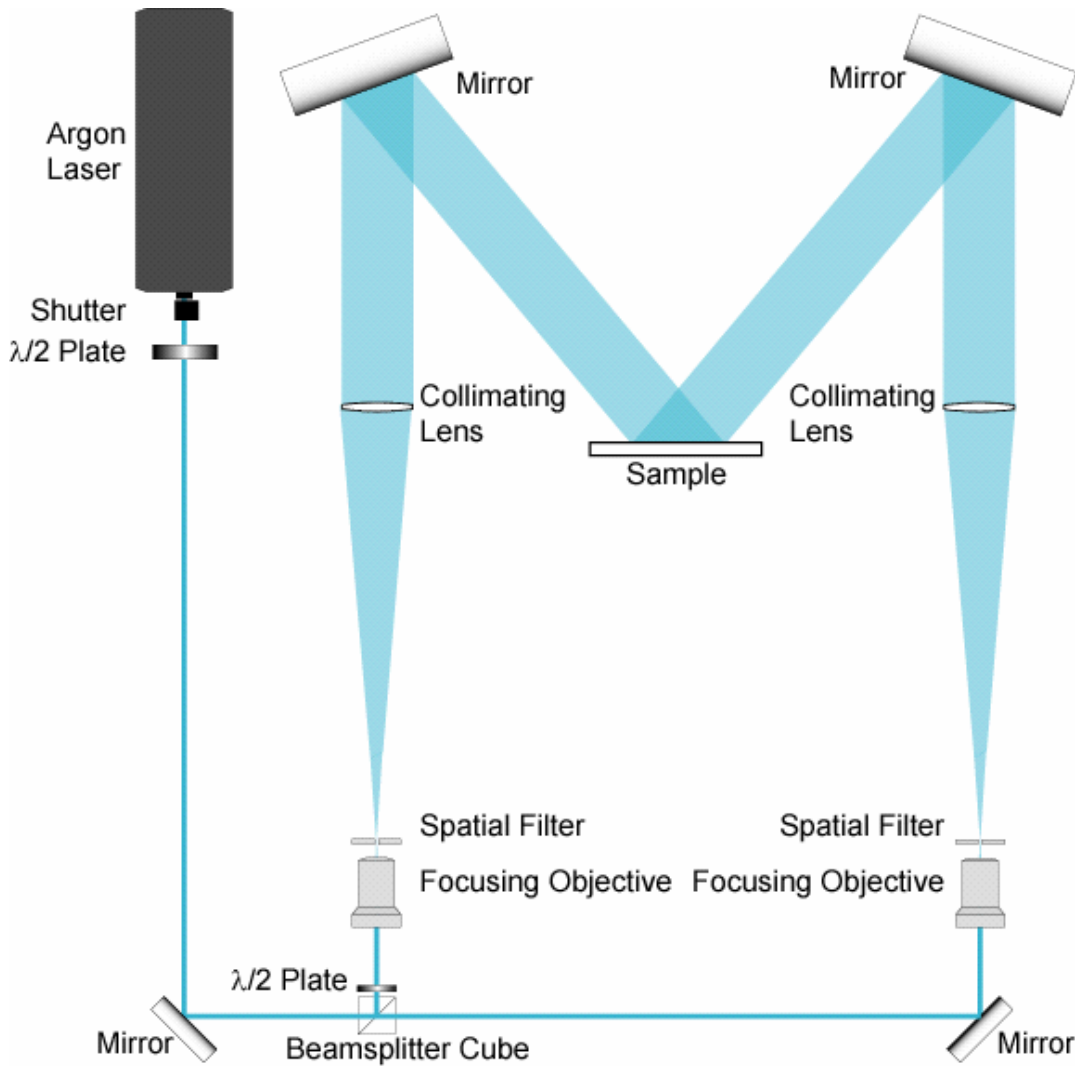
Figure 6.4 Diagram of final recording assembly

From Figure 6.4, we can see that all spatial filtering is done after the beamsplitter cube. Thus, two spatial filters are required. Moving the spatial filter after the beamsplitter cube allows beam degradation due to dust particles on the beamsplitter to be filtered out. Also, when the beam passes through the beamsplitter, it has not yet been expanded and is not clipped by apertures in the beamsplitter cube mount. The only components that could add to the beam degradation are the lenses and the mirrors, which are not very difficult to clean. The collimating lenses have a

long focal length. Therefore, before the beam is collimated it is expanded such that the portion of the Gaussian profile that is collimated is nearly uniform. Because the beams travel along the edges of the table, the sample can move to any point along the center of the table. Thus, a wide range of periods can be recorded with this assembly. Based on the possible angles of the two beams in this assembly, we should be able to record any period from .2 μm to 2.4 μm. Additionally we added two iris diaphragms to each path, to eliminate stray light. One iris is placed before the objective lens to block reflected light, and another is placed after the spatial filter, and adjusted such that light just fills the collimating lens. In this assembly, there is a difference in the two path lengths of about a meter. This difference in path length does not prevent us from recording the diffraction gratings because the coherence length of our laser source is longer than the difference in path length.

Some examples of gratings recorded with this assembly are now given. Figure 6.5 shows a Scanning Electron Microscope (SEM) image of a 1 μm grating that was recorded with our assembly.
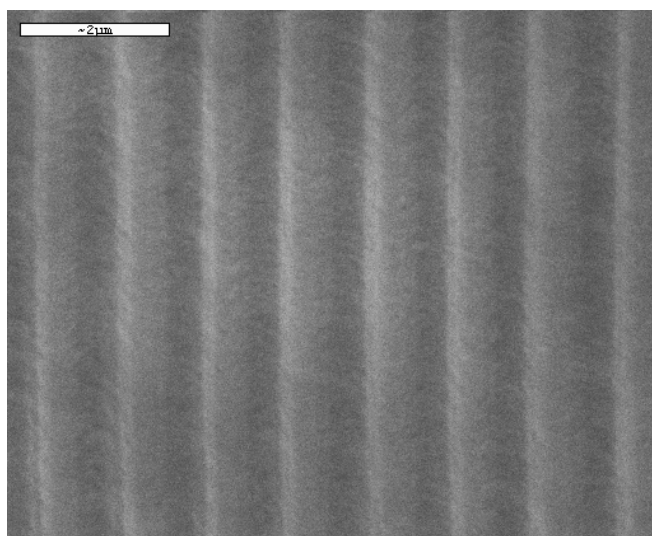
Figure 6.5 SEM image of 1 μm period grating

Also with this assembly, we have been able to record gratings with periods as small as .517 μm. Figure 6.6 shows an SEM image of a .517 μm grating recorded with this assembly.
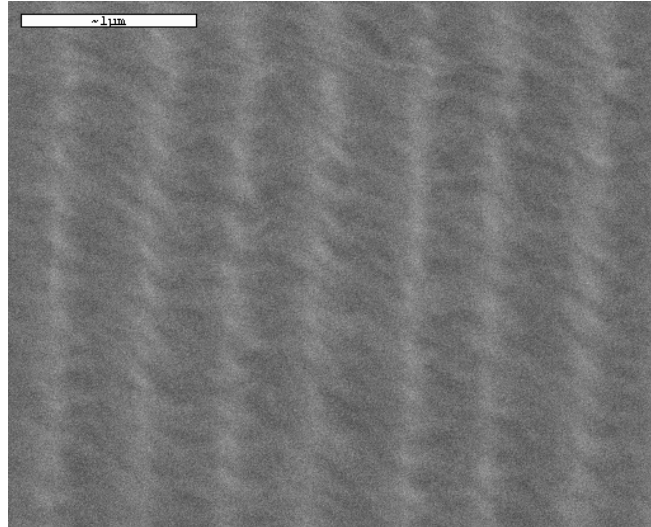
Figure 6.6 SEM image of .517 μm grating

6.2.4   Further Possible Improvements

There are further improvements that could be made to this assembly in terms of power efficiency. As discussed earlier, our method for obtaining uniform intensity is essentially to throw away power by expanding out the Gaussian profile beam, and collimating only the center, more uniform intensity section. A better way would be to use aspheric lenses to focus the Gaussian profile to a flat profile. In this way, we could get uniform intensity without a loss of power. Another option would be to use a hologram to transform the intensity profile [22-26]. Both of these methods are costly, and it may be that we can accomplish our goals in this research without them.

106

This recording assembly should be able to fulfill all of our requirements, and allow us to fabricate diffraction gratings for use in grating couplers, as well as many other potential applications.

6.3   Experiment to Determine Dosage for Recording Gratings in Photoresist

This section presents some experimentation that was done to find the dosage that produces the diffraction grating with the maximum possible amplitude. Figure 6.7 shows the swing curve for this photoresist provided by the manufacturer for the recording wavelength of 365 nm. The swing curve relates the required dosage to the thickness of the photoresist film.
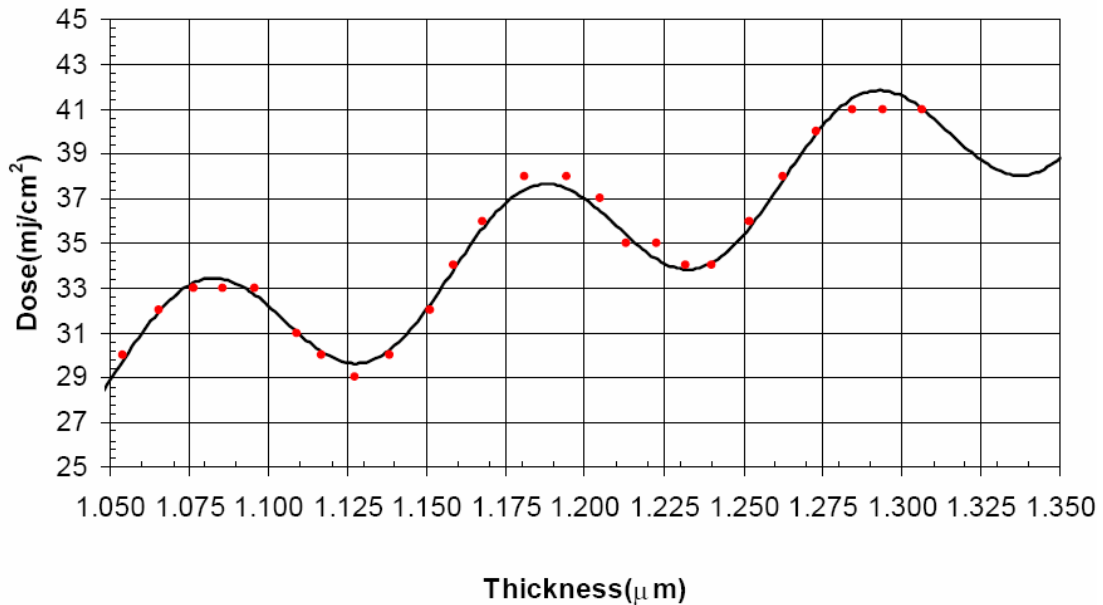
Figure 6.7 I-line swing curve for AZ® 3312 photoresist

From Figure 6.7, we see that the required dosage for a 1 μm film thickness is about 29 mJ/cm^2. The actual dosage that we need varies from the number given by Figure 6.7 because instead of recording using uniform intensity light, our light has sinusoidal intensity variation, but for our experimentation, we use the dosage of 29

mJ/cm^2 as the starting point. The method of this experiment is to record gratings of varying dosages and find the dosage that gives the best results.

6.3.1 Experimental Metric

In order to determine which grating is the best, we need to first select an appropriate experimental metric that we can measure for each case. The metric must correlate to the desired grating feature, namely the amplitude of the grating. Once a grating is fabricated, an easy quantity to measure is the efficiency of the diffractive orders. If the efficiency of the diffractive orders correlates to grating amplitude, meaning that there is a one to one relationship, then the efficiency can be used as the experimental metric. To test this requirement, we use rigorous coupled wave analysis and calculate the efficiency of the diffraction grating based on the amplitude of the grating. Because our photoresist thickness is 1 μm, the maximum possible grating amplitude that we are able to achieve in photoresist gratings is 1 μm. Here, we need to assume something about the shape of our grating. While the interference pattern that we are recording has sinusoidal variation, what is actually recorded in the photoresist may not be sinusoidal due to nonlinearities in the photoresist. Because of this uncertainty, we analyze three structures: binary, sinusoidal, and triangular. The gratings that we record are somewhat like these structures, and if all three structures show similar behavior, then we can assume that the grating we record also shows similar behavior. Figure 6.8-Figure 6.13 show plots of the efficiency of the +1 transmitted order and the +1 reflected order at different angles of incidence for binary, sinusoidal, and triangular diffraction gratings. These gratings are assumed to be photoresist (n=1.6) gratings on a glass (n=1.5) substrate.

108
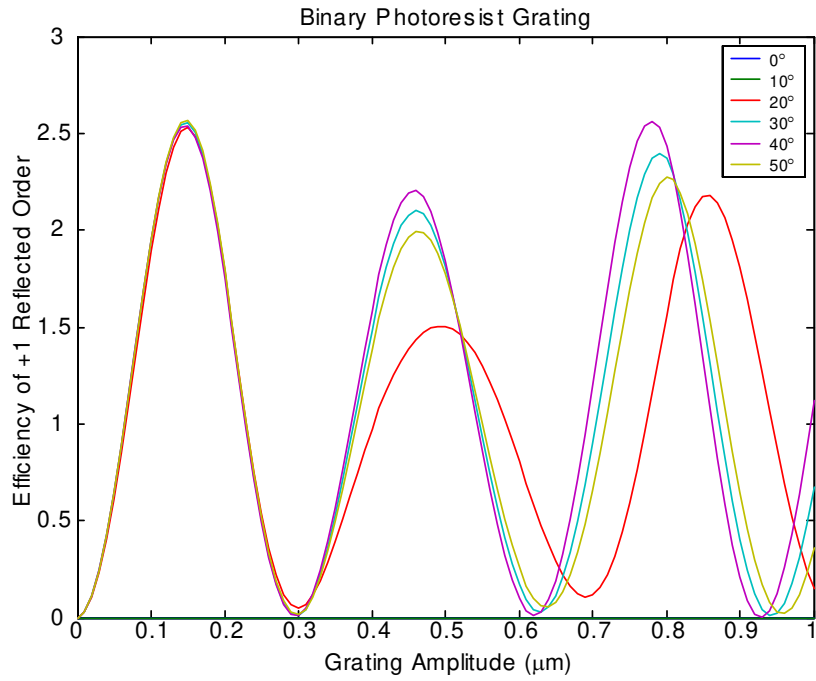
Figure 6.8 Plot of efficiency of reflected orders of binary photoresist grating as a function of grating amplitude
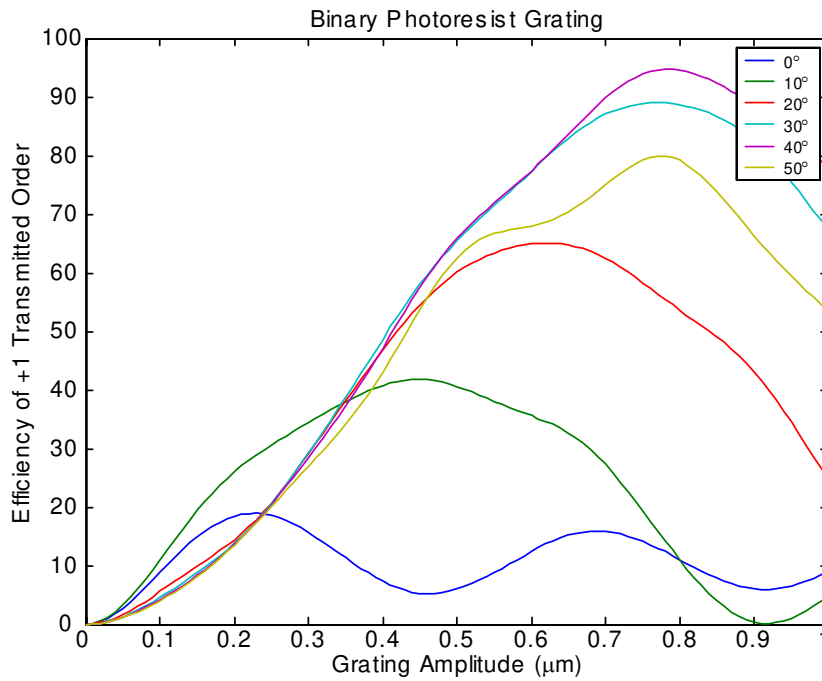
Figure 6.9 Plot of efficiency of transmitted orders of binary photoresist grating as a function of grating amplitude
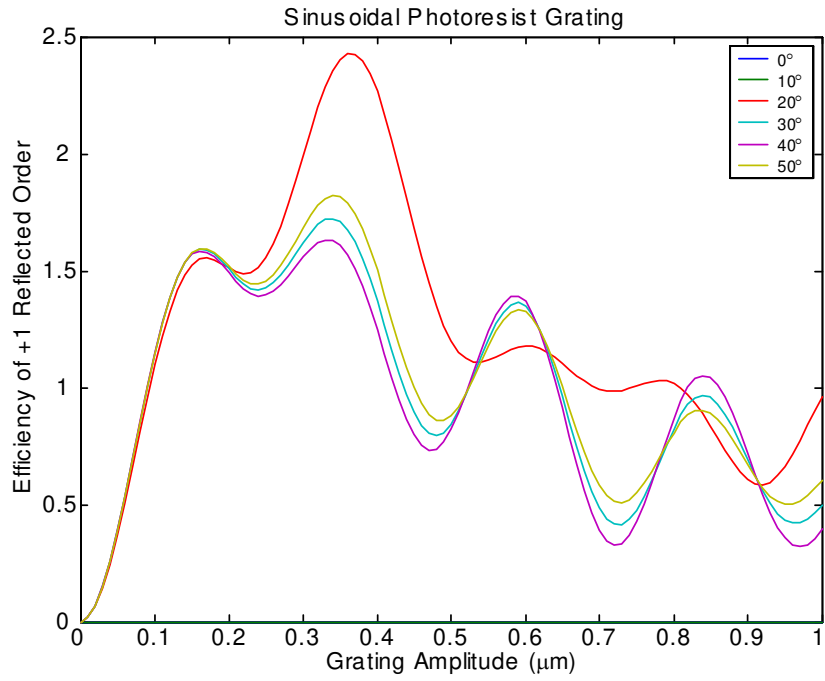
Figure 6.10 Plot of efficiency of reflected orders of sinusoidal photoresist grating as a function of grating amplitude
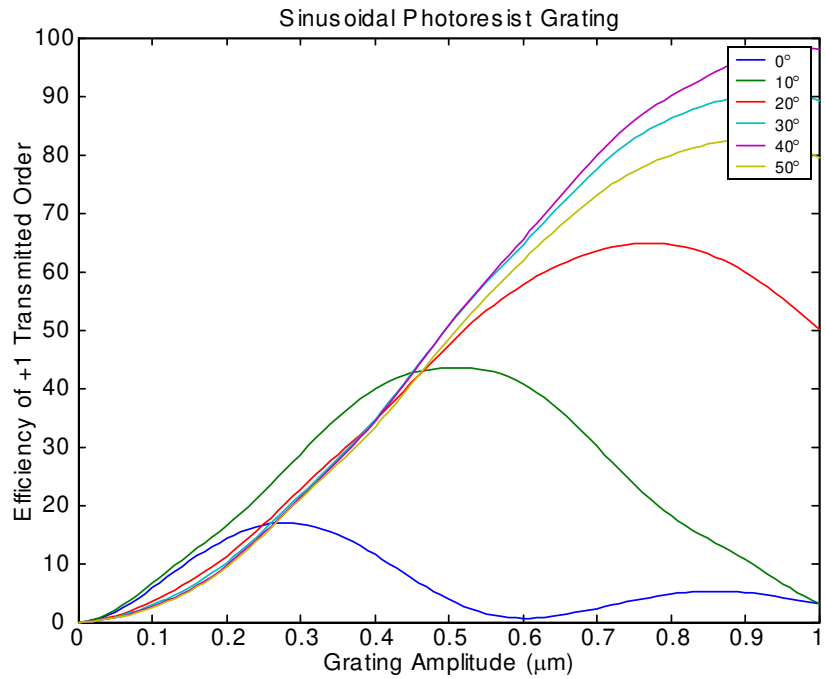
Figure 6.11 Plot of efficiency of transmitted orders of sinusoidal photoresist grating as a function of grating amplitude
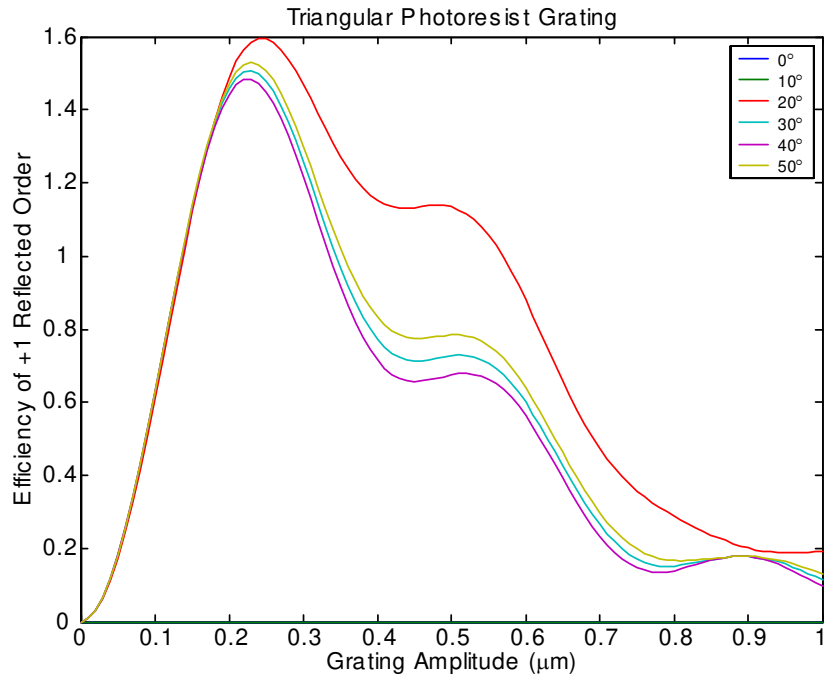
Figure 6.12 Plot of efficiency of reflected orders of triangular photoresist grating as a function of grating amplitude
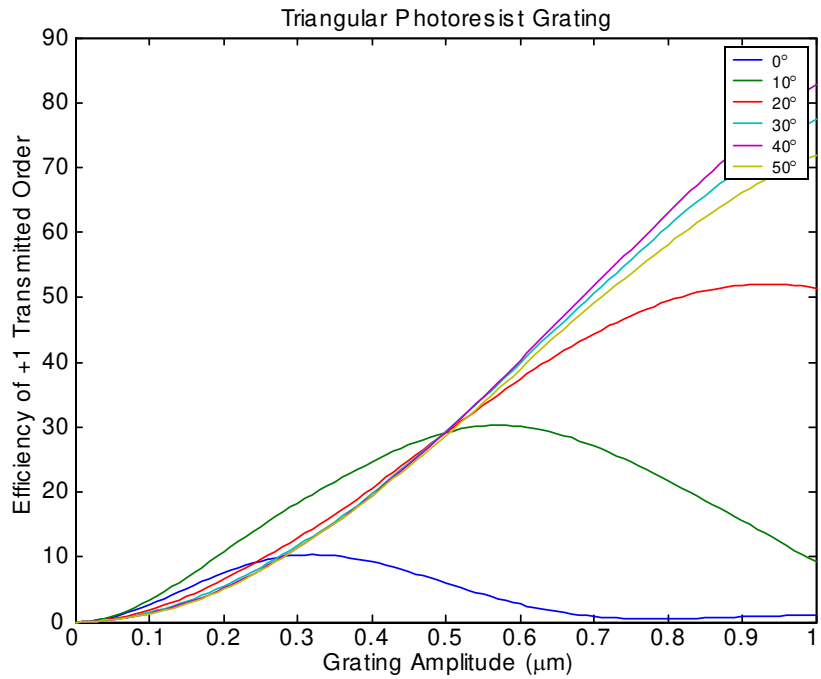
Figure 6.13 Plot of efficiency of transmitted orders of triangular photoresist grating as a function of grating amplitude

111

As Figure 6.8-Figure 6.13 illustrate, all of the structures exhibit similar behavior. Therefore, the grating that we record should also exhibit similar behavior. The reflected efficiencies have several oscillations, and would thus be unsuitable for use as an experimental metric. However, the transmitted orders for each structure increase slower and reach their maxima later with respect to grating amplitude. This behavior is even more pronounced at certain angles. Therefore, by measuring the efficiency of the transmitted order at a specific angle for different exposure times, we should be able to determine the optimal dosage. We assume that as the dosage time increases, the grating amplitude increases up to a point where the maximum amplitude is reached based on the intensity contrast of our sinusoidal interference pattern, and then decreases as the grating pattern reaches the substrate surface. As we measure the efficiency of the transmitted order, it should vary the same as the grating amplitude, and the grating with the maximum transmitted efficiency is the grating with the maximum grating amplitude.

6.3.2   Experimental Results for Exposure Time

Using the experimental procedure and metric described above, we attempted to characterize the optimal dosage for a 0.517 μm photoresist diffraction grating. The efficiency measurements were done at an angle of 20º, and the dosage range was from about 50 mJ/cm^2 to 67 mJ/cm^2. Figure 6.14 shows the results of the experiment.

112

Measured Transmitted Efficiency of +1 Diffracted Order
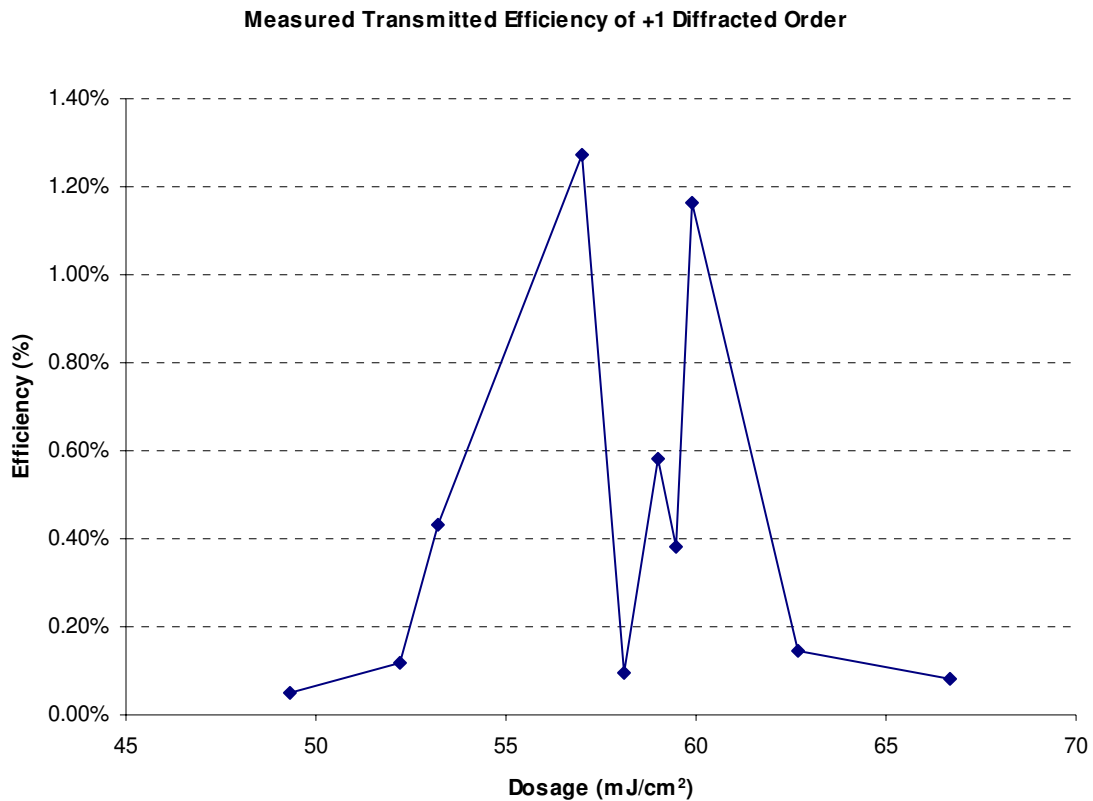
Figure 6.14 Results of dosage optimization experiment

As seen in Figure 6.14, the experimental results vary from what was expected. It is likely that process variations are affecting the results, and that the dosage may not be the only variable that is changing. However, from these results we can infer that the optimal dosage is likely somewhere in the range of 52 to 62 mJ/cm^2. As a second experiment, a series of exposures at 52.2 mJ/cm^2 were taken so that we could get an idea of the repeatability of our results. Figure 6.15 shows the results of this second test.

Repeatability of Exposure
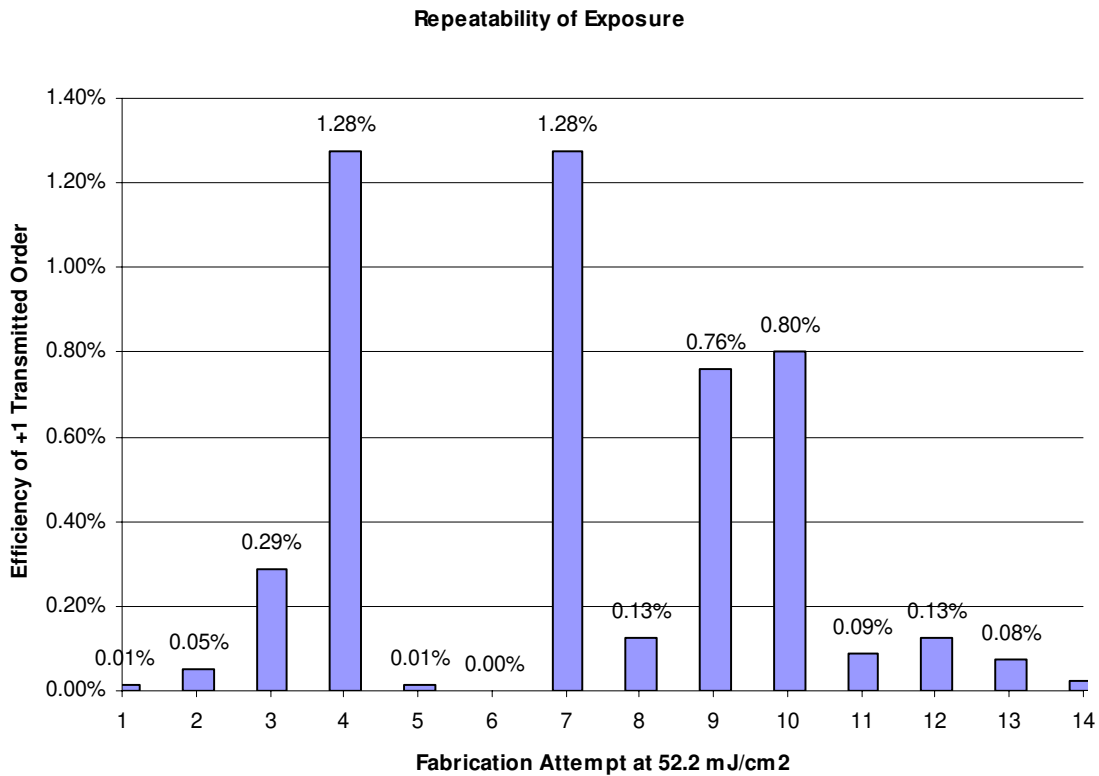
Figure 6.15 Variation of results at the same dosage

As Figure 6.15 shows, there is about as much variation in exposing different samples with the same dosage as there is in exposing different samples at different dosages. These results show that we have some serious variations in our process that are not being accounted for. Some possible culprits might be photoresist thickness variations, laser power fluctuations during exposure, laser polarization drift during exposure, vibrations of recording assembly during exposure, or photoresist developing variations. Each sample was measured more than once and similar results were obtained each time. Therefore, the differences in results are not likely due to inconsistent measurement techniques. It is possible that the variations could be due in part to nonuniformities within the gratings themselves, and that the point where the

measurement is taken is differs between samples; however, in observing the gratings under ambient light, those with high measured efficiencies diffract the ambient light strongly, while those with low measured efficiencies do not. In the effort to fabricate a diffraction grating, these reasons for process variation are not thoroughly investigated as a part of this thesis. Our results have shown that while the process is not repeatable to a high degree, we can make gratings that have reasonable efficiencies. The best efficiency that we have observed is about 1.28%, which from Figure 6.8-Figure 6.13 corresponds to grating amplitudes in the range of 50-80 nm. From the design of the grating couplers in Chapter 4, the required grating amplitude for photoresist gratings was in the range of 18-20 nm, which is attainable within these results. Therefore, we make gratings at the dosage of 52.2 mJ/cm^2, and those samples that come out well are used in further fabrication steps, while samples that do not are attributed to low yield and recycled. The above results have shown that we can manufacture diffraction gratings that have grating amplitudes in the design range for our grating couplers. While we do see a variation in our yield, we are able to manufacture gratings with desirable amplitude.

Chapter 7

7   Grating Coupler Results

So far in this thesis, the design, and analysis of grating couplers has been
presented. The grating coupler fabrication process has been discussed. In this
chapter the results of a fabricated grating coupler is presented. The quantities that are
measured to characterize our grating couplers are the period of the grating, the angle
at which the grating couples light into the waveguide, the input coupling efficiency,
and the decay loss parameter of the output grating. This chapter shows the results of
all of these measurements, and discusses the results in relation to the expected
theoretical results.

7.1   Atomic Force Microscope Image of Fabricated Grating Coupler

The Figures below are Atomic Force Microscope (AFM) images of the
grating recorded with a dosage of 52.2 mJ/cm^2. As these AFM data show, the
gratings have a nearly sinusoidal profile.
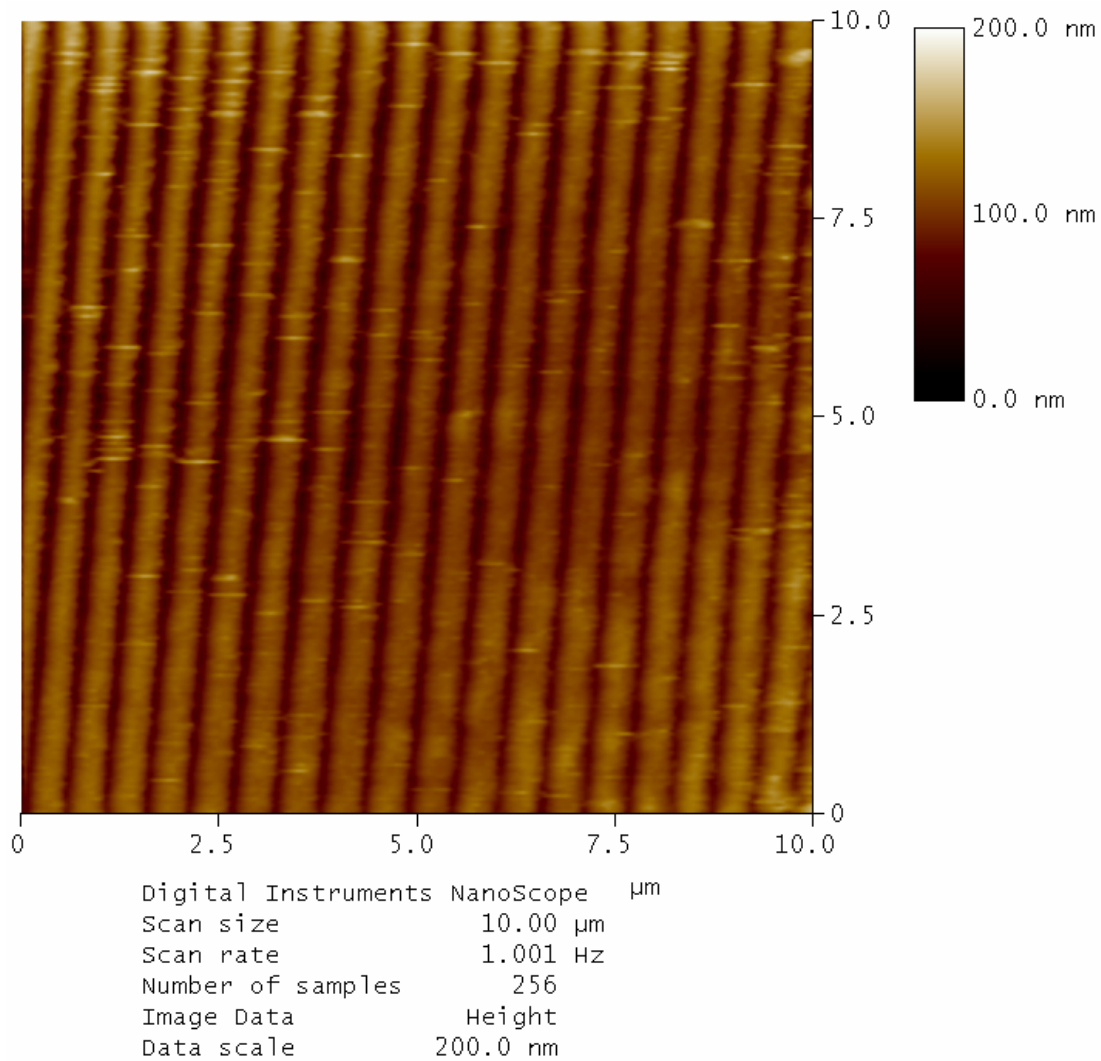
Figure 7.1 AFM image of surface of diffraction grating

Figure 7.1 shows that the gratings are in straight lines as was expected and are fairly uniform. The short horizontal lines on the image are artifacts of the AFM probe.
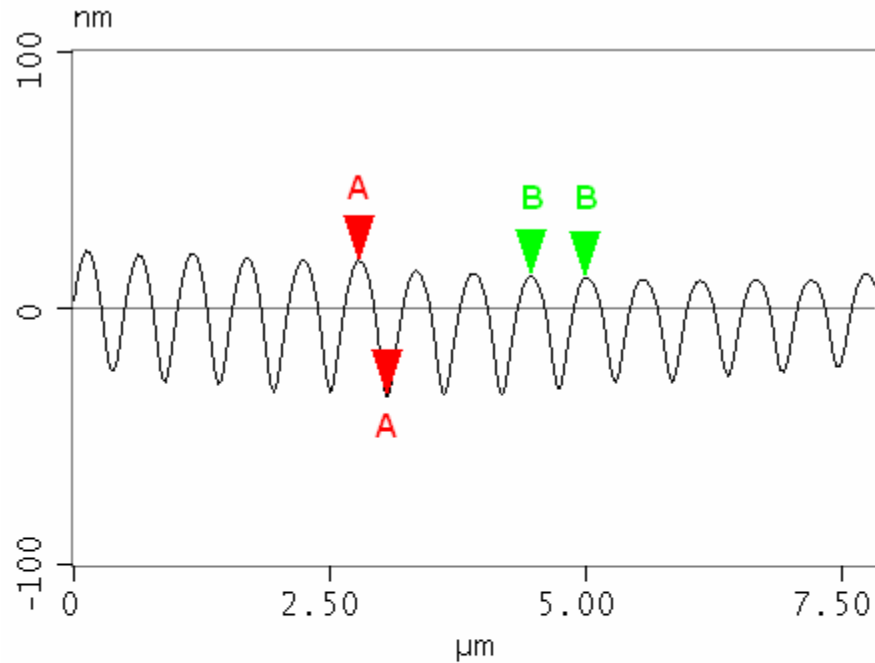
Figure 7.2 Cross sectional analysis of diffraction grating from AFM

Figure 7.2 shows that the amplitude of the sinusoidal grating is 54.684 nm. The measurement for the period is 546.88 nm, but this value could be off by as much as 20 nm due to the resolution of the AFM scan in the horizontal direction. A more precise measurement of the grating period is given in the next section.

7.2   Measurement of Grating Period

The measurement of the grating period is done by rotating the sample on a motorized rotation stage until the +1 reflected diffractive order is retro reflected onto the incident beam. This situation is illustrated in Figure 7.3.
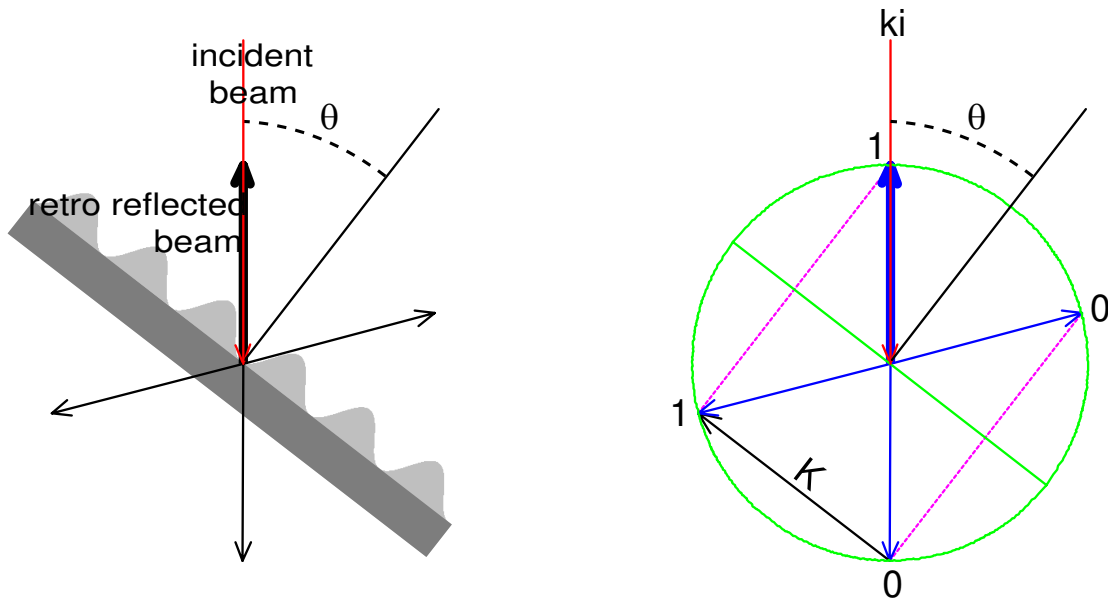
Figure 7.3 Measurement of the grating period

The incident beam is passed through an iris diaphragm and the angle is tuned until the retro reflected beam is centered on the hole in the iris diaphragm. Our motorized rotational stage has a resolution of a hundredth of a degree; therefore, the angle that is measured is precise to a fraction of a percent. Once the angle of retro reflection is found, the period of the grating can be easily calculated. From the k-space diagram of Figure 7.3, it is readily seen that

$$\left|\mathbf{K}\right| = 2\left|\mathbf{k}_i\right|\sin\theta .\qquad\qquad (8.1)$$

Substituting into (8.1) and rearranging the expression gives

$$\Lambda = \frac{\lambda}{2\sin\theta}.$$
(8.2)

By measuring the angle of retro reflection and using equation (8.2) the period of the

diffraction grating can be easily measured. For our grating coupler, the measured

period is 0.528 µm, which is slightly higher than the design value.

7.3   Results for Input Coupling Angle and Efficiency

The input coupling angle and efficiency is highly dependant on the interaction

with the diffraction grating and the waveguide. Figure 7.4 below shows a Scanning

Electron Microscope (SEM) cross-sectional image of the fabricated grating coupler.
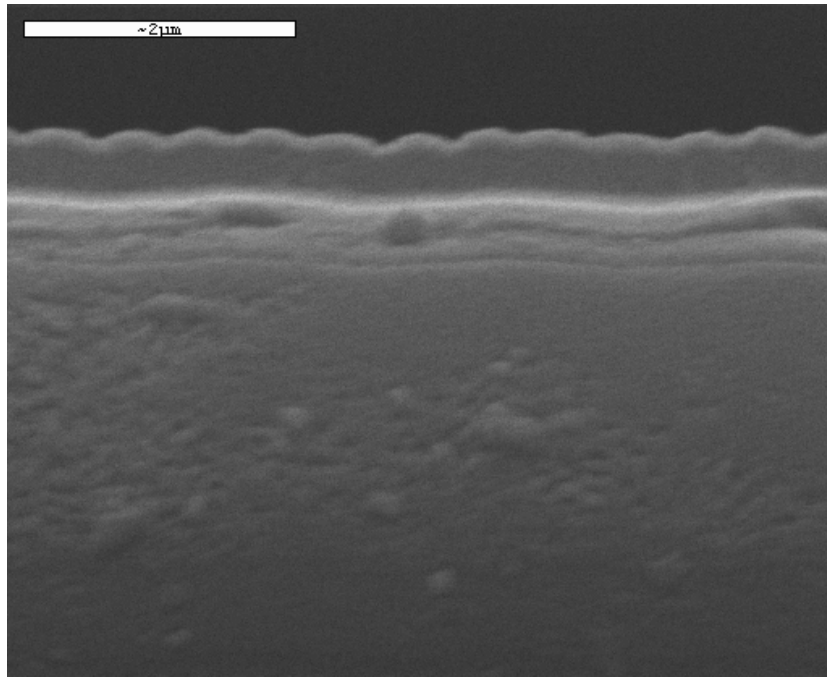
Figure 7.4 SEM image of fabricated grating coupler

In Figure 7.4, the bright line going across the image is the nitride waveguide.

On top of this is a photoresist layer, with the sinusoidal gratings on the top. From this

image it appears that the sinusoidal gratings are about 40-60 nm deep, and that the

gratings are separated from the waveguide layer by about 400-600 nm of unexposed photoresist. This structure is different from the assumed design given in Chapter 4.

7.3.1   Effect of Excess Photoresist beneath Grating

The design of the grating coupler assumed that the gratings would be adjacent to the waveguide, but Figure 7.4 shows that this is not the case. We now look at the effect of having excess photoresist beneath the diffraction grating. Figure 7.5 shows plots of the decay parameter, α_r, and the effective index, n_{eff}, for the 0.517 μm period binary photoresist grating designed in Chapter 4 as a function of thickness of photoresist beneath the grating.
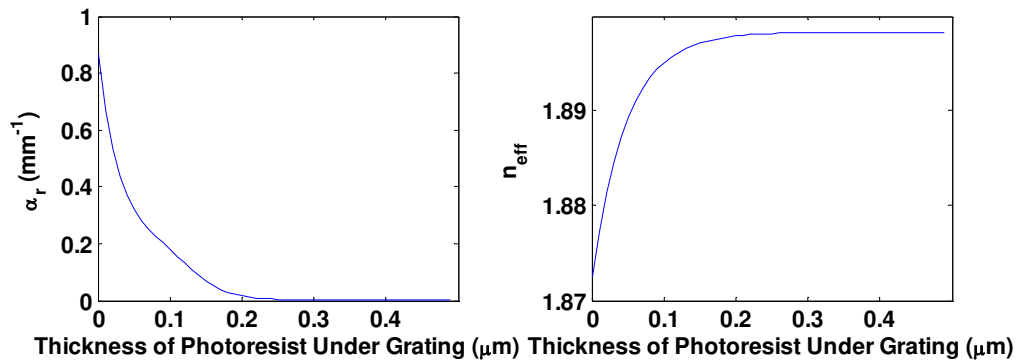
Figure 7.5 Effect of excess photoresist under grating on α_r and n_{eff}

As Figure 7.5 shows, the value of α_r decreases rapidly as the photoresist thickness increases. This is expected because the grating's interaction on the guided wave will decrease as the grating moves away because the evanescent fields decay exponentially. Also, the effective index settles to a constant value. This value is the effective index of the nitride waveguide with a photoresist cladding on top. By the time the photoresist thickness reaches 200 nm, the grating ceases altogether to

122

interact with the mode in the nitride at all, and the radiation parameter is essentially

zero. From this information, the conclusion seems that with a photoresist layer of

400-600 nm, we cannot couple directly into the nitride waveguide; however as Figure

7.4 shows, there is a thick photoresist slab as well. The photoresist is thick enough

that it also will support guided modes that we can couple into.

7.3.2 Measurement of Coupling Angle and Efficiency

To measure the coupling angle, we use the assembly shown in Figure 7.6.

detector

P_t

Motorized
Rotational
Stage

θ_i
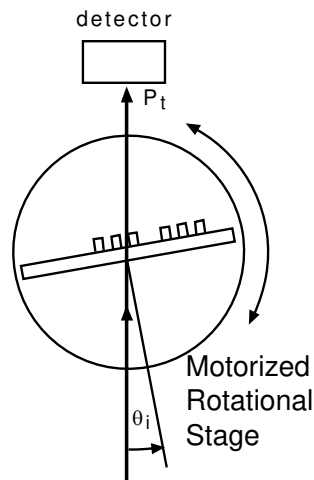
Figure 7.6 Schematic of basic grating coupler testing assembly

The basic testing assembly consists of a motorized rotational stage that the

sample is mounted on. The incident light is from a HeNe laser. The laser beam

passes through the center of the axis of rotation. A detector measures the undiffracted

through power. The sample is rotated, and when the coupling angle is reached, there

is a visible streak of light in the waveguide. With our measurement assembly we can

adjust the angle of incidence by hundredths of a degree. Once the angular range of

coupling is determined qualitatively, we can rotate the sample, and measure the

intensity of the undiffracted beam as shown in Figure 7.6. In our measurement assembly, both the rotational stage and the detector are interfaced with LABVIEW^{TM} and the undiffracted intensity is measured as a function of rotation angle. When the sample is rotated such that the incident beam is at the coupling angle, the incident power is coupled into the guided mode of the waveguide. The observed effect is a sharp decrease in the power of the undiffracted beam. The range of angles for coupling should be small, and the dip in the undiffracted intensity should be narrow. For the fabricated grating coupler structure, we were able to observe coupling, and Figure 7.7 shows a plot of the undiffracted transmitted power as a function of angle of incidence.
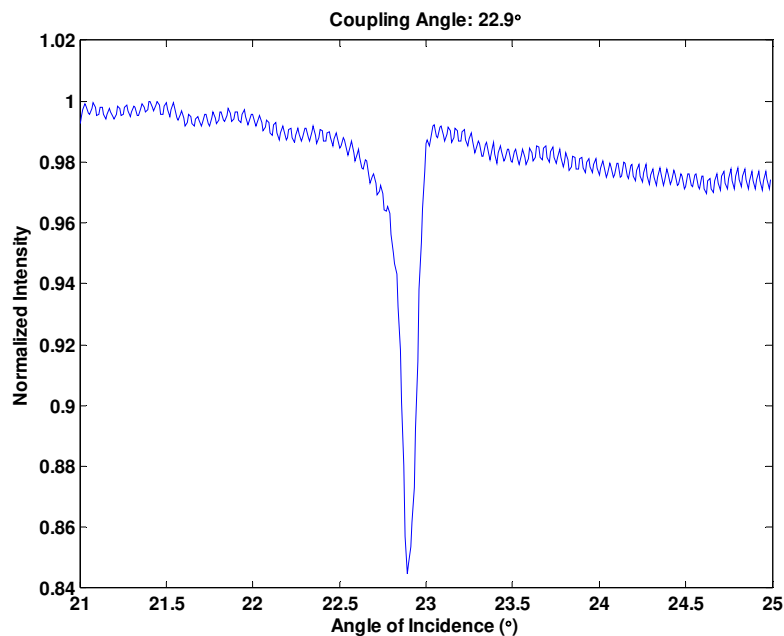
Figure 7.7 Normalized transmitted power as a function of incidence angle

As Figure 7.7 shows, there is a narrow dip in the transmitted power at 22.9°. This coupling angle is not the same as the designed angle of 35.57° because we are

not coupling directly into the nitride mode as designed. If the dip in the transmitted

power is only accounted for due to power being coupled into the waveguide, then the

coupling efficiency is about 16%.

7.3.3   Effective Index at Coupling Angle

To explain the coupling that we observe, let us look at the effective refractive

index of the coupled diffracted beam. Above, the coupling angle was measured at

22.9º, and the period of the diffraction grating was measured at 0.528 µm. Using

equation (4.2) for the effective index of the -1 diffracted order, which is the coupling

order, the effective index of the coupling beam is 1.5876. This effective index is

lower than the effective index of the photoresist, which is about 1.6. Therefore, the

input beam is coupling into a mode in the photoresist slab and not into the nitride

waveguide.

7.3.4   Modes in the Coupler Structure

As a further explanation, we can analyze the modes of the coupler structure.

Because we know what the effective index is of the mode that we couple into and we

have ranges for the material thicknesses and indices of refractions, we make

assumptions about the exact material parameters of our structure. These assumptions

are given in the table below.

Table 7.1 Material parameters used in analyzing fabricated coupler

refractive index of substrate	1.515
refractive index of nitride	2.15
thickness of nitride	200 nm
refractive index of photoresist	1.64
thickness of photoresist	590 nm

With the parameters given above, we can use a numerical solver for multilayer waveguides to calculate the electric field profiles and the propagation constants of the modes of in the coupler region.

In the coupler region, there are two modes. The effective index of the fundamental mode is 1.9502, and the effective index of the higher order mode is 1.5876. The effective index of the higher order mode is the same as the effective index of the mode that we are coupling into, and has most of its energy in the photoresist region. The fundamental mode is only guiding in the nitride region, and we are not coupling directly into this mode. The two modes are orthogonal, but if we launch into the higher order photoresist mode, light may scatter due to waveguide nonuniformities into the fundamental nitride mode. The electric field intensity profiles for both of these modes are shown in the figure below.
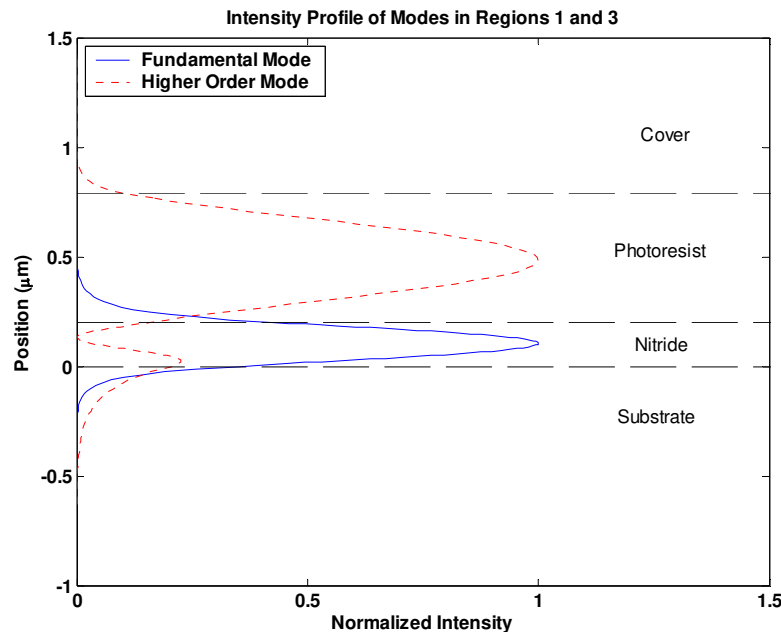
Figure 7.8 Intensity profiles of both modes in Region 1 and 3 of the fabricated grating coupler

7.4   Measurement of Output Coupling Performance

In order to observe output coupling, the light must be coupled into the nitride waveguide at some point and back into the output coupler. A diagram of our fabricated coupler structure is shown below.
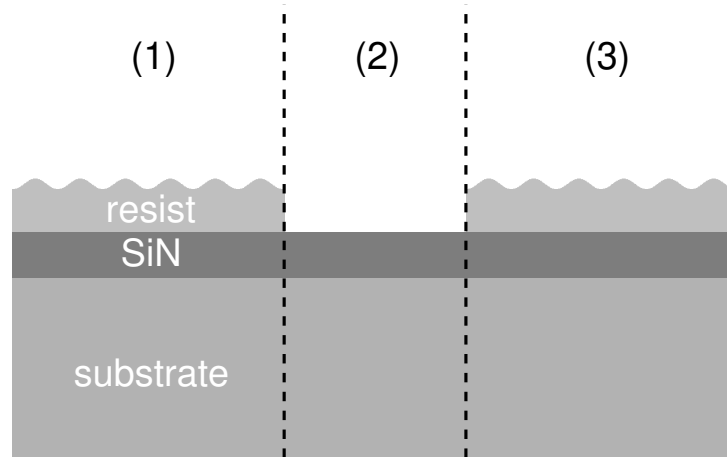
Figure 7.9 Diagram of fabricated grating coupler

There are three regions in Figure 7.9. Regions 1 and 3 are the input and output coupler regions respectively. Region 2 connects the input and output couplers through the nitride waveguide. If there is any overlap between the fields in regions 1 and 3 with the fields in region 2, then power is coupled between the input and output couplers, although there is scattering loss due to modal mismatch.

7.4.1   Modes in the Bare Nitride Waveguide

In the bare nitride region, there is only one mode. The effective index of this mode is 1.92. We can perform an overlap integral on the electric fields of the photoresist mode in regions 1 and 3 with the electric fields of the fundamental mode of region 2. The resulting percentage is the amount of light that is coupled into region 2 from region 1, neglecting scattering. The overlap between these two modes

is 1.1%. Because we go through one transition from region 1 into region 2, and another transition from region 2 to region 3, the total efficiency through both interfaces is 0.012%. The electric field intensity profile for the single mode in region 2 is shown in the figure below.
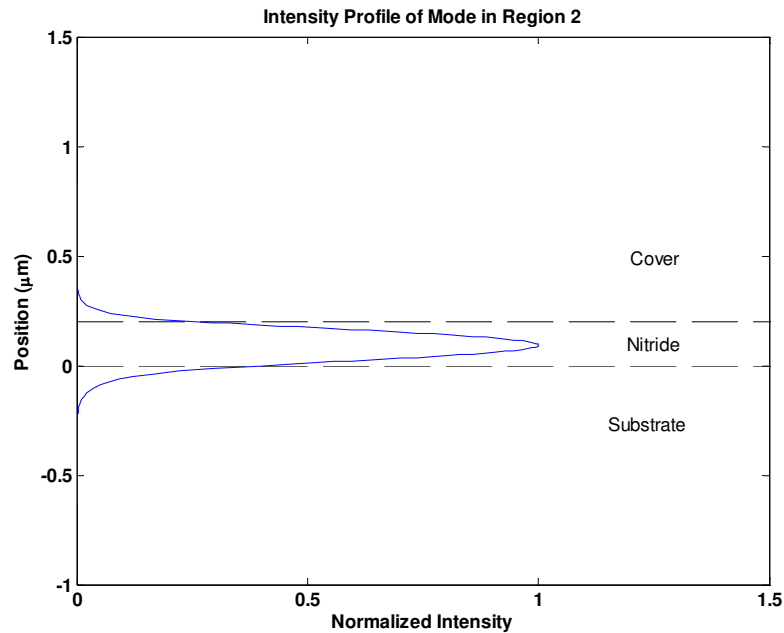
Figure 7.10 Intensity Profile of the mode in region 2 of the fabricated grating coupler

The above analysis has shown that it is possible to couple light between both couplers with very low efficiency. Although the light is launched at first into the photoresist slab, it is coupled into the mode of the nitride waveguide at the interface between region 1 and region 2 and also possibly from scattering. At the interface between regions 2 and 3, light is coupled back into the photoresist slab, and out of the photoresist through the diffraction grating. Thus, if we get enough power into the structure, we should be able to measure the output intensity profile of the grating coupler.

7.4.2   Measurement of Output Intensity Profile

In order to measure the output intensity profile, the sample is placed at the coupling angle determined by the methods in the previous section. The assembly used for this measurement is shown in Figure 7.11.
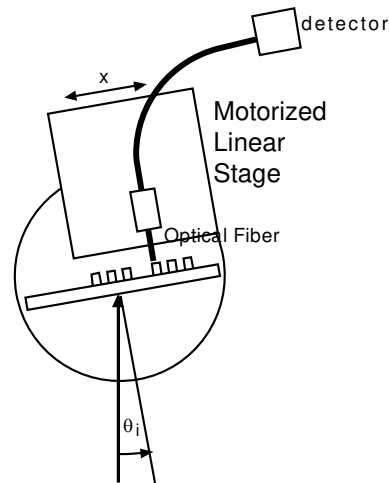
Figure 7.11 Augmented measurement assembly for scanning intensity of output beam

The optical fiber is a graded index multi-mode fiber with a core diameter of 52 μm. Because the multimode fiber has a larger numerical aperture than single mode fiber, our measurements have a larger angular tolerance. Also, more light is coupled into the fiber giving us more sensitivity to low intensity light. One end of the optical fiber is mounted on a motorized linear stage. The other end is placed in the detector. Both the detector and the linear stage are interfaced with LABVIEW$^{\text{TM}}$ and the intensity is measured as a function of the position of the optical fiber. If the diffraction grating is uniform, the intensity profile should be a decaying exponential as explained in Chapter 4. By measuring the intensity profile, we can fit the measurement to an estimate of the decay parameter.

129

Using the configuration shown in Figure 7.11, we were able to scan the intensity profile of the output beam with an optical fiber. Figure 7.12 shows the intensity profile measured by the fiber scan.
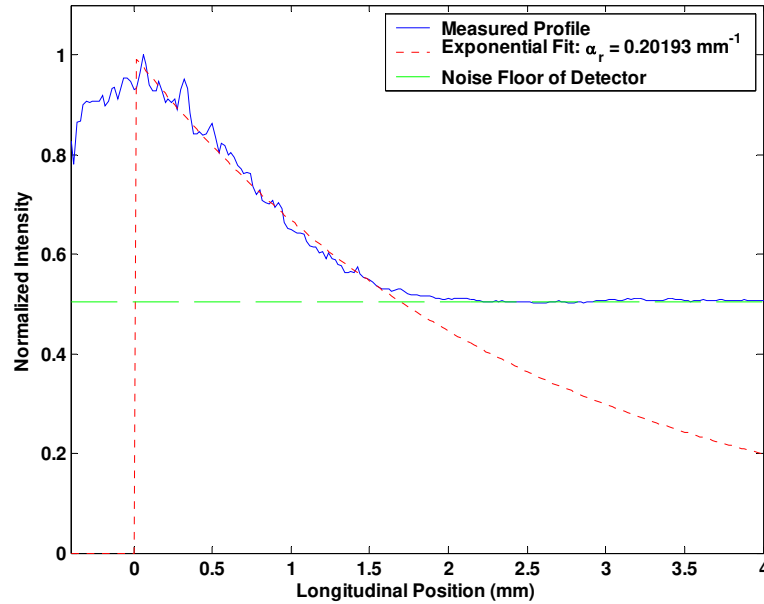
Figure 7.12 Intensity profile of the out-coupled beam at the grating surface

Figure 7.12 also shows the exponential curve that best fits this intensity profile. From these results, we see that the value of our decay parameter is about 0.2 mm^{-1}. This value is lower than the optimal design value of 0.8788 mm^{-1}. This result is consistent with our input coupling efficiency being lower. Because the decay parameter is lower, the overlap integral is smaller. With a decay parameter of 0.2 cm^{-1}, the value of the overlap integral of the decaying exponential with the input Gaussian shaped beam is only 45.8%, which alone reduces the input coupling efficiency to 12% from the cover, which is more consistent with the result shown in Figure 7.7.

7.5   Discussion of Results

The results so far have shown that we were successful in making a grating coupler, but that the measured results differ from the theoretical design. We can now compare our measured result with calculations based on our grating coupler structure. We use the values from Table 7.1, and the effective index of the photoresist slab mode to calculate the loss parameter of our structure and the efficiencies of the orders. If we assume a grating amplitude of 40 nm, the calculated value for α_r is 0.813 mm^{-1}. This value is larger than the measured value, but is close, based on the number of assumptions we have made in our analysis. The power splitting ratio into the cover first order beam is 25.8%, and the power splitting ratio into the substrate first order beam is 72.8%. The overlap integral between our input laser beam and the outcoupled intensity profile with the simulated value of α_r is 80%. Therefore if the assumptions are correct, we should be able to couple in 20% of the input power. These calculated values are qualitatively close to the experimental values.

Chapter 8

8   Conclusion

8.1   Summary

The theory, design, and fabrication of grating couplers for a slab waveguides is the emphasis of this thesis. Because this is the first research done in this area at Brigham Young University, all of the fabrication processes had to be developed from the ground up. These processes as well as the theory of the design of diffractive grating couplers have been given for the use of later researchers in this area.

A grating coupler was fabricated by holographic recording in photoresist with a period of 0.528 µm to couple light into a photoresist and silicon nitride waveguide. The results showed that this coupling was achieved at an angle of 22.9º. The input efficiency of this grating coupler was measured to be about 16%. The out-coupled beam from the grating coupler was measured and the radiation decay parameter for the grating coupler was determined to be about 0.2 mm^{-1}. These experimental values differ from the design values, but the discrepancies have been accounted for, and it has been shown that the results are in accordance with theory.

8.2 Future Work

There is much more research that can be done in the area of diffractive optics. This work has focused on the design of slab grating couplers. Other areas for future development include the further characterization of fabrication processes, the investigation into other methods of grating fabrication, using grating couplers in conjunction with optical fibers, and the investigation of other integrated optical devices based on diffraction gratings.

Perhaps the most important area that future research may address is solving the problem of the excess photoresist slab beneath our diffraction gratings. Some possible solutions to this problem could be using thinner photoresist, using the RIE to etch the gratings down, or to explore different fabrication methods. Also, as the results given in Chapter 7 showed, there are some variations in our processes. These variations were not found and corrected as a part of this research, because we were able to fabricate desirable gratings with a low yield. Further research should be done to find the cause of and eliminate these process variations. If these variations can be eliminated than better quality diffraction gratings can be fabricated with repeatability.

Investigation into alternate methods for grating fabrication should also be pursued. First, it would be beneficial to use thinner photoresist for our diffraction grating recording. We must either find thinner photoresist from a manufacture, or be able to mix the resist with solvents so that it spins on thinner. Thinner photoresist allows for shorter exposure times, which makes our process more immune to vibrations. Also thinner photoresist allows us to be sure that our diffraction gratings

are adjacent to the substrate surface, which was a process that we had little control over in this research.

The Electro Optics lab at Brigham Young University has been investigating in-fiber devices for many years. The platform of research is the D-fiber. Further research should be done to attempt to place gratings onto a D-fiber. With our recording techniques, gratings could be placed on the fibers that would act as selective wavelength filters.

Finally, there are many other integrated optical devices that should be studied in further research. Some of these potential research areas include: integrated spectrometers, chemical sensors, optical interconnects, volume gratings, focusing gratings for improved alignment tolerance, non homogeneous grating couplers for improved coupling efficiency, and novel phase mask topologies.

APPENDIX

Appendix A

A   **Fabrication Steps**

This Appendix outlines the most current fabrication steps at the time of the writing of this thesis. These steps are in no means definitive, and with further optimization could be significantly improved.

A.1 Slide Cleaning

It is important that before any photoresist or film of any kind is deposited on the slide, that the surface of the slide be clean. Below are two procedures for slide cleaning.

A.1.1 Piranha Etch

Piranha Etching gets its name from its ability to dissolve organic compounds. Special care must be taken with this procedure, and appropriate safety precautions must be used. The substrates should be cleaned with acetone and isopropanol and dried before being placed in the piranha etch, as the piranha etch is only used to remove residues. The hot etch solution should always be kept in an open container. Metallic compounds should never be put in the piranha etching solution. The Piranha etch should only be done in a well ventilated area. The procedures are as follows:

- Heat 3 parts concentrated sulfuric acid (H_2SO_4) in a glass beaker to 70º C

139

- Add 1 part 30% hydrogen peroxide (H_2O_2) to the sulfuric acid

- The solution will begin to bubble and will heat up even more as the chemicals begin to react

- Immediately place the substrate to be cleaned into the piranha etch

- Let the substrate soak in the piranha etch for at least 15 minutes

- After a while the chemical reaction will begin to be completed

- When the etching solution has cooled to below room temperature, carefully pour the spent solution into an appropriately marked waste container.

A.1.2 SC1 Solution

SC1 or Standard Clean 1 solution is not as dangerous as piranha etching, and can be used to remove residual organic materials and some metallic substances. This cleaning procedure should also be done in a well ventilated area, and the substrates should be cleaned with acetone and isopropanol and dried first. The procedures are as follows

- Combine 5 parts DI water, 1 part ammonium hydroxide (NH_4OH), and 1 part 30% hydrogen peroxide (H_2O_2) in a glass beaker

- Heat the solution to 70º C. Solution will begin to bubble off oxygen

- Submerge substrate in the solution for at least 10 minutes

- Allow solution to cool

- Solution may be diluted and disposed of down the drain

A.2 PECVD Procedures

The PECVD, or plasma enhanced chemical vapor deposition, is used to deposit thin films onto substrates. The films that we are interested are silicon nitride (Si_3N_4) and silicon dioxide (SiO_2). Here only the recipes used for deposition will be given. A step by step usage of the PECVD itself can be found on the cleanroom website.

A.2.1 Silicon Nitride Deposition

The recipe used to deposit silicon nitride is as follows.

- Ammonia flow rate: 2.5% MFC

- Silane flow rate: 89.5% MFC

- RF power: 100 W

- Pressure: .9 Torr

- Temperature: 240º C

- Deposition rate: 70 Å/min

A.2.2 Silicon Dioxide Deposition

The recipe used to deposit silicon dioxide is as follows.

- Silane flow rate: 70% MFC

- Nitrous oxide flow rate: 26% MFC

- RF power: 120 W

- Pressure: .515 Torr

- Temperature: 250º C

- Deposition rate: 200 Å/min

A.3 Photoresist Application

After the slides have been cleaned, and the desired film, if any, has been deposited. The slides are ready to be coated with photoresist. The process is as follows:

- Soak the slides in SurPass 3000 adhesion promoter for 60 seconds

- Rinse slides and blow dry

- Mount slides on spinner

- Apply AZ 3312 Photoresist

- Spin at 5000 rpm for 60 seconds

- Soft bake at 90º C for 90 seconds

- Slides should be kept in dark container until exposure

A.4 Exposure Procedures

Once the slides are coated with photoresist, they are ready to have the holographic diffraction grating recorded in them. This process is as follows:

- Allow the Laser to warm up for about 15 minutes

- Power reading on laser head should be 60 mW

- Check the alignment of the spatial filters

- Measure the power in both beams and, if needed, adjust half wave plate to equalize them

- Dial in desired exposure time into electronic shutter

- Mount sample on the sample holder

- Open shutter

- After desired amount of time, shutter will close automatically

- If desired, mark slide with permanent marker for identification later

- Place slide back into dark container

A.5   Developer Procedures

After the patterns have been recorded in the photoresist, they must be developed in the cleanroom. Also, additional features may be recorded into the photoresist such as the input and output strips for a grating coupler. These processes are as follows:

- Take samples back into the cleanroom

- If desired, record any additional patterns into the photoresist with the mask aligner

- Place the slide into a sample holder

- Immerse the sample in AZ 300 MIF developer for 60 seconds while agitating the sample.

- Place the sample in the nitrogen bubble tank for about 30 seconds

- Rinse the sample in DI water

- Blow dry with nitrogen gas

A.6   RIE Procedures

After the sample has been developed it may be desirable to further process the sample with the RIE. We can use either an O_2 based plasma, which should only etch photoresist, or we can use an O_2 and CF_4 based plasma to etch either nitride or silicon dioxide. The recipes for these plasmas are as follows:

A.6.1   O$_2$ plasma

- Oxygen flow rate: 3.1 sccm

- Pressure: 50 mTorr

- RF power: 100 W

A.6.2   O$_2$ and CF$_4$ based plasma

- Oxygen flow rate: 3.1 sccm

- CF4 flow rate: 25 sccm

- Pressure: 50 mTorr

- RF power: 100 W

Appendix B

B **Code Documentation**

This Appendix documents the MATLAB code used for all of the analysis in

this thesis. There are codes to analyze diffraction angle, diffraction efficiency, and

grating couplers.

B.1 K-Space Analysis

B.1.1 diffract.m

```
function [D_mat]=diffract2(lambda,ni,nt,L,thetai,p)
%function [D_mat]=diffract2(lambda,ni,nt,L,thetai,p)
%returns array containing the transmitted diffracted angle,
%the order number for each diffracted order, and the reflected
%diffracted angle.  Also can produce k-space plot of the diffraction.
%
%Parameters:
%lambda: wavelength of incident light in microns
%ni: index of refraction of incident medium
%nt: index of refraction for transmitted medium
%L: period of the grating in microns
%thetai: angle of incident light in degrees
%p: 1 for plot, 0 for no plot

q=ceil(L*(ni*sin(thetai*(pi/180))-
nt)/lambda):1:floor(L*(ni*sin(thetai*(pi/180))+nt)/lambda);
thetad=-asin((-ni*sin(thetai*(pi/180))*L+q*lambda)/nt/L)*180/pi;
thetar=-asin(nt*sin(thetad*pi/180)/ni)*180/pi;
D_mat=[thetad' q' thetar'];
2*pi/L

%plot the figure
if p==1
    kt=2*pi*nt/lambda;
    ki=2*pi*ni/lambda;
    arrowb(ki,[0 0],thetai,'red')
    for v=1:length(q)
        if q(v) <0
            arrowt(2*pi/L,[(q(v)+1)*2*pi/L+kt*sin(pi/180*thetad(find(q==0)))...
                    -kt*cos(pi/180*thetad(find(q==0)))],90,'black');
        elseif q(v) >0
            arrowt(2*pi/L,[(q(v)-1)*2*pi/L+kt*sin(pi/180*thetad(find(q==0)))...
                    -kt*cos(pi/180*thetad(find(q==0)))],-90,'black');
        end
        pl=line([-(q(v))*2*pi/L+kt*sin(pi/180*thetad(find(q==0)))...
                -(q(v))*2*pi/L+kt*sin(pi/180*thetad(find(q==0)))],...
            [-kt*cos(pi/180*thetad(find(q==0))) ki*cos(pi/180*thetai) ]);
```

```
    set(pl,'Linestyle',':','Color','m')
    if q(v)==0
        arrowt(kt,[0 0],thetad(v),'b')
        if isreal(thetar(v))
            arrowt(-ki,[0 0],thetar(v),'b')
        end
    else
        arrowt(kt,[0 0],thetad(v))
        if isreal(thetar(v))
            arrowt(-ki,[0 0],thetar(v))
        end
    end
    text(1.1*kt*sin(thetad(v)*pi/180),-1.1*kt*cos(thetad(v)*pi/180)...
        ,num2str(q(v)),'HorizontalAlignment','center')
end
hold on;
plot(linspace(-ki,ki,1000),sqrt(ki^2-(linspace(-ki,ki,1000)).^2),'g')
plot(linspace(-kt,kt,1000),-sqrt(kt^2-(linspace(-kt,kt,1000)).^2),'g')
plot([-max(ki,kt) max(ki,kt)],[0 0],'g');
axis off;
title(['K-Space Diagram for \lambda = ' num2str(lambda) '\mum and \Lambda ='
num2str(L) '\mum'])
end
```

B.2   Free Space Rigorous Coupled Wave Analysis

B.2.1   Description

I now briefly discuss the MATLAB program for free space diffraction

efficiency, and its interface. The MATLAB file that does all of the computation is

called *sr_rcwa2.m*. This file computes the diffracted amplitudes of a multilayer

lamellar surface-relief grating for an arbitrarily polarized unit amplitude wave,

incident from an arbitrary angle and plane of incidence in an isotropic lossless cover

medium. The grating and substrate media can be lossy, but must be isotropic. There

are several input parameters that *sr_rcwa2.m* needs to perform this computation. All

of these parameters are set in an input file called *sr_in.m*. Table B.8.1 describes all of

the variables that are set in *sr_in.m*.

Table B.8.1 Description of variables for MATLAB implementation of rigorous coupled wave analysis

Variable	Description
NumOrds	Number of diffractive orders maintained
nc	Region 1 (cover) refractive index
ns	Region 3 (substrate) refractive index
Ngrat	Number of grating slices

Period	Grating period in microns
depth	Vector containing grating depth for each grating; size is 1xNgrat
ng	Vector containing groove refractive indices for each grating; size is 1xNgrat
Nr	Vector containing ridge refractive indices for each grating; size is 1xNgrat
FilFac	Vector containing the percent fill factor for the ridges of each grating; size is 1xNgrat
Disp	Vector containing ridge displacements in fractions of a period for each grating; size is 1xNgrat
Lambda0	Free space wavelength in microns
theta0	Polar angle of incidence in degrees
phi0	Azimuthal angle of incidence in degrees
Psi	Polarization angle
Delta	Input wave retardation phase from TE to TM

B.2.2   Grating Description in MATLAB Implementation

In order to understand some of the variables in the table above, I now explain how the diffraction grating is represented in this MATLAB code. The representation used follows the method given in [75]. As stated in the derivation of rigorous coupled wave analysis, a diffraction grating is sliced into thin slabs, and their permittivity distribution is expressed in terms of a Fourier series. Each of these slabs is treated as a binary grating and in this code is characterized by a filling factor, a ridge displacement, a grating depth, a ridge refractive index, and a groove refractive index. By characterizing the slices this way, the Fourier series expression is a well-known analytic expression. The filling factor represents the percentage of the period that the ridge occupies. The displacement represents the shift of the ridge in the x direction expressed in terms of percentage of the grating period. The depth is, of course, the height of the slab grating. The specifications for the slabs are expressed starting at the top of the grating and ending at the bottom of the grating. Figure B.1 demonstrates this representation.
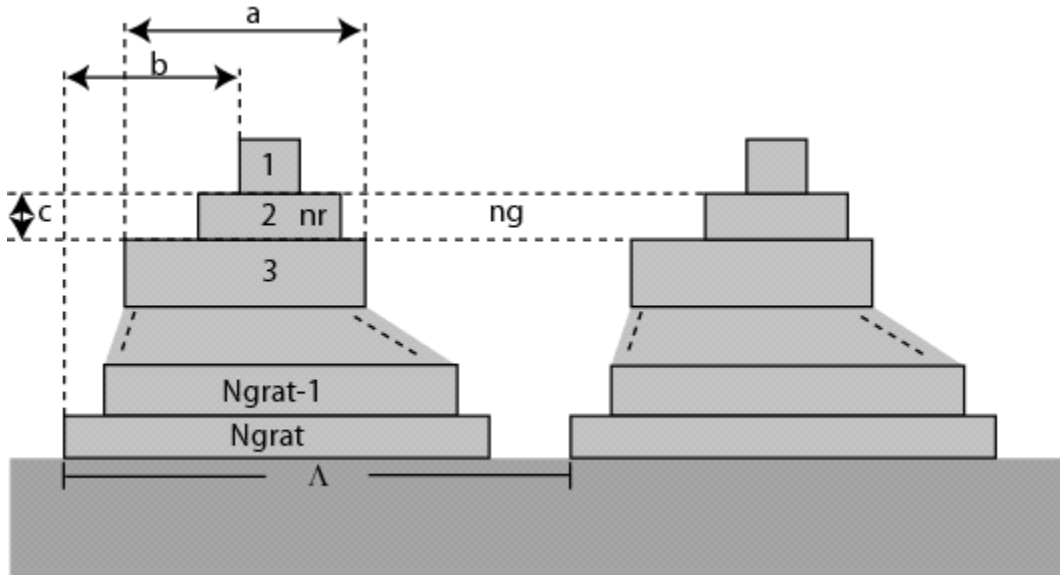
Figure B.1 Demonstration of geometry used in MATLAB rigorous coupled wave analysis code

In Figure B.1 we see that the slabs are numbered from top to bottom. The length labeled "a" corresponds to the filling factor for ridge 3, with length a = FilFac(3)*Period. The length labeled "b" corresponds to the displacement for ridge 1, and can be expressed as   b = Disp(1)*Period. The quantity labeled "c" is the depth of ridge 2. Figure B.1 also illustrates the ridge and groove refractive indices for slab number 2. All of these quantities are defined for each slab grating in this formulation of the rigorous coupled-wave analysis.

For binary gratings, only one slab is needed to represent the grating. For a blazed grating, if a total amplitude is defined, then the MATLAB expression for the appropriate displacement, filling factors, and depth vectors is:

```
%Blazed Grating
FilFac=(linspace(1/Ngrat,1-1/Ngrat,Ngrat));
Disp=(linspace(.5/Ngrat,.5-.5/Ngrat,Ngrat));
depth=Amplitude/Ngrat*ones(1,Ngrat);
```

where "Amplitude" is the total amplitude of the grating. For a sinusoidal grating, the

MATLAB expression for the appropriate displacement, filling factors, and depth

vectors is:

```
%Sinusoidal Grating
FilFac=fliplr(acos(linspace(-1+1/Ngrat,1-1/Ngrat,Ngrat))/pi);
Disp=(.5*ones(1,Ngrat));
depth=Amplitude/Ngrat*ones(1,Ngrat);
```

The above expressions enable the analysis of any binary, blazed, or sinusoidal

grating.

B.2.3   sr_in.m

```
%
% TE Multilayer test cases
%
%

NumOrds=21;

nc     = 1.0;           % Region 1 refractive index
ns     = 1.5;           % Region 3 refractive index

%   Grating region parameters

Ngrat  = 1;            % Number of gratings
Period =.8;            % Grating period in microns for all gratings
depth  = [.1] % grating depths in microns
ng     = [ns];             % Groove indicies
nr     = [nc];             % Ridge indices
FilFac = [.5];        % Filling factors
Disp   = [0];              % Ridge displacements in fractions of 1 Period

%   Angle of incidence and wavelength information

lambda0 = .6328;            % Freespace wavelength in microns
theta0  = 0;        % Polar angle of incidence (deg)
phi0    = 0;            % Azimuthal angle of incidence (deg)
psi     = 0;              % Polarization angle (deg): 0 => TE,  90 => TM
delta   = 0;              % Input wave retardation phase from TE to TM (deg)
```

B.2.4   sr_rcwa.m

```
%       SR_RCWA computes the diffracted amplitudes of a multilayer
%       lamellar surface-relief grating for an arbitrarily polarized unit
%       amplitude wave, incident from an arbitrary angle and plane
%       of incidence in an isotropic lossless cover medium.  The grating
%       and substrate media can be lossy, but must be isotropic.
%       The analysis is Rigorous Coupled Wave Analysis, as presented in
%
%       M. G. Moharam, E. B. Grann, D. A. Pommet, and
%       T. K. Gaylord "Formulation for stable and efficient
%       implementation of the rigorous coupled-wave analysis
%       of binary gratings," J. Opt. Soc. Am. A, vol. 12,
%       pp. 1068-1076, May 1995.
%
%       and
%
```

```
%       M. G. Moharam, E. B. Grann, D. A. Pommet, and
%       T. K. Gaylord "Stable implementation of the rigorous
%       coupled-wave analysis of surface-relief gratings:
%       enhanced transmittance matrix approach," J. Opt. Soc.
%       Am. A, vol. 12, pp. 1068-1076, May 1995.
%
%       User must edit sr_in.m to set up the input parameters.
%
%       Author: Dave Brundrett
%
%       Revised by Stephen M. Schultz
%

%clear all;
%close all;
%    Define the program constants.

j=sqrt(-1);
deg=pi/180;
t0=clock;

sr_in;

%    Define the dimensioning variables

Nmax   = (NumOrds-1)/2;           % NumMax is the highest order number retained,
I      = (-Nmax:Nmax)';           % I is the order index,
p      = (NumOrds+1)/2;           % and p is the index of the zeroth order.

%    Set up the input variables

%    Change angles to radians

theta0=theta0*deg;
phi0=phi0*deg;
delta=delta*deg;

%    Define the relative permittivities

epsc    = nc^2;                             % Cover     relative permittivity
epss    = ns^2;                             % Substrate relative permittivity

%    Define the grating vector and the wavevectors
k0  = 2*pi/lambda0;                              % Freespace wavevector
K  = 2*pi/Period;                         % Grating vector

kc  = k0*nc;                               % Region 1 wavevector components
kx = kc*sin(theta0)*cos(phi0) - I*K;        %
ky = kc*sin(theta0)*sin(phi0)*ones(size(kx)); %

kzc = sqrt(kc^2 - kx.^2 - ky.^2);          %
bad_indices=find((real(kzc)-imag(kzc))<0);   % locate incorrect signs
kzc(bad_indices)=-kzc(bad_indices);          % correct the signs

ks  = k0*ns;                               % Region 3 wavevector components
kzs = sqrt(ks^2 - kx.^2 - ky.^2);          %
bad_indices=find((real(kzs)-imag(kzs))<0);   % locate incorrect signs
kzs(bad_indices)=-kzs(bad_indices);          % correct the signs

%    Define the diffraction angles

tc = -atan2(kx,kzc);               % Cover     order polar angles
ts = -atan2(kx,kzs);               % Substrate order polar angles

if abs(phi0) > 1e-6,               % Diffraction plane azimuthal angles
   phi_d=atan2(ky,kx);          %
else                              %
   phi_d=zeros(size(kx));       %
end                               %

%    Define some auxillary matrices and vectors

Zm     = zeros(NumOrds,NumOrds);
Zv     = zeros(NumOrds,1);
Dv     = Zv;   Dv(p)=1;
Zv2    = [Zv;Zv];
Eye    = eye(NumOrds);
Kx     = diag(kx)/k0;
Kxsq   = Kx.^2;
Ky     = diag(ky/k0);
Kysq   = Ky.^2;
```

```matlab
Kzc   = diag(kzc)/k0;
Kzcsq = Kzc.^2;
Kzs   = diag(kzs)/k0;
Kzssq = Kzs.^2;
M     = NumOrds-1;


%
%   Trap out planar diffraction cases, otherwise do the full-blown problem
%

if phi0==0,

   if (psi==0|psi==180|psi==-180),
      psi=psi*deg;
      temp1=Eye;
      fmat=Eye;
      gmat=j*Kzs;
      for ii=Ngrat:-1:1,
         epsg    = ng(ii).^2;                      % Groove permittivity
         epsr    = nr(ii).^2;                      % Ridge permittivity
         epsG    = (1-FilFac(ii))*epsg + FilFac(ii)*epsr; % average grating
permittivity
         iepsG   = (1-FilFac(ii))/epsg + FilFac(ii)/epsr; % average inverse grating
permittivity
         Sinc    = sin(pi*FilFac(ii)*[ 1:M])./(pi*[ 1:M]);
            vm      = (  epsr -   epsg)*fliplr(Sinc);
            v0 = epsG;
            vp = (  epsr -   epsg)*Sinc;
         v       = [vm v0 vp].*exp(-j*2*pi*Disp(ii)*[-M:M]);
            ivm     = (1/epsr - 1/epsg)*fliplr(Sinc);
            iv0 = iepsG;
            ivp = (1/epsr - 1/epsg)*Sinc;
            iv = [ivm iv0 ivp].*exp(-j*2*pi*Disp(ii)*[-M:M]);
            Epsilon = toeplitz(fliplr( v(1:NumOrds)), v(NumOrds:2*NumOrds-1));
            Alpha   = toeplitz(fliplr(iv(1:NumOrds)),iv(NumOrds:2*NumOrds-1));
         clear Sinc v iv vm iivm v0 iv0 vp ivp

         A       = Kxsq - Epsilon;
         [W,V]=eig(A);
         Q=sqrt(V);
         M0=W*Q;
         E=expm(-k0*Q*depth(ii));
         v=[W,W;M0,-M0]\[fmat;gmat];
            temp2=v(1:NumOrds,:)\E;
            temp3=E*v(NumOrds+1:2*NumOrds,:)*temp2;
            temp1=temp1*temp2;
            fmat=W+W*temp3;
            gmat=M0-M0*temp3;
      end
      gfi=gmat/fmat;
      RHS=-gfi(:,p); RHS(p)=RHS(p) + j*kzc(p)/k0;
      Rs=[gfi + j*Kzc]\RHS;
      Ts=(temp1/fmat)*(Rs + Dv);
%      [Rs Ts]
      Rx=Zv;
      Ry=Rs*cos(psi)*exp(+j*delta/2);
      Rz=Zv;
      Tx=Zv;
      Ty=Ts*cos(psi)*exp(+j*delta/2);
      Tz=Zv;
      IR=(abs(Rs).^2) .* real(kzc ./ kzc(p)) * 100;
      IT=(abs(Ts).^2) .* real(kzs ./ kzc(p)) * 100;
  elseif (psi==90|psi==-90),
      psi=psi*deg;
      temp1=Eye/ns;
      fmat=Eye;
      gmat=j*Kzs/ns^2;
      for ii=Ngrat:-1:1,
         epsg    = ng(ii)^2;                       % Groove permittivity
         epsr    = nr(ii)^2;                       % Ridge permittivity
         epsG    = (1-FilFac(ii))*epsg + FilFac(ii)*epsr; % average grating
permittivity
         iepsG   = (1-FilFac(ii))/epsg + FilFac(ii)/epsr; % average inverse grating
permittivity
         Sinc    = sin(pi*FilFac(ii)*[ 1:M])./(pi*[ 1:M]);
            vm      = (  epsr -   epsg)*fliplr(Sinc);
            v0 = epsG;
            vp = (  epsr -   epsg)*Sinc;
            v   = [vm v0 vp].*exp(-j*2*pi*Disp(ii)*[-M:M]);
            ivm     = (1/epsr - 1/epsg)*fliplr(Sinc);
            iv0 = iepsG;
```

```matlab
            ivp = (1/epsr - 1/epsg)*Sinc;
            iv  = [ivm iv0 ivp].*exp(-j*2*pi*Disp(ii)*[-M:M]);
            Epsilon = toeplitz(fliplr( v(1:NumOrds)), v(NumOrds:2*NumOrds-1));
            Alpha   = toeplitz(fliplr(iv(1:NumOrds)),iv(NumOrds:2*NumOrds-1));
        clear Sinc v iv vm iivm v0 iv0 vp ivp
%
            B  = Kx*(Epsilon\Kx) - Eye;
        [W,V]=eig(Alpha\B);
        Q=sqrt(V);
        M0=Alpha*W*Q;
        E=expm(-k0*Q*depth(ii));
        v=[W,W;M0,-M0]\[fmat;gmat];
            temp2=v(1:NumOrds,:)\E;
            temp3=E*v(NumOrds+1:2*NumOrds,:)*temp2;
            temp1=temp1*temp2;
            fmat=W+W*temp3;
            gmat=M0-M0*temp3;
        end
        gfi=gmat/fmat;
        RHS=-gfi(:,p); RHS(p)=RHS(p) + j*kzc(p)/k0/epsc;
        Rp=[gfi + j*Kzc/nc^2]\RHS;
        Tp=(temp1/fmat)*(Rp + Dv)*nc;
%        [Rp Tp]
        Rx=-Rp.*cos(tc)*sin(psi)*exp(-j*delta/2);
        Ry= Zv;
        Rz= Rp.*sin(tc)*sin(psi)*exp(-j*delta/2);
        Tx= Tp.*cos(ts)*sin(psi)*exp(-j*delta/2);
        Ty= Zv;
        Tz= Tp.*sin(ts)*sin(psi)*exp(-j*delta/2);
        IR=(abs(Rp).^2).*real(kzc./kzc(p))*100;
        IT=(abs(Tp).^2).*real(kzs./kzc(p))*100;
    else
        psi=psi*deg;
        [Ws,Vs]=eig(A);
        Qs=sqrt(Vs);
        M0s=Ws*Qs;
        M1s=j*Kzc*Ws;
        M2s=j*Kzs*Ws;
        [Wp,Vp]=eig(Alpha_I*B);
        Qp=sqrt(Vp);
        M0p=Alpha*Wp*Qp;
        M1p=j*Kzc*Wp/epsc;
        M2p=j*Kzs*Wp/epss;
        RHSs = Zv2; RHSs(p) = j*2*kzc(p)/k0;
        RHSp = Zv2; RHSp(p) = j*2*kzc(p)/k0/epsc;
        Es=expm(-k0*Qs*depth);
        Xs=[(M1s+M0s)      (M1s-M0s)*Es;
            (M2s-M0s)*Es (M2s+M0s)  ];
        Cs=inv(Xs)*RHSs;  Cps=Cs(1:NumOrds,1); Cms=Cs(NumOrds+1:2*NumOrds,1);
        Rs=Ws*(Cps+Es*Cms) - RHSs(1:NumOrds)/(j*2*kzc(p)/k0);
        Ts=Ws*(Es*Cps + Cms);
        IRs=(abs(Rs).^2).*real(kzc./kzc(p))*100
        ITs=(abs(Ts).^2).*real(kzs./kzc(p))*100;
        Ep=expm(-k0*Qp*depth);
        Xp=[(M1p+M0p)      (M1p-M0p)*Ep;
            (M2p-M0p)*Ep (M2p+M0p)  ];
        Cp=inv(Xp)*RHSp;  Cpp=Cp(1:NumOrds,1); Cmp=Cp(NumOrds+1:2*NumOrds,1);
        Rp=Wp*(   Cpp + Ep*Cmp) - RHSp(1:NumOrds)/(j*2*kzc(p)/k0/epsc);
        Tp=Wp*(Ep*Cpp +    Cmp)*nc/ns;
        IRp=(abs(Rp).^2).*real(kzc./kzc(p))*100;
        ITp=(abs(Tp).^2).*real(kzs./kzc(p))*100;
        Rx=-Rp.*cos(tc)*sin(psi)*exp(-j*delta/2);
        Ry= Rs *        cos(psi)*exp(+j*delta/2);
        Rz= Rp.*sin(tc)*sin(psi)*exp(-j*delta/2);
        Tx= Tp.*cos(ts)*sin(psi)*exp(-j*delta/2);
        Ty= Ts          *cos(psi)*exp(+j*delta/2);
        Tz= Tp.*sin(ts)*sin(psi)*exp(-j*delta/2);
        IR=IRs*cos(psi)^2 + IRp*sin(psi)^2;
        IT=ITs*cos(psi)^2 + ITp*sin(psi)^2;
    end

else,

    psi=psi*deg;
    ux0=sin(psi)*cos(theta0)*cos(phi0)*exp(-j*delta/2) ...
      - cos(psi)             *sin(phi0)*exp(+j*delta/2);
    uy0=sin(psi)*cos(theta0)*sin(phi0)*exp(-j*delta/2) ...
      + cos(psi)             *cos(phi0)*exp(+j*delta/2);
    Kxy=Kx*Ky;
    Kyzc=Kysq+Kzcsq;
    Kyzs=Kysq+Kzssq;
```

152

```
    Kxzc=Kxsq+Kzcsq;
    Kxzs=Kxsq+Kzssq;
    Eye=eye(NumOrds);


        epsg    = ng^2;                       % Groove permittivity
        epsr    = nr^2;                       % Ridge permittivity
        epsG    = (1-FilFac)*epsg + FilFac*epsr; % average grating permittivity
        iepsG   = (1-FilFac)/epsg + FilFac/epsr; % average inverse grating
permittivity
    Sinc    = sin(pi*FilFac*[ 1:M])./(pi*[ 1:M]);

        vm      = (  epsr -   epsg)*fliplr(Sinc);
        v0      = epsG;
        vp      = (  epsr -   epsg)*Sinc;
        v       = [vm v0 vp].*exp(-j*2*pi*Disp*[-M:M]);
        Epsilon = toeplitz(fliplr( v(1:NumOrds)), v(NumOrds:2*NumOrds-1));
    Epsilon_I=inv(Epsilon);

        ivm     = (1/epsr - 1/epsg)*fliplr(Sinc);
        iv0     = iepsG;
        ivp     = (1/epsr - 1/epsg)*Sinc;
        iv      = [ivm iv0 ivp].*exp(-j*2*pi*Disp*[-M:M]);
    Alpha   = toeplitz(fliplr(iv(1:NumOrds)),iv(NumOrds:2*NumOrds-1));
    Alpha_I=inv(Alpha);
        A   = Kxsq - Epsilon;
     B  = Kx*(Epsilon\Kx) - Eye;

    Ainv=inv(A);
    Binv=inv(B);
    [Ws,Vs]=eig(Kysq + Kx*Epsilon_I*Kx*Alpha_I - Alpha_I);
    [Wu,Vu]=eig(A+Kysq);
    Qs=sqrt(Vs);
    Qu=sqrt(Vu);
    clear Vu Vs
    Dx=Zv; Dx(p)=ux0;
    Dy=Zv; Dy(p)=uy0;
    Es=expm(-k0*Qs*depth);
    Eu=expm(-k0*Qu*depth);
    X25=-Ainv*Kxy*Ws;
    X27= Ainv*Wu*Qu;
    X37= j*Kzc*Wu;
    X45= j*Kzc*Binv*Ws*Qs;
    X47=-j*Kzc*Binv*Kx*Epsilon_I*Ky*Wu;
    X78=-j*Kzs*Wu;
    X86= j*Kzs*Binv*Ws*Qs;
    X88= j*Kzs*Binv*Kx*Epsilon_I*Ky*Wu;
    X=[Eye,   Zm,    Zm,    Zm,    -Ws,    -Ws*Es,  Zm,       Zm;
       Zm,    Eye,   Zm,    Zm,    X25,    X25*Es, X27,    -X27*Eu;
       Kxy,   Kyzc,  Zm,    Zm,    Zm,      Zm,     X37,     X37*Eu;
       Kxzc,  Kxy,   Zm,    Zm,    X45,    -X45*Es, X47,     X47*Eu;
       Zm,    Zm,    Eye,   Zm,    -Ws*Es, -Ws,     Zm,       Zm;
       Zm,    Zm,    Zm,    Eye,   X25*Es, X25,    X27*Eu, -X27;
       Zm,    Zm,    Kxy,   Kyzs,  Zm,      Zm,     X78*Eu,  X78;
       Zm,    Zm,    Kxzs,  Kxy,   -X86*Es, X86,    X88*Eu,  X88];
    RHS=[-Dx;-Dy;Kxy*Dx + Kyzc*Dy; Kxzc*Dx + Kxy*Dy; Zv; Zv; Zv; Zv];
    F=inv(X)*RHS;
    Rx=F(1:NumOrds,1); Ry=F(NumOrds+1:2*NumOrds,1);
    Tx=F(2*NumOrds+1:3*NumOrds,1); Ty=F(3*NumOrds+1:4*NumOrds,1);
    bad_indices=find(kzc==0); kzc(bad_indices)=-j*1e-16*ones(size(bad_indices));
    Rz=-(Rx.*kx + Ry.*ky)./kzc;
    bad_indices=find(kzs==0); kzs(bad_indices)=-j*1e-16*ones(size(bad_indices));
    Tz=-(Tx.*kx + Ty.*ky)./kzs;
    IR = (abs(Rx).^2 + abs(Ry).^2 + abs(Rz).^2).* real(kzc./kzc(p)) * 100;
    IT = (abs(Tx).^2 + abs(Ty).^2 + abs(Tz).^2).* real(kzs./kzc(p)) * 100;
end

%     Sum the efficiencies.

%SUM=sum(IR+IT);


Eff_mat=[I,IR,IT];
```

153

B.3 Grating Coupler Analysis

B.3.1   Description

I now briefly describe the MATLAB code implementation for analyzing a grating coupler. The overall process is to first specify the fixed parameters of the problem, calculate the propagation constant of the waveguide without the grating, define the variable grating parameters, calculate α_r, and finally calculate the power distribution into each diffractive order.

The basic parameters of the problem are set in the file *mlayer_in*. The basic parameters that need to be set are listed in Table B.8.2.

Table B.8.2 Description of variables that must be declared in MATLAB script mlayer_in.m

lambda0	free space wavelength
FilFac	fill factors for grating layers
Disp	ridge displacements of grating layers
NumOrds	number of orders retained in analysis

Additionally the following global variables need to be declared and set.

Table B.8.3 Additional global variables that must be declared in MATLAB implementation of grating coupler analysis

lr	free space wavelength
nf	refractive index of waveguide
nc	refractive index of cover
ns	refractive index of substrate
ngrat	refractive index of grating
h	height of waveguide

Additional global variables that are determined later in the code, but must be declared are listed below.

154

Table B.8.4 Additional global variables in MATLAB implementation

Depth	depth vector = [grating depth, waveguide depth]
KX	the grating vector

The first step is to calculate the guided mode propagation constant of the waveguide. This is done with the file *temode.m* to calculate k_{x0}. This file requires the optimization toolbox, and calls the function *te.m* to perform the optimization. The output of *temode.m* is the effective index of refraction for the guided mode, Neff and the propagation constant kxo.

The next step is to specify the grating. Often these values are adjusted in a loop. The variables describing the grating that need to be set at this point are

Table B.8.5 variables to specify important grating parameters

theta	angle of incidence in degrees
KX1	the grating vector
period	the grating period
d	the grating height

After the grating is described, the next step is to begin finding the complex propagation constant. The complex propagation constant is stored in a variable u2 with u2(1) being the real part of the propagation constant, and u2(2) being the imaginary part. We need an initial guess, and the best guess is to set u2(1) equal to kxo as solved from *temode.m*. A good starting guess for u2(2) depends on the description of the grating. Usually a good starting point would be to set the grating height to a small value and give an initial guess for u2(2) of 0, and gradually increase the grating depth. At each grating depth level, a good initial guess is the value of

155

u2(2) calculated from the previous level, or a projected value based on a curve fit of the previously calculated values. This process is repeated until the desired level is reached. The file that is used to find the complex propagation constant is called *find_eff*. This file does an optimization routine, and the function that is used in the optimization is called *intfun.m*. The function *intfun.m* calls the function that does the rigorous coupled wave analysis solving, which in this development is called *mlayer.m*. The program *mlayer.m* uses the parameters set in the file *mlayer_in.m*. The input to the rigorous coupled wave solver is the variable beta, the complex propagation constant. The output of the rigorous coupled wave solver is the variable Ro, which, in the optimization routine, we want to be very large. After the optimization routine is over, *find_eff.m* returns the optimal value of the propagation constant in the variable u2. The value of u2(1) is β, the real part of the propagation constant, and the value of u2(2) is α_r the radiation decay parameter and imaginary part of the propagation constant.

The last step is to calculate the power distribution ratios. The program *pwr_surf.m* uses the variables beta and KX to calculate the efficiencies of the beams diffracted into the cover and substrate. The efficiencies of the beams in the cover are returned in the variables R1-R2, and the efficiencies of the beams in the substrate are returned in the variables T1-T3.

A summary of this computational process is given in Figure B.2.

specify general
parameters

↓

calculate propagation constant
without grating ⟷ **temode.m**
output: Neff, kxo ⟷ **te.m**

↓

setup variable
grating parameters

↓

calculate
α,β ⟷ **find_eff.m**
output: u ⟷ **intfun.m**
input: u
output: 1/Ro ⟷ **mlayer.m**
calls **mlayer_in.m**
input: beta
output: Ro

↓

calculate power
distributions ⟷ **pwr_surf.m**
input: KX1, beta
output: Ri, Ti
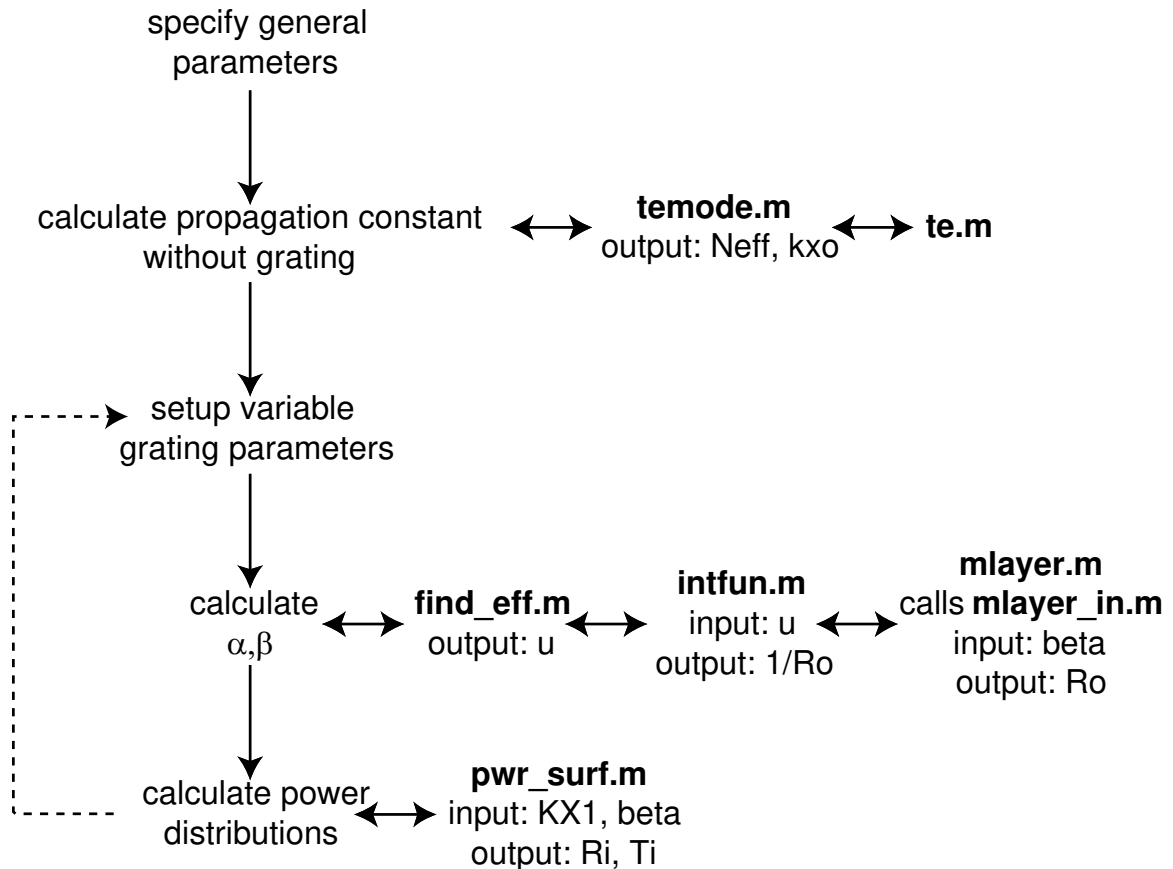
Figure B.2 Computational process for MATLAB implementation to solving for complex propagation constant in grating coupler

B.3.2 example.m

```
% This file contains an example of the calculation of
% a surface relief grating coupler
%
fprintf(1,'This file contains instructions and an example\n')
pause

%set up global vaiables
global lr h nf ns nc KX depth ngrat

fprintf(1,'(1) Set up the basic parameters\n')
fprintf(1,'change the following parameters in the file mlayer_in.m\n')
fprintf(1,'lambda0,nc,ns,FilFac,Disp,NumOrds\n')
pause

fprintf(1,'set the following paramters\n')
fprintf(1,'lr: wavelength\n')
fprintf(1,'nf: waveguide index\n')
fprintf(1,'nc: cover index\n')
fprintf(1,'ns:substrate index\n')
fprintf(1,'ngrat: grating index\n')
fprintf(1,'depth: waveguide and grating thickness (depth=[grating, waveguide])\n')
lr=1
ko=2*pi/lr;
nf=1.5
nc=1
ns=1.46
ngrat=1.5
```

157

```
h=1
pause
depth(2)=h

fprintf(1,'(2) Calculate guided mode propagation constant\n')
fprintf(1,'run temode.m to calculate kxo (requires optimization toolbox)\n')
fprintf(1,'this program is for a single layer slab waveguide with TE polarization\n')
fprintf(1,'the grating will change the effective index but it is initially
ignored.\n')
pause
temode
pause

fprintf(1,'(3) Specify the grating\n')
fprintf(1,'   KX1=2*pi/period: the grating vector \n')
fprintf(1,'      (KX1 can be a vector)\n')
fprintf(1,'   d: the grating height\n')
fprintf(1,'      (d is a vector the same length as KX1)\n')

fprintf(1,'design the grating to have an outcoupled angle of 5 degrees\n')
pause

theta=5
fprintf(1,'ko*sin(theta)=Neff*ko-KX1\n')
KX1=Neff*ko-ko*sin(theta*pi/180)
period=2*pi/KX1
d=0.1*ones(size(KX1));
pause

fprintf(1,'(4) Calculate alpha\n')
fprintf(1,'u2=beta+j alpha\n')
fprintf(1,'set u2(1)= kxo (from temode)\n')
fprintf(1,'guess a value for u2(2) (u2(2)=-2)\n')
pause

%beta=u2(1)+j*u2(2)/1000;
%alpha=imag(u2)*1000

ui=[]; %the imaginary part
ur=[]; %the real part

u2(1)=kxo; %the guess is the propagation constant of the original waveguide
u2(2)=-2;
for lp=1:length(KX1)
        KX=KX1(lp);
    depth(1)=d(lp);
        find_eff %a file that finds the complex propagation constant
        lp
    %intfun(u2) calculates the resonance that should be close to zero
        if intfun(u2)>.001
                fprintf(1,'Could not find resonance\n')
                fprintf(1,'You need to play around with u2 until you find the
resonance\n')
        end
        ur(lp)=u2(1);
        ui(lp)=u2(2);
end
fprintf(1,'alpha in mm^{-1}\n')
ui
pause

fprintf(1,'(5) Calculate R1,R2,T1,T2,T3\n')
fprintf(1,'run pwr_surf.m\n')
pause
pwr_surf %a file that calculates the power distribution ratios
        % R1 is the first order into air (this is the desired order)
        % R2 is the second order into air (should be zero for this problem)
        % T1 T2 T3 are the orders into the glass substrate




fprintf(1,'(6) What is the fraction of the total outcoupled power (Po=1)\n')
fprintf(1,'Pout=1-exp(-2*alpha*L)\n')

fprintf(1,'What is coupler length for an outcoupled power .99\n')
fprintf(1,'Pout=.99=1-exp(-2*alpha*L)\n')

L=log(.01)/(2*ui) %units of mm
```

B.3.3 mlayer_in.m

```
%
% TE Multilayer test cases
%
%
global period
NumOrds=21;

nc     = 1.0;           % Region 1 refractive index
ns     = 1.46;                 % Region 3 refractive index
nf     = 1.5;

%   Grating region parameters

Ngrat  = 2;                    % Number of gratings
Period = 0.8;                  % Grating period in microns for all gratings
depth  = [.1,1.15];            % grating depths in microns
ng     = [nc,nf];              % Groove indicies
nr     = [ngrat,nf];           % Ridge indices
FilFac = [.5,.5];              % Filling factors
Disp   = [0,0];                % Ridge displacements in fractions of 1 Period

%   Angle of incidence and wavelength information

lambda0 = lr;  % Freespace wavelength in microns
theta0  = 0;               % Polar angle of incidence (deg)
phi0    = 0;               % Azimuthal angle of incidence (deg)
psi_    = 0;               % Polarization angle (deg): 0 => TE,  90 => TM
delta   = 0;               % Input wave retardation phase from TE to TM (deg)
D=Disp;
F=FilFac;
```

B.3.4 temode.m

```
global lr h nf ns nc

Neff=[];
kxo=[];
no=100;

%lr=.85;
%h=1;
%nf=1.54;
%ns=1.456;
%nc=1.0;


nn1=min([nc,ns]);
nn2=max([nc,ns]);

ko=2*pi/lr;

stp=.0001;

while no~=length(kxo)

        N=nn2:stp:nf;
        kfx=ko.*sqrt(nf^2-N.^2);
        gc=ko.*sqrt(N.^2-nc^2);
        gs=ko.*sqrt(N.^2-ns^2);

        BB1=tan(kfx.*h);
        BBtop=kfx.*(gs+gc);
        BBbot=kfx.^2-gs.*gc;

        BB2=BBtop./BBbot;

    %Plot result
        plot(N,BB1,'b')
        hold
        plot(N,BB2,'r')
        hold
        axis([nn2 nf -30 30])
        zoom 'on'
        grid 'on'
```

159

```
                hc=(pi+atan(sqrt((nn2^2-nn1^2)/(nf^2-nn2^2))))/(2*pi/lr*sqrt(nf^2-nn2^2));
                V=2*pi*h/lr*sqrt(nf^2-nn2^2);
                ate=(nn2^2-nn1^2)/(nf^2-nn2^2);
                no=floor(1+1/pi*(V-atan(sqrt(ate))));

                BB=BB1-BB2;
                sBB=sign(BB);
                dBB=diff(sBB);
                I=find(abs(dBB)>0);
                if I(1)==1
                        I(1)=2;
                end
                J=find(sign(BB1(I-1))-sign(BB1(I+1))==0 & sign(BB2(I-1))-sign(BB2(I+1))==0);
                I=I(J);

                for kxoind=1:max(size(I))
                        Neff(kxoind)=fminbnd('te',N(I(kxoind)-1),N(I(kxoind)+1));
                        kxo(kxoind)=Neff(kxoind)*ko;
                end
                Neff

                stp=stp*.1;
        end

clear BB1 BB2 BBtop BBbot kfx N gc gs nn1 nn2 no
clear BB sBB dBB I J stp kxoind stp I J ate ans V
```

B.3.5 te.m

```
function ans=te(N)

global NumOrds lr depths ns epsmods KX KZS layers nsub ncov u2

global h
nf = ns;
nc = ncov;

ko=2*pi/lr;


kfx=ko.*sqrt(nf^2-N.^2);
gc=ko.*sqrt(N.^2-nc^2);
gs=ko.*sqrt(N.^2-nsub^2);

ans=abs(tan(kfx.*h)-(kfx.*(gs+gc))./(kfx.^2-gc.*gs));
```

B.3.6 find_eff.m

```
% FIND_EFF.M finds the complex quality beta0 for a
% given grating vector KX, and depth
%
% The resonance is narrow, thus a good starting point is needed.
% Loop the real part and then the imaginary part until a good
% starting point is reached then do the optimization
%

global lr h nf ns nc KX depth ngrat

% define upper and lower search bounds
vlb=[9. -90];
vub=[19 0];
options(1)=0;
options(2:3)=[1e-7 1e-7];
options(14)=200;
options(16)=1e-22;
options(17)=1e-6;

if intfun(u2)<.7
        ff=constr('intfun',u2,options,vlb,vub);
        if (ff(1)>(u2(1)-.01) & ff(1)<(u2(1)+.01))
                done=1;
                u2=ff;
        end
end

mm=100;
```

```
str=-.1;
endr=.1;
sti=-.5*u2(2);
endi=.5*u2(2);
done=2;
pass=1;
exit_it=1;

streal=str;
endreal=endr;
stimag=sti;
endimag=endi;


while intfun(u2)>1e-5 & exit_it~=2

% Vary the imaginary part of u2
        for jj=1:mm;
                u=u2;
                nn=stimag+2*endimag/mm*(jj-1);
                u(2)=u2(2)+nn;
                f1(jj)=intfun(u);
                fi1(jj)=u(2);
        end
        subplot(2,1,1)
        plot(fi1-u2(2),f1,'b')
        title(['u2(2) = ',num2str(u2(2))])
        pause(1)

% Find the minimum value
        II=find(f1==min(f1));
        II=II(1);
% If the minium value in not an end point
% make it the new imaginary part and reduce the search range
        if II~=1 & II~=100
                u2(2)=fi1(II);
                stimag=fi1(max([II-3,1]))-u2(2);
                endimag=-stimag;

% If the minimum is at an end point
        elseif II==1
                u2(2)=fi1(II);
                endimag=5*(fi1(100)-u2(2));
                stimag=-endimag;
                done=3;
        elseif II==100
                u2(2)=fi1(II);
                stimag=5*(fi1(1)-u2(2));
                endimag=-stimag;
                done=3;
        end

% If the value is low enough do the optimization

        if intfun(u2)<.7
                ff=constr('intfun',u2,options,vlb,vub);
                if (ff(1)>(u2(1)-.01) & ff(1)<(u2(1)+.01))
                        done=1;
                        u2=ff;
                end
        end

        if done~=1

% Vary the real part of u2
                for jj=1:mm;
                        u=u2;
                        nn=streal+2*endreal/mm*(jj-1);
                        u(1)=u2(1)+nn;
                        f2(jj)=intfun(u);
                        fr1(jj)=u(1);
                end
                subplot(2,1,2)
                plot(fr1-u2(1),f2,'b')
                title(['u2(1) = ',num2str(u2(1))])
                pause(1)

% Find the minimum
                KK=find(f2==min(f2));
                KK=KK(1);
        % If not an end point
```

161

```
                            if KK~=1 & KK~=100
                                    u2(1)=fr1(KK);
                                    streal=fr1(max([KK-3,1]))-u2(1);
                                    endreal=-streal;
              % If an endpoint
                            elseif KK==1
                                    endreal=5*(fr1(100)-u2(1));
                                    streal=-endreal;
                                    if pass==1 & done==3
                                            exit_it=2;
                                            fprintf(1,'error\n')
                                    end
                            elseif KK==100
                                    streal=5*(fr1(1)-u2(1));
                                    endreal=-streal;
                                    if pass==1 & done==3
                                            exit_it=2;
                                            fprintf(1,'error\n')
                                    end
                            end

% Do the optimization if value low enough
                    if intfun(u2)<.7
                            ff=constr('intfun',u2,options,vlb,vub);
                            if (ff(1)>(u2(1)-.01) & ff(1)<(u2(1)+.01))
                                    done=1;
                                    u2=ff;
                            end
                    end

        end
        pass=pass+1; % The number of passes

        if pass>10 % Give up too many passes
                exit_it=2;
        end
end


clear f1 f2 ff fi1 fr1 str sti streal stimag endi endr
clear endreal endimag KK II exit_it done mm  pass jj nn
```

B.3.7   intfun.m

```
function [f,g]=intfun(u)

global lr h nf ns nc KX depth ngrat

beta0=u(1)+j*u(2)/1000;  %the complex propagation constant to be optimized

f=abs(1/mlayer(beta0));

% the contraints for the optimization
g(1)=-u(1)+8.; %Re(beta0)>10
g(2)=u(1)-16;  %Re(beta0)<16
g(3)=u(2);     %Imag(betao)<0
g(4)=-u(2)-100;        %Imag(beta0)>-100

return
```

B.3.8   mlayer.m

```
function ANS=mlayer(beta0)

%       MLAYER computes the diffracted amplitudes of a multilayer
%       lamellar surface-relief grating for an arbitrarily polarized unit
%       amplitude wave, incident from an arbitrary angle and plane
%       of incidence in an isotropic lossless cover medium.  The grating
%       and substrate media can be lossy, but must be isotropic.
%       The analysis is Rigorous Coupled Wave Analysis, as presented in
%
%       M. G. Moharam, E. B. Grann, D. A. Pommet, and
%       T. K. Gaylord "Formulation for stable and efficient
%       implementation of the rigorous coupled-wave analysis
%       of binary gratings," J. Opt. Soc. Am. A, vol. 12,
%       pp. 1068-1076, May 1995.
```

162

```
%
%        and
%
%        M. G. Moharam, E. B. Grann, D. A. Pommet, and
%        T. K. Gaylord "Stable implementation of the rigorous
%        coupled-wave analysis of surface-relief gratings:
%        enhanced transmittance matrix approach," J. Opt. Soc.
%        Am. A, vol. 12, pp. 1068-1076, May 1995.
%
%        Usage is ANS=Mlayer(beta0)
%
%        where beta0 is the complex propagation constant,
%        and ANS contains the zero order reflected complex amplitude
%
%        User must edit mlayer_in.m to set up the input parameters.
%
%        Author: Dave Brundrett
%
%        Revised by Stephen M. Schultz
%


%   Define the program constants.

global lr h nf ns nc KX depth ngrat
          % add any variables here and in INTFUN.M and in FIND_EFF.m
              % remove the variables from MLAYER_IN.M

j=sqrt(-1);
deg=pi/180;
t0=clock;

mlayer_in;

%   Define the dimensioning variables

Nmax   = (NumOrds-1)/2;          % NumMax is the highest order number retained,
I      = (-Nmax:Nmax)';          % I is the order index,
p      = (NumOrds+1)/2;          % and p is the index of the zeroth order.

%   Set up the input variables

%   Change angles to radians

%theta0=theta0*deg;
phi0=phi0*deg;
delta=delta*deg;

%   Define the relative permittivities

epsc    = nc^2;                            % Cover      relative permittivity
epss    = ns^2;                            % Substrate relative permittivity

%   Define the grating vector and the wavevectors
k0  = 2*pi/lambda0;                            % Freespace wavevector
%K  = 2*pi/Period;                       % Grating vector
K   = KX;

kc  = k0*nc;                               % Region 1 wavevector components
%kx = kc*sin(theta0)*cos(phi0) - I*K;
%ky = kc*sin(theta0)*sin(phi0)*ones(size(kx)); %
kx  = beta0-I*K;
ky  = zeros(size(kx));

kzc = sqrt(kc^2 - kx.^2 - ky.^2);          %
bad_indices=find((real(kzc)-imag(kzc))<0);     % locate incorrect signs
kzc(bad_indices)=-kzc(bad_indices);            % correct the signs

ks  = k0*ns;                             % Region 3 wavevector components
kzs = sqrt(ks^2 - kx.^2 - ky.^2);          %
bad_indices=find((real(kzs)-imag(kzs))<0);     % locate incorrect signs
kzs(bad_indices)=-kzs(bad_indices);            % correct the signs

%   Define the diffraction angles

tc = -atan2(kx,kzc);                 % Cover      order polar angles
ts = -atan2(kx,kzs);                 % Substrate order polar angles

if abs(phi0) > 1e-6,            % Diffraction plane azimuthal angles
   phi_d=atan2(ky,kx);           %
else                            %
```

163

```
    phi_d=zeros(size(kx));          %
end                                 %

%    Define some auxillary matrices and vectors

Zm    = zeros(NumOrds,NumOrds);
Zv    = zeros(NumOrds,1);
Dv    = Zv;   Dv(p)=1;
Zv2   = [Zv;Zv];
Eye   = eye(NumOrds);
Kx    = diag(kx)/k0;
Kxsq  = Kx.^2;
Ky    = diag(ky/k0);
Kysq  = Ky.^2;
Kzc   = diag(kzc)/k0;
Kzcsq = Kzc.^2;
Kzs   = diag(kzs)/k0;
Kzssq = Kzs.^2;
M     = NumOrds-1;


%
%   Trap out planar diffraction cases, otherwise do the full-blown problem
%

if phi0==0,

    if (psi_==0|psi_==180|psi_==-180),
       psi_=psi_*deg;
       temp1=Eye;
       fmat=Eye;
       gmat=j*Kzs;
       for ii=Ngrat:-1:1,
         epsg   = ng(ii)^2;                        % Groove permittivity
         epsr   = nr(ii)^2;                        % Ridge permittivity
         epsG   = (1-FilFac(ii))*epsg + FilFac(ii)*epsr; % average grating
permittivity
         iepsG  = (1-FilFac(ii))/epsg + FilFac(ii)/epsr; % average inverse grating
permittivity
         Sinc   = sin(pi*FilFac(ii)*[ 1:M])./(pi*[ 1:M]);
         vm     = (  epsr -   epsg)*fliplr(Sinc);
         v0     = epsG;
         vp     = (  epsr -   epsg)*Sinc;
         v      = [vm v0 vp].*exp(-j*2*pi*Disp(ii)*[-M:M]);
         ivm    = (1/epsr - 1/epsg)*fliplr(Sinc);
         iv0    = iepsG;
         ivp    = (1/epsr - 1/epsg)*Sinc;
         iv     = [ivm iv0 ivp].*exp(-j*2*pi*Disp(ii)*[-M:M]);
         Epsilon = toeplitz(fliplr( v(1:NumOrds)), v(NumOrds:2*NumOrds-1));
         Alpha   = toeplitz(fliplr(iv(1:NumOrds)),iv(NumOrds:2*NumOrds-1));
          clear Sinc v iv vm iivm v0 iv0 vp ivp
%
         A      = Kxsq - Epsilon;
%        B      = Kx*Epsilon_I*Kx - Eye;
          [W,V]=eig(A);
          Q=sqrt(V);
          M0=W*Q;
          E=expm(-k0*Q*depth(ii));
          v=[W,W;M0,-M0]\[fmat;gmat];
          temp2=v(1:NumOrds,:)\E;
          temp3=E*v(NumOrds+1:2*NumOrds,:)*temp2;
          temp1=temp1*temp2;
          fmat=W+W*temp3;
          gmat=M0-M0*temp3;
       end
       gfi=gmat/fmat;
       RHS=-gfi(:,p); RHS(p)=RHS(p) + j*kzc(p)/k0;
       Rs=[gfi + j*Kzc]\RHS;
       Ts=(temp1/fmat)*(Rs + Dv);
%      [Rs Ts]
       Rx=Zv;
       Ry=Rs*cos(psi_)*exp(+j*delta/2);
       Rz=Zv;
       Tx=Zv;
       Ty=Ts*cos(psi_)*exp(+j*delta/2);
       Tz=Zv;
       IR=(abs(Rs).^2)  .* real(kzc ./ kzc(p)) * 100;
       IT=(abs(Ts).^2)  .* real(kzs ./ kzc(p)) * 100;
 elseif (psi_==90|psi_==-90),
       psi_=psi_*deg;
       temp1=Eye/ns;
```

164

```
        fmat=Eye;
        gmat=j*Kzs/ns^2;
        for ii=Ngrat:-1:1,
          epsg    = ng(ii)^2;                               % Groove permittivity
          epsr    = nr(ii)^2;                               % Ridge permittivity
          epsG    = (1-FilFac(ii))*epsg + FilFac(ii)*epsr; % average grating
permittivity
          iepsG   = (1-FilFac(ii))/epsg + FilFac(ii)/epsr; % average inverse grating
permittivity
          Sinc    = sin(pi*FilFac(ii)*[ 1:M])./(pi*[ 1:M]);
          vm      = (  epsr -   epsg)*fliplr(Sinc);
          v0      = epsG;
          vp      = (  epsr -   epsg)*Sinc;
          v       = [vm v0 vp].*exp(-j*2*pi*Disp(ii)*[-M:M]);
          ivm     = (1/epsr - 1/epsg)*fliplr(Sinc);
          iv0     = iepsG;
          ivp     = (1/epsr - 1/epsg)*Sinc;
          iv      = [ivm iv0 ivp].*exp(-j*2*pi*Disp(ii)*[-M:M]);
          Epsilon = toeplitz(fliplr( v(1:NumOrds)), v(NumOrds:2*NumOrds-1));
          Alpha   = toeplitz(fliplr(iv(1:NumOrds)),iv(NumOrds:2*NumOrds-1));
          clear Sinc v iv vm iivm v0 iv0 vp ivp
%
          B       = Kx*(Epsilon\Kx) - Eye;
          [W,V]=eig(Alpha\B);
          Q=sqrt(V);
          M0=Alpha*W*Q;
          E=expm(-k0*Q*depth(ii));
          v=[W,W;M0,-M0]\[fmat;gmat];
          temp2=v(1:NumOrds,:)\E;
          temp3=E*v(NumOrds+1:2*NumOrds,:)*temp2;
          temp1=temp1*temp2;
          fmat=W+W*temp3;
          gmat=M0-M0*temp3;
        end
        gfi=gmat/fmat;
        RHS=-gfi(:,p); RHS(p)=RHS(p) + j*kzc(p)/k0/epsc;
        Rp=[gfi + j*Kzc/nc^2]\RHS;
        Tp=(temp1/fmat)*(Rp + Dv)*nc;
%        [Rp Tp]
        Rx=-Rp.*cos(tc)*sin(psi_)*exp(-j*delta/2);
        Ry= Zv;
        Rz= Rp.*sin(tc)*sin(psi_)*exp(-j*delta/2);
        Tx= Tp.*cos(ts)*sin(psi_)*exp(-j*delta/2);
        Ty= Zv;
        Tz= Tp.*sin(ts)*sin(psi_)*exp(-j*delta/2);
        IR=(abs(Rp).^2).*real(kzc./kzc(p))*100;
        IT=(abs(Tp).^2).*real(kzs./kzc(p))*100;
    else
        psi_=psi_*deg;
        [Ws,Vs]=eig(A);
        Qs=sqrt(Vs);
        M0s=Ws*Qs;
        M1s=j*Kzc*Ws;
        M2s=j*Kzs*Ws;
        [Wp,Vp]=eig(Alpha_I*B);
        Qp=sqrt(Vp);
        M0p=Alpha*Wp*Qp;
        M1p=j*Kzc*Wp/epsc;
        M2p=j*Kzs*Wp/epss;
        RHSs = Zv2; RHSs(p) = j*2*kzc(p)/k0;
        RHSp = Zv2; RHSp(p) = j*2*kzc(p)/k0/epsc;
        Es=expm(-k0*Qs*depth);
        Xs=[(M1s+M0s)    (M1s-M0s)*Es;
            (M2s-M0s)*Es (M2s+M0s)   ];
        Cs=inv(Xs)*RHSs;  Cps=Cs(1:NumOrds,1); Cms=Cs(NumOrds+1:2*NumOrds,1);
        Rs=Ws*(Cps+Es*Cms) - RHSs(1:NumOrds)/(j*2*kzc(p)/k0);
        Ts=Ws*(Es*Cps + Cms);
        IRs=(abs(Rs).^2).*real(kzc./kzc(p))*100
        ITs=(abs(Ts).^2).*real(kzs./kzc(p))*100;
        Ep=expm(-k0*Qp*depth);
        Xp=[(M1p+M0p)    (M1p-M0p)*Ep;
            (M2p-M0p)*Ep (M2p+M0p)   ];
        Cp=inv(Xp)*RHSp;  Cpp=Cp(1:NumOrds,1); Cmp=Cp(NumOrds+1:2*NumOrds,1);
        Rp=Wp*(  Cpp + Ep*Cmp) - RHSp(1:NumOrds)/(j*2*kzc(p)/k0/epsc);
        Tp=Wp*(Ep*Cpp +   Cmp)*nc/ns;
        IRp=(abs(Rp).^2).*real(kzc./kzc(p))*100
        ITp=(abs(Tp).^2).*real(kzs./kzc(p))*100;
        Rx=-Rp.*cos(tc)*sin(psi_)*exp(-j*delta/2);
        Ry= Rs *        cos(psi_)*exp(+j*delta/2);
        Rz= Rp.*sin(tc)*sin(psi_)*exp(-j*delta);
        Tx= Tp.*cos(ts)*sin(psi_)*exp(-j*delta/2);
```

165

```
        Ty= Ts            *cos(psi_)*exp(+j*delta/2);
        Tz= Tp.*sin(ts)*sin(psi_)*exp(-j*delta/2);
        IR=IRs*cos(psi_)^2 + IRp*sin(psi_)^2;
        IT=ITs*cos(psi_)^2 + ITp*sin(psi_)^2;
    end

else

    psi_=psi_*deg;
    ux0=sin(psi_)*cos(theta0)*cos(phi0)*exp(-j*delta/2) ...
      - cos(psi_)                 *sin(phi0)*exp(+j*delta/2);
    uy0=sin(psi_)*cos(theta0)*sin(phi0)*exp(-j*delta/2) ...
      + cos(psi_)                 *cos(phi0)*exp(+j*delta/2);
    Kxy=Kx*Ky;
    Kyzc=Kysq+Kzcsq;
    Kyzs=Kysq+Kzssq;
    Kxzc=Kxsq+Kzcsq;
    Kxzs=Kxsq+Kzssq;
    Eye=eye(NumOrds);
    Ainv=inv(A);
    Binv=inv(B);
    [Ws,Vs]=eig(Kysq + Kx*Epsilon_I*Kx*Alpha_I - Alpha_I);
    [Wu,Vu]=eig(A+Kysq);
    Qs=sqrt(Vs);
    Qu=sqrt(Vu);
    clear Vu Vs
    Dx=Zv; Dx(p)=ux0;
    Dy=Zv; Dy(p)=uy0;
    Es=expm(-k0*Qs*depth);
    Eu=expm(-k0*Qu*depth);
    X25=-Ainv*Kxy*Ws;
    X27= Ainv*Wu*Qu;
    X37= j*Kzc*Wu;
    X45= j*Kzc*Binv*Ws*Qs;
    X47=-j*Kzc*Binv*Kx*Epsilon_I*Ky*Wu;
    X78=-j*Kzs*Wu;
    X86= j*Kzs*Binv*Ws*Qs;
    X88= j*Kzs*Binv*Kx*Epsilon_I*Ky*Wu;
    X=[Eye,  Zm,   Zm,    Zm,    -Ws,      -Ws*Es,  Zm,        Zm;
        Zm,   Eye,  Zm,    Zm,    X25,      X25*Es,  X27,     -X27*Eu;
        Kxy,  Kyzc, Zm,    Zm,    Zm,       Zm,      X37,      X37*Eu;
        Kxzc, Kxy,  Zm,    Zm,    X45,     -X45*Es,  X47,      X47*Eu;
        Zm,   Zm,   Eye,   Zm,    -Ws*Es, -Ws,      Zm,        Zm;
        Zm,   Zm,   Zm,    Eye,   X25*Es, X25,      X27*Eu, -X27;
        Zm,   Zm,   Kxy,   Kyzs,  Zm,       Zm,      X78*Eu,   X78;
        Zm,   Zm,   Kxzs,  Kxy,  -X86*Es, X86,      X88*Eu,   X88];
    RHS=[-Dx;-Dy;Kxy*Dx + Kyzc*Dy; Kxzc*Dx + Kxy*Dy; Zv; Zv; Zv; Zv];
    F=inv(X)*RHS;
    Rx=F(1:NumOrds,1); Ry=F(NumOrds+1:2*NumOrds,1);
    Tx=F(2*NumOrds+1:3*NumOrds,1); Ty=F(3*NumOrds+1:4*NumOrds,1);
    bad_indices=find(kzc==0); kzc(bad_indices)=-j*1e-16*ones(size(bad_indices));
    Rz=-(Rx.*kx + Ry.*ky)./kzc;
    bad_indices=find(kzs==0); kzs(bad_indices)=-j*1e-16*ones(size(bad_indices));
    Tz=-(Tx.*kx + Ty.*ky)./kzs;
    IR = (abs(Rx).^2 + abs(Ry).^2 + abs(Rz).^2).* real(kzc./kzc(p)) * 100;
    IT = (abs(Tx).^2 + abs(Ty).^2 + abs(Tz).^2).* real(kzs./kzc(p)) * 100;
end

%       Sum the efficiencies.

%SUM=sum(IR+IT);

%        Form the output matrix

%ANS=[I Ry Ty];
ANS=[Ry(p)];

%fprintf('\n       Sum of efficiencies = %g %%\n',SUM)
%fprintf('        Elapsed time is %g seconds\n\n\n',etime(clock,t0))
```

B.3.9 pwr_surf.m

```
%%%%%%%%%%%%%%%%%%%%%%%%%%%%%%%%%%%%%%%%%%%%%%%%%%%%%%%%
% This program calculates the percent of the power into
% each mode
%
global lr h nf ns nc KX depth ngrat
```

```matlab
% The poynting vector is calculated at the cover and
% substrate boundaries.

mlayer_in
ii=-(NumOrds-1)/2:1:(NumOrds-1)/2;
p=(NumOrds-1)/2+1;

for jj=1:length(KX1)
        KX=KX1(jj);      %get the parameters for each point
     depth(1)=d(jj);
        jj;
        beta0=ur(jj)+j*ui(jj)/1000;
        f(jj)=abs(1/mlayer(beta0));

        rt=mlayer2(beta0);    %this function calculates the R & T
        R=rt(:,1);
        T=rt(:,2);
        R(p)=0;          % throw out non-diffracted orders
        T(p)=0;

        k1z=rt(:,3);
        k4z=rt(:,4);
        kx=real(rt(:,5));

        II=find(abs(kx)>ko*nc);                %find which orders are propagating
        JJ=find(abs(kx)>ko*ns);
        II1=find(abs(kx)<ko*nc);
        JJ1=find(abs(kx)<ko*ns)-p;
        [aa,I]=sort(abs(JJ1));
        JJ1=JJ1(I)+p;

%       R(p)=0;
%       T(p)=0;
        R(II)=zeros(size(II));
        T(JJ)=zeros(size(JJ));


%calculate the poynting vectors
        poyntr=abs(R).^2.*real(k1z);
        poyntt=abs(T).^2.*real(k4z);

%normalize the poynting vectors to sum to 1
        percr=poyntr./(sum(poyntr)+sum(poyntt));
        perct=poyntt./(sum(poyntr)+sum(poyntt));

        R1(jj)=percr(II1(1));
        T1(jj)=perct(JJ1(1));
        if length(II1)>1              %if the second order exist
                R2(jj)=perct(II1(2));
        else
                R2(jj)=0;
        end

        if length(JJ1)>2              %if the second order exist
                T3(jj)=perct(JJ1(3));
                T2(jj)=perct(JJ1(2));
        elseif length(JJ1)>1
                T3(jj)=0;
                T2(jj)=perct(JJ1(2));
        else
                T3(jj)=0;
                T2(jj)=0;
        end
end

if max(f)>1e-3
        'There is an error'
        'f > 1e-3'
        II=find(f>1e-3)
end

clear JJ II II1 JJ1 poyntr poyntt k1z k4z percr perct R T sz jj beta0
clear ans rt phi0 psi theta0
```
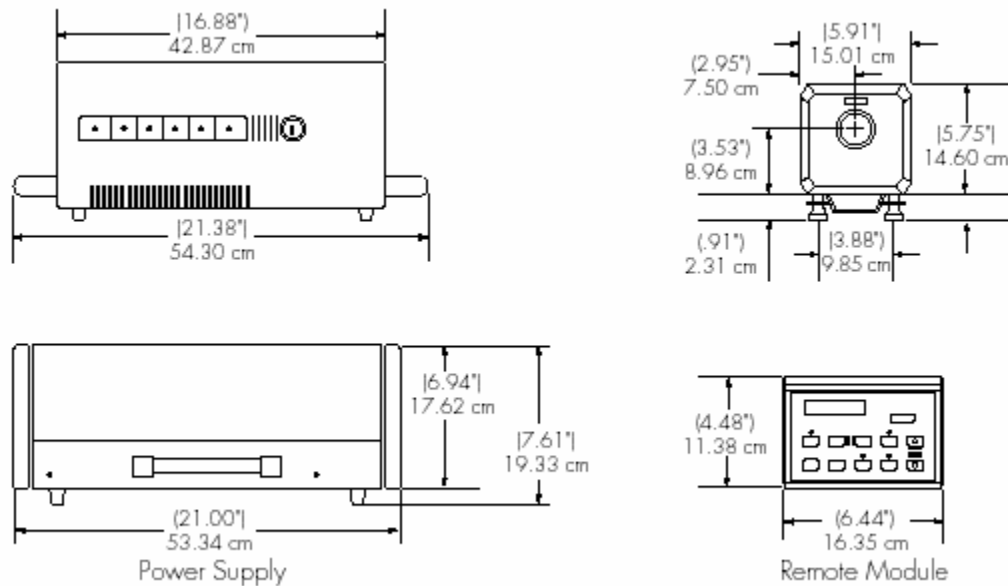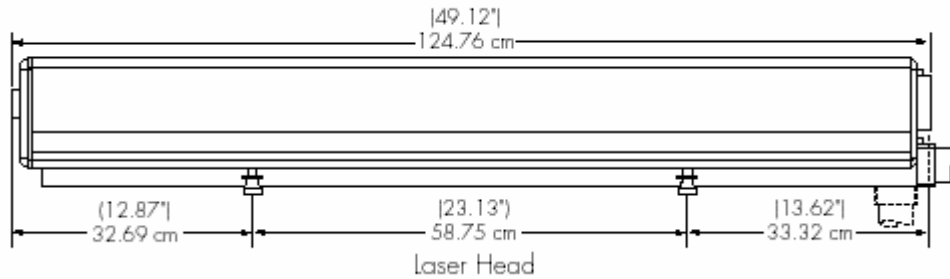
Appendix C

C   List of Components

        This appendix includes most of the optics and components used in our
recording assembly. Some of the mounts for the optics are also included. Not
included are posts, post holders and bases used to hold the optics on the table.

C.1   COHERENT INNOVA 306C Argon Laser

49.12"
124.76 cm

(12.87")
32.69 cm

(23.13")
58.75 cm

(13.62")
33.32 cm

Laser Head

	Multiline Visible	Single-line 488.0nm, TEM00	Single-line 514.5nm, TEM00
Output Power (W)	6	1.8	2.4

Standard Single-line Power Specifications

Argon Wavelength (nm)	1090	528.7	501.7	496.5	476.5	472.7	465.8	457.9	454.5	333.6-363.8	351.1	363.8
TEM_{00} Output Power (W)	0.07	0.42	0.48	0.72	0.72	0.24	0.18	0.42	0.14	0.5	0.17	0.17

Optional Single-line Power Specifications

Maximum Tube Discharge Current	Minimum Tube Discharge Current	
	High Field	Low Field
50 Amps	20 Amps	15 Amps

Maximum/Minimum tube Current

| Long-Term Power Stability		
	30 Min. Period	**8 Hour Period**
Light Regulation Mode		
With PowerTrack[1]	± 0.5%	± 1.0%
Without PowerTrack[2]	± 0.5%	N/A
Current Regulation Mode		
With PowerTrack[1]	± 1.0%	± 1.0%
Without PowerTrack[2]	± 2.0%	N/A
Beam Pointing Stability[2]		
Angle	< 5 μrad/°C change in air or water temperature	
Offset	< 5 μm/°C change in air or water temperature	
Optical RMS Noise[3]		
All models	0.20%	
Notes: (1) After fifteen minute warm-up (2) After one hour warm-up (3) Measured with a 10 Hz to 2 MHz photo diode at 514.5 nm		

Power Stability, Beam Pointing Stability and Noise Specifications

Characteristic	TEM_{00} Beam Measurement @ 514.5 nm

Beam Diameter @ 1/e² points at output mirror	1.5 mm	
Virtual Beam Waist Location (measured from the output mirror towards the high reflector)	1.2 m	
Beam Divergence (full angle)	0.5 mrad	
Cavity Length		
Single-line	1.16 m	
Multiline	1.14 m	

Beam Parameters

C.2   Newport 845HP Electronic Shutter System
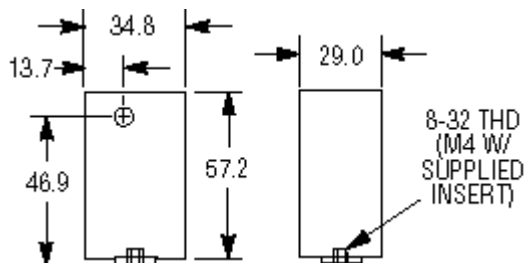
Specifications

Shutter		
Aperture	5.6 mm	
Height	46.9 mm	
Maximum Optical Power	5 W CW	
Cable	2.44 m (8 ft) terminated in a 4-pin DIN connector	
Electrical Input	Positive or negative pulse with 5-30 V amplitude into 13 Ω	
Dimensions [in. (mm)]	2.25 x 1.35 x 1.14 (57.2 x 34.3 x 29)	
Controller		
Shutter Response Time	<3 msec	
Exposure Duration	10 msec–990 sec	
Timing Accuracy	0.05% ± 10 μsec	
Maximum Repetition Rate	10 Hz	
Operating Modes	TIME:	Timed shutter opening
Operating Modes	MANUAL:	Open and close shutter independent of time setting
Operating Modes	START:	Initiates time or manual exposure
Operating Modes	RESET:	Closes shutter
Operating Modes	DELAY:	Optional 10 sec delay before shutter opening
Pushbutton Cable [ft (m)]	8 (2.44)	
Power Requirements	115 VAC at 100 mA or 230 VAC at 50 mA	
Dimensions [in. (mm)]	3.25 x 6.00 x 6.25 (82.6 x 152.4 x 158.8)	

C.3 Newport 10RP02-08 Quartz λ/2 Plate @ 354.7 nm
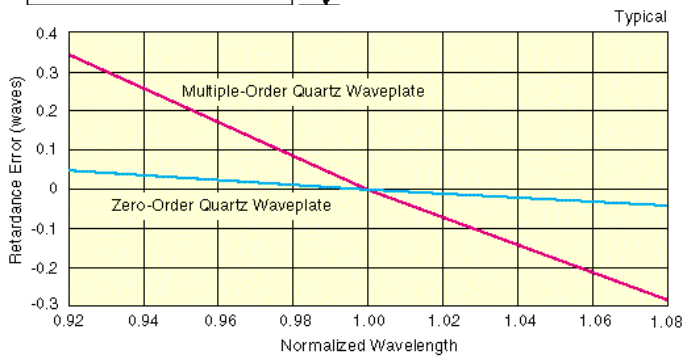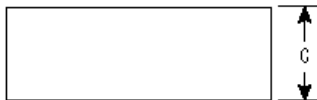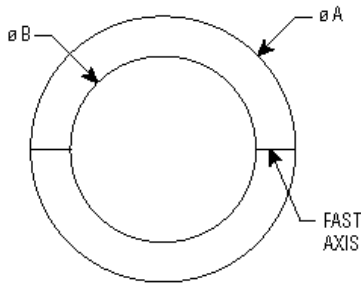
	Dimension (mm)		
Model	øA	øB	C
10RP	25.4	15.0	9.7

Specifications

Material	Quartz, schlieren grade
Construction	Two plates, air spaced
Retardation	λ/4 or λ/2
Retardation Accuracy	±λ/300
Wavefront Distortion	≤λ/10 at 632.8 nm over the full aperture
Surface Quality	10-5 scratch-dig
Wedge	<1 arc sec
Diameter Tolerance	+0/-0.076 mm
Inside Diameter Tolerance	+0.25/-0 mm
Thickness Tolerance	+0/-0.25 mm
Antireflection Coating	Laser Line V-coating, R <0.25%
Cleaning	Non-abrasive method, acetone or isopropyl alcohol on lens tissue recommended, caution: fragile, thin optic
Damage Threshold	2 MW/cm^2 CW, 2 J/cm^2 with 10 nsec pulses, typical

C.4   Newport RSP-1T Rotation Stage
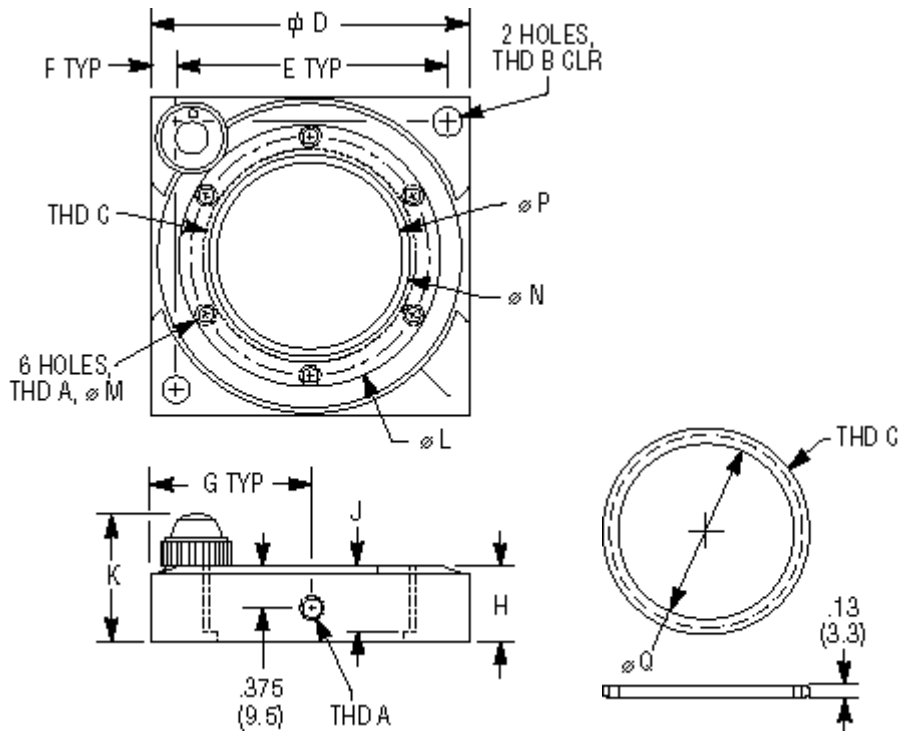
	Thread			Dimension [in. (mm)]											Thread
Model	A	B	C	D	E	F	G	H	J	K	L	M	N	P	Q	R
RSP-1T	8-32	1/4-20	1.063-20	2.5	2.0	0.25	1.25	0.56	0.50	1.07	2.18	1.375	1.01	0.875	0.755	8-32

Specifications

	RSP-1, RSP-1T
Rotation per knob turn	60°
Sensitivity (arc min)	4
Load Capacity [lb (N)]	10 (44.5)
Maximum Off-Axis Load (horiz.) [in-lb (Nm)]	35 (4)
Maximum Drive Torque [in-lb (Nm)]	10 (1.2)
Runout (radial and axial) [in. (μm)]	<0.001 (25)

C.5 Newport 900 3-Axis Spatial Filter
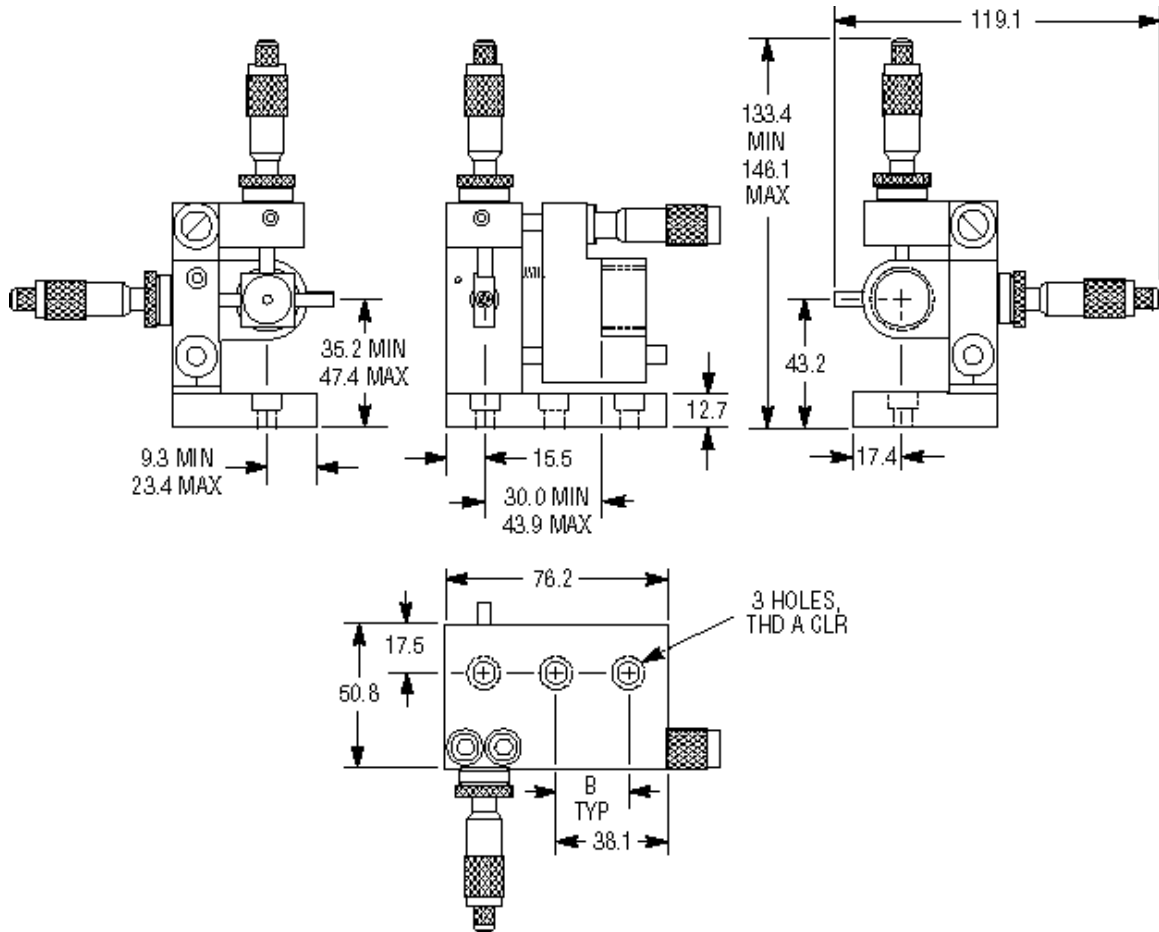
	Thread	Dimension [in. (mm)]
Model (Metric)	A	B
900 (M-900)	1/4-20 (M6)	25.4 (25.0)

Specifications

	Travel Range (mm)	Resolution (μm)
X axis	13	<2
Y axis	13	<2 μm
Z axis, optical	13	<2 mm

C.6 Newport M-10X Objective Lens

Model	Magnification	Numerical Aperture (NA)	Focal Length (mm)	Working Distance (mm)	Clear Aperture (mm)
M-10X	10x	0.25	16.5	5.5	7.5

C.7 Newport 900PH-5 5 micron pinhole

Specifications

Material	Molybdenum
Outside Diameter	9.525 ±0.125 mm
Thickness	15.24 μm (13 μm for 1 μm aperture)
Mounting Thread	0.875-20 (910PH Series)
Damage Threshold	75 MW/cm^2 CW, 700 mJ/cm^2 with 10 nsec pulses, typical
Aperture Diameter (μm)	5 ±0.75

C.8 Melles Griot 03 PBS 127 Polarizing Beamsplitter Cube
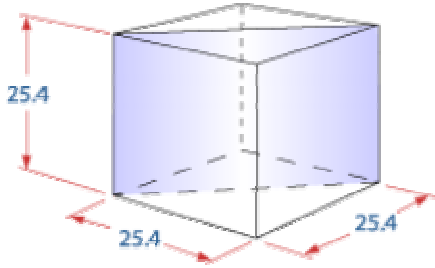
dimensions in mm
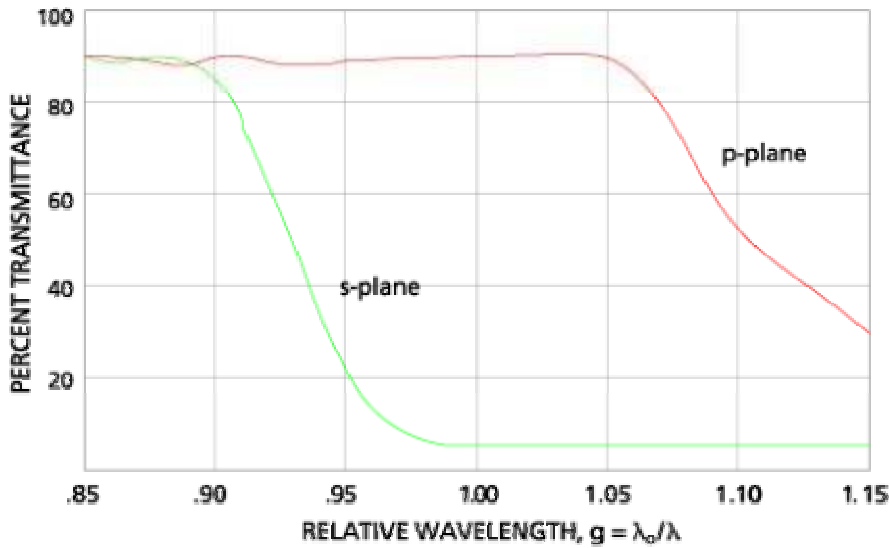
Specifications:

Dimension:	25.4 ± 0.3 mm
Material	UV grade synthetic fused silica
Wavelength (nm)	351
Principal Transmittance	>90% for p polariztion
Principal Reflectance	>95% for s polariztion
Surface Quality	20-10 scratch and dig
Transmitted Wavefront Distortion	$<\lambda/2$ at 632.8 nm
Entrance/Exit Face Flatness	$<\lambda/8$ at 632.8 nm
Beam Deviation	<5 arc minutes
Transmission (straight through)	46%
Transmission (polarizer pair)	41%
Extinction Ratio	0.05
Coating	Laser-line multilayer antireflector with R <0.2

C.9 Newport CH-1 Beamsplitter Cube Mount
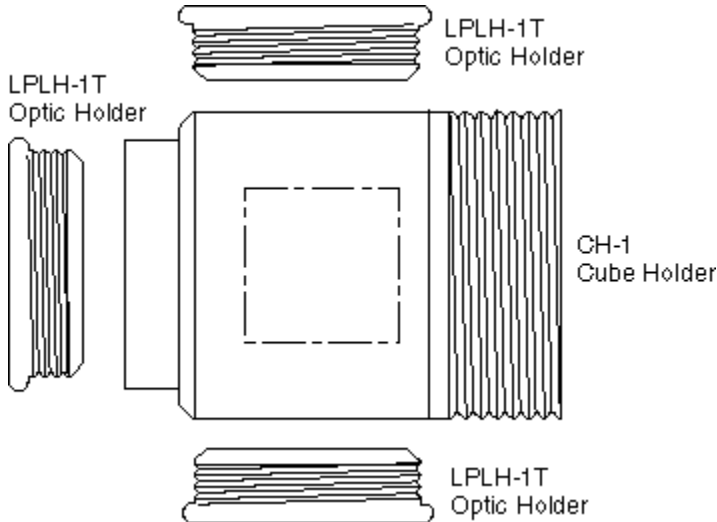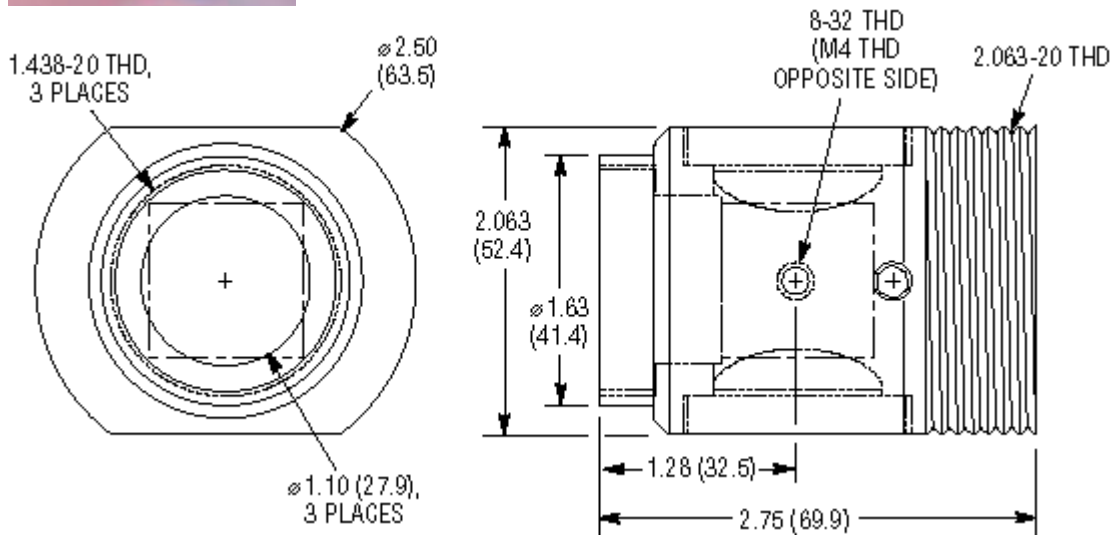
C.10 Newport SBX070-AR.10 Biconvex Lens
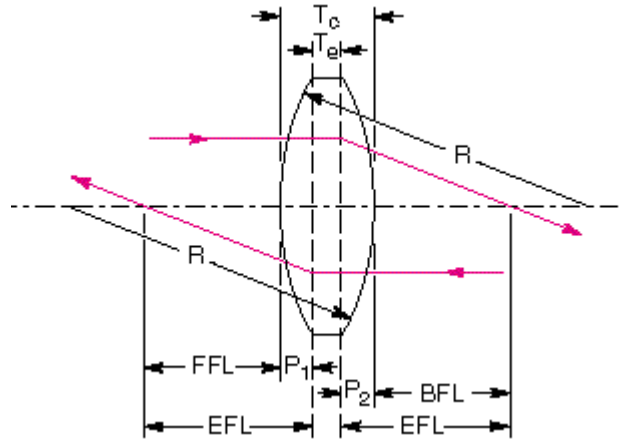
Model	Diameter (mm)	EFL (mm)	f/#	BFL, FFL (mm)	P$_1$ (mm)	P$_2$ (mm)	T$_c$ (mm)	R (mm)
SBX070	50.8	1000	19.7	988.73	1.27	-1.27	3.703	917.459

Specifications

Focal Length at 546.1 nm	±1%
Material	UV grade fused silica
Wavelength	195–2100 nm, uncoated
Surface Accuracy	≤3 fringes (1.5λ) power, 1/4 fringe (λ/8) irregularity at 546.1 nm over the clear aperture
Clear Aperture	≥central 90% of diameter
Surface Quality	40-20 scratch-dig
Centration, Spherical Lenses	≤3 arc min
Diameter Tolerance	+0/-0.1 mm
Center Thickness (T$_c$) Tolerance	±0.1 mm
Edge Thickness (T$_e$)	3.0 mm, Nominal Value
Chamfers	0–0.8 mm face width x 45° ±15°, typical
Antireflection Coating	AR.10, AR.14, AR.16, AR.18: broadband, multilayer antireflection coating, R$_{avg}$ <0.5% AR.33: laser line, multilayer V-coat, R$_{max}$ <0.25%
Durability	MIL-C-675C, moderate abrasion
Cleaning	Non-abrasive method, acetone or isopropyl alcohol on lens tissue recommended
Damage Threshold	AR.10: 100 W/cm^2 CW, 1 J/cm^2 with 10 nsec pulses, typical Other AR coated: 100 W/cm^2 CW, 2 J/cm^2 with 10 nsec pulses, typical

C.11 Newport LH-2 Lens Mount
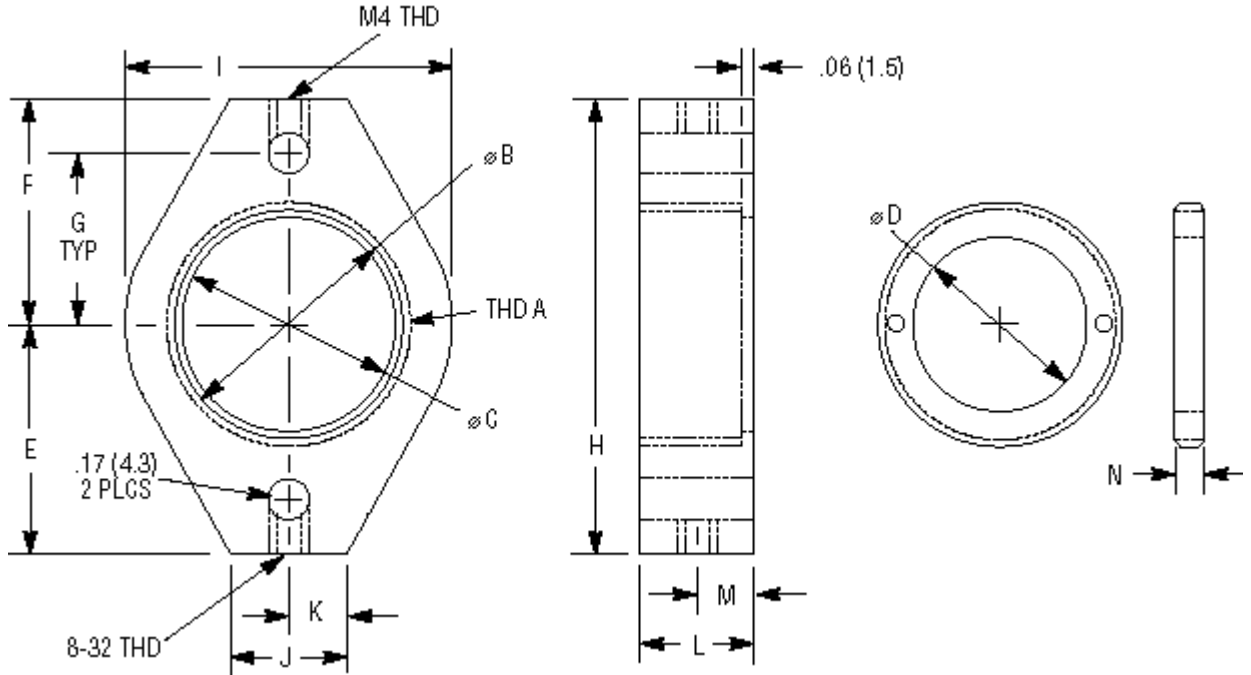
	Thread	Diameter [in. (mm)]		Dimension [in. (mm)]			
Model	A	B MIN.	C	D	E	F	G
LH-2	2.063-20	2.008 (51.0)	1.937 (49.2)	1.690 (42.9)	1.500 (38.1)	1.500 (38.1)	1.250 (31.8)
	H	I	J	K	L	M	N
	3.000 (76.2)	2.407 (61.1)	0.500 (12.7)	0.250 (6.4)	0.500 (12.7)	0.250 (6.4)	0.127 (3.2)

C.12 Newport 605-4 Precision Gimbal Mount

Specifications

	605-4
Coarse/Fine Range (each axis)	360°/10°
Sensitivity with AJS Adjustment Screws (arc sec)	4
Sensitivity with DM-13 Differential Micrometers (arc sec)	0.3
Vernier Graduations (arc min)	15
Orthogonality (arc min)	1

1.00 (25.0)
1.37 (34.8)
.850 (21.6)

10-32 SET SCREW

∅ 3.812 (96.8)
∅ 4.063 (103.2)

6.37 (161.8)
4.00 (101.6)
1.25 (31.8)

LOCK

∅ 5.75 (146.1)

3 SLOTS, 1/4-20 (M6) CLR

4.25 (108.0)
2.000 (50.0)
1.000 (25.0)
.375 (9.5)
.500 (12.7) TYP
2.00 (50.0) TYP

180
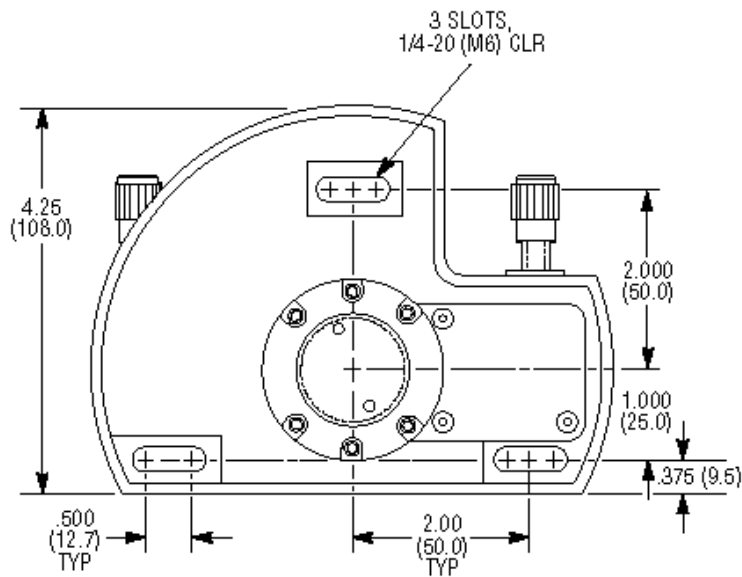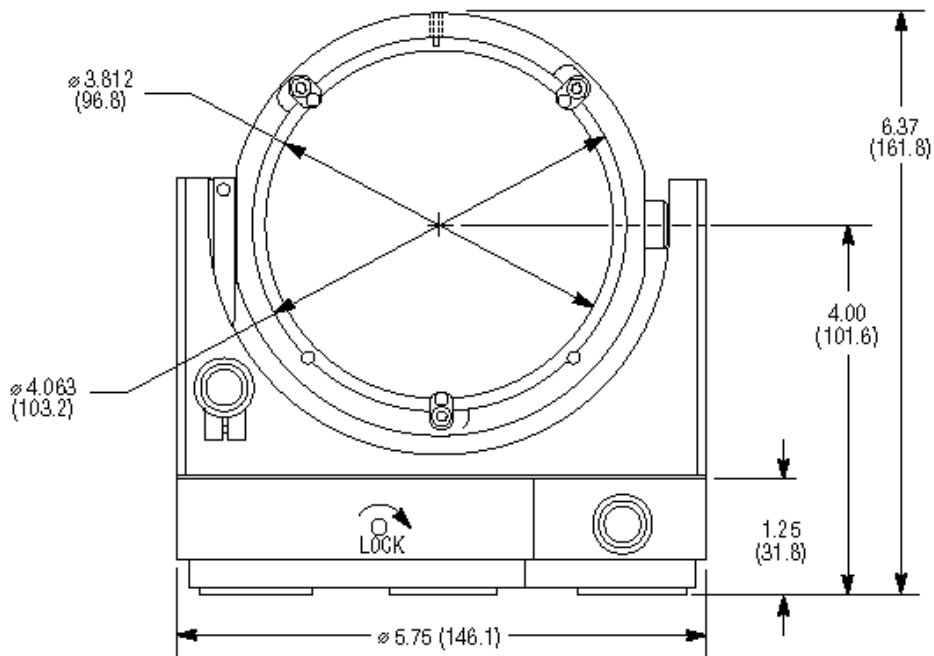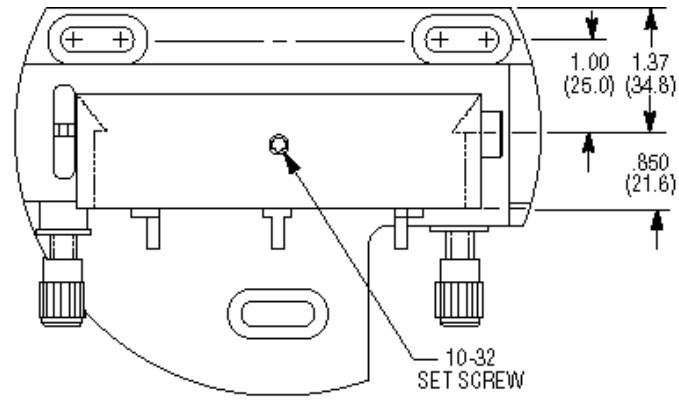
C.13 Newport Broadband Metallic Mirrors 20D10
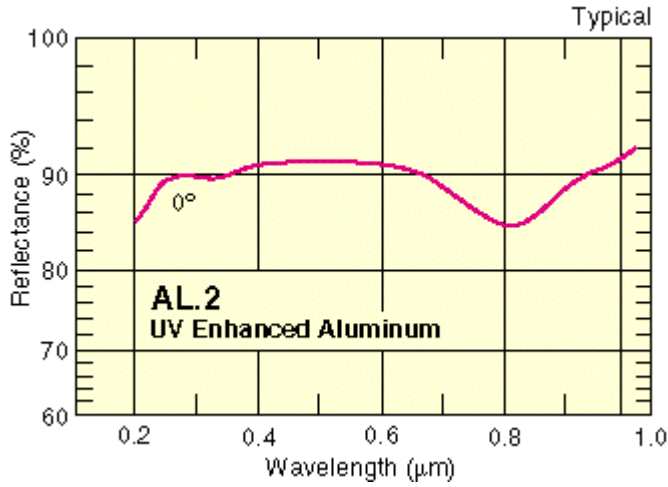
Substrate Number	Diameter [in. (mm)]	Thickness [in. (mm)]	Material	Surface Flatness	Surface Quality
20D10	2.0 (50.8)	0.5 (12.7)	Pyrex®	λ/5	20-10

Specifications

Diameter [in. (mm)]	0.5 (12.7)–4.0 (101.6)	+0/-0.13 mm
	6.0 (152.4) & 8.0 (203.2)	+0/-0.25 mm
	Elliptical Minor Axis Tolerance	+0/-0.18 mm
	Elliptical Major Axis Tolerance	+0/-0.25 mm
Thickness [in. (mm)]	0.5 (12.7)–4.0 (101.6)	±0.25 mm
	6.0 (152.4) & 8.0 (203.2)	±0.38 mm
	Elliptical	±0.25 mm
Clear Aperture	≥central 80% of diameter	
Chamfers [in. (mm)]	0.5 (12.7) & 1.0 (25.4)	0.25–0.76 mm face width x 45° ±15°
	1.181 (30.0)–4.0 (101.6)	0.38–1.14 mm face width x 45° ±15°
	6.0 (152.4) & 8.0 (203.2)	0.51–1.52 mm face width x 45° ±15°
	Elliptical	0.38–1.14 mm face width x 45° ±15°
S_2 Surface	Ground	
Durability	MIL-M-13508C	
Cleaning	Non-abrasive method, acetone or isopropyl alcohol on lens tissue recommended	
Damage Threshold	AL.2, 50 W/cm^2 CW, 5 mJ/cm^2 with 10 nsec pulses at 308 nm, typical ER.1, 100 W/cm^2 CW, 10 mJ/cm^2 with 10 nsec pulses at 532 nm, typical ER.2, 1000 W/cm^2 CW, 1 J/cm^2 with 10 nsec pulses at 1064 nm, typical	

C.14 Melles Griot 02MPG 017/023 Round Flat Mirror with Enhanced Aluminum Coating

typical reflectance curve

normal incidence ——
45° incidence
s-plane ——
p-plane - - - - - -
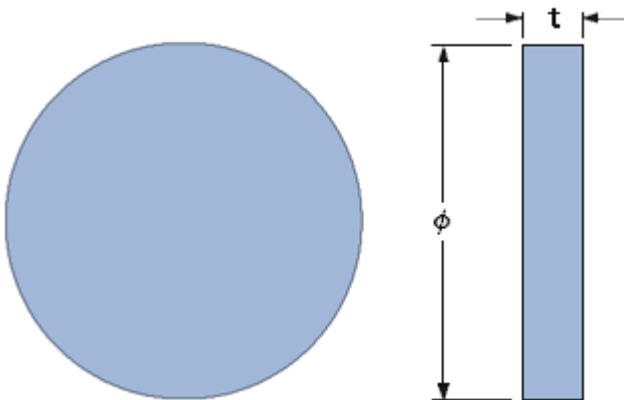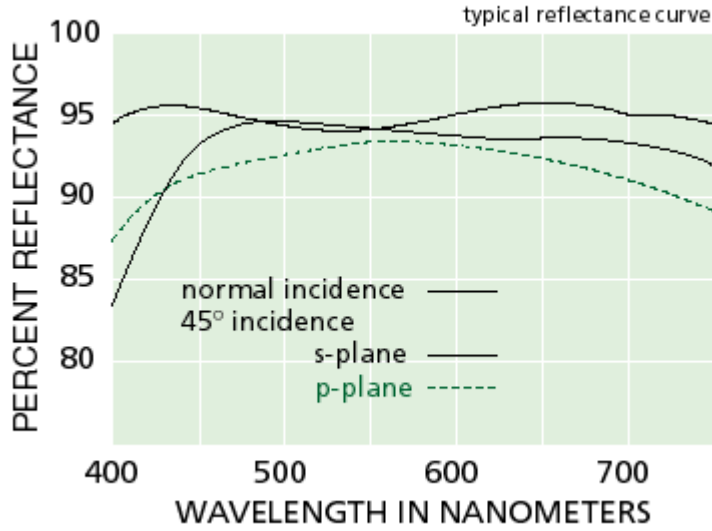
Detailed Specifications:

Diameter :	100 +0/-0.15 mm
Thickness (t) :	19 ± 0.25 mm
Flatness :	λ /10
Surface Quality :	60-40 Scratch and Dig
Clear Aperture :	90 mm
Parallelism :	3 arc minutes
Material :	LEBG
Standard Coating :	Protected Aluminum /011
Wavelength :	450-750 nm

References

[1]   J. Strong, "The Johns Hopkins University and diffraction gratings," *J. Opt. Soc. Am.*, vol. 50, pp. 1148-1152, Dec. 1960, quoting G. R. Harrison.

[2]   P. R. Haugen, S. Rychnovsky, and A. Husain, "Optical interconnects for high speed computing," *Opt. Engr.*, vol. 25, pp. 1076-1084, Oct. 1986.

[3]   D. A. B. Miller, "Optics for low-energy communication inside digital processors: Quantum detectors, sources, and modulators as efficient impedance converters," *Opt. Lett.*, vol. 14, pp. 146-148, Jan. 1989.

[4]   L. B. Aronson and L. Hesselink, "Photorefractive waveguide switches for optical interconnects," *Proc. SPIE*, vol. 1212, pp. 304-314, 1990.

[5]   H. Kogelnik and T. P. Sosnowski, "Holographic thin film couplers," *The Bell System Technical Journal*, vol. 49, pp. 1602-1608, Sept. 1970.

[6]   C. Zhao and R. Chen, "Performance consideration of three-dimensional optoelectronic interconnection for intra-multichip-module clock signal distribution," *Appl. Opt.*, vol. 36, pp. 2537-2544, Apr. 1997.

[7]   J. H. Harris, R. K. Winn, and D. G. Dalgoutte, "Theory and design of periodic couplers," *Appl Opt.*, vol. 11, pp. 2234-2241, Oct. 1972.

[8]   A. Katzir, A. C. Livanos, J. B. Shellan, and A. Yariv, "Chirped gratings in integrated optics," *IEEE J. Quantum Electron.*, vol. 13, pp. 296-304, Apr. 1977.

[9]   D. Heitmann and R. V. Pole, "Two-dimensional focusing holographic grating coupler," *Appl. Phys. Lett.*, vol. 37, pp. 585-587, Oct. 1980.

[10]   M. Li, J. Bengtsson, M. Hagberg, A. Larsson, and T. Suhura, "Off-plane computer-generated waveguide hologram," *IEEE J. Selected Topics in Quantum Electron.*, vol 2, pp. 226-235, June 1996.

[11]   M. Li, P. Modh, S. Kristjansson, A. Larsson, C. Silfvenius, and G. Landgren, "Demonstation of computer-generated waveguide hologram on InGa AsP-InP

waveguide for 1550-nm optical wavelength," *IEEE Phot. Lett.*, vol 9. pp. 958-960, July 1997.

[12]   N. Streibl, R. Vokel, J. Schwider, P. Habel, and N. Lindlein, "Parallel optoelectronic interconnections with high packing density through a light-guiding plate using grating couplers and field lenses," *Opt. Commun.*, vol 99, pp. 167-161, June 1993.

[13]   S. H. Song and S. D. Jung, "Back-board optical signal interconnection module using focusing grating coupler arrays," U. S. Patent No. 5,469,518 assigned to Electronics and Telecommunications Research Institute, issued 21 Nov 1995.

[14]   I. Shariv, Y. Amitai, A. A. Friesem, "Compact holographic beam expander," *Opt. Lett.*, vol. 18, pp. 1268-1270, Aug. 1993.

[15]   R. Shechter, Y. Amitai, A. A. Friesem, "Compact Beam Expander with Linear Gratings," *Appl. Opt. OT*, vol. 41, pp. 1236-1240, March 2002.

[16]   D L. Brundrett, T. K. Gaylord, E. N. Glytsis, "Polarizing mirror/absorber for visible wavelengths based on a silicon subwavelength grating: design and fabrication," *Appl. Opt.*, vol. 37, pp. 2534-2541, May 1998.

[17]   D. C. Flanders, "Submicrometer periodicity gratings as artificial anisotropic dielectrics," *Appl. Phys. Lett.*, vol 42, pp. 492-494, 1983.

[18]   S. Aoyama and T. Yamashita, "Grating beam splitting polarizer using multilayer resist method," *Proc SPIE*, vol. 1545, pp. 241-250, 1991.

[19]   E. N. Glytsis and T. K. Gaylord, "High-spatial-frequency binary multilevel stairstep gratings: polarization-selective mirrors and broadband antireflection surfaces," *Appl. Opt.*, vol 31, 4459-4470, 1992.

[20]   M. Schmitz, R. Brauer, and O. Bryngdahl, "Gratings in the resonance domain as polarizing beamsplitters," *Opt. Lett.*, vol 20, pp. 1830-1831, 1995.

[21]   R. C. Tyan, A. A. Salvekar, H. P. Chou, C. C. Cheng, A. Scherer, P. C. Sun, F. Xu, and Y. Fainman, "Design, fabrication, and characterization of form-birefringent multilayer polarizing beamsplitter," *J. Opt. Soc. Am. A*, vol. 14, pp. 1627-1636, 1997.

[22]   I. Koudela, M. Miler, M. Skalsky, "Holographic optical element converting the Gaussian laser beam into a more uniform one," *Proc. SPIE*, vol. 2169, pp. 84-88, 1984.

[23]   M. Quintanilla and A. M. de Frutos, "Holographic filter that transforms a Gaussian into a uniform beam," *Appl. Opt.*, vol. 20, pp. 879-880, 1981.

[24]   C. Y. Han, Y. Ishii, and K. Murata, "Reshaping collimated laser beams with Gaussian profile to uniform profiles," *Appl. Opt.*, vol. 22, pp. 3644-3647, Nov. 1983.

[25]   F. S. Roux, "Intensity distribution transformation for rotationally symmetric beam shaping," *Opt. Engr.*, vol. 30, pp. 529-536, 1991.

[26]   C. C. Aleksoff, K. K. Ellis, and B. D. Neagle, "Holographic conversion of a Gaussian beam to a near-field uniform beam," *Opt. Engr.*, vol. 30, pp. 537-543, 1991.

[27]   S. Ura, T. Suhara, H. Nishihara, and J. Koyama, "An integrated-optic disk pickup device," *J. Lightwave Tech.*, vol. 4, pp. 913-918, July 1986.

[28]   S. Nishiwaki, J. Asada, and S. Uchida, "Optical head employing a concentric-circular focusing grating coupler," *Appl. Opt.*, vol. 33, pp. 1819-1827, Apr. 1994.

[29]   S. Nishiwaki, Y. Taketomi, S. Uchida, T. Tomita, and J. Asada, "Optical head apparatus including a waveguide layer with concentric or spiral periodic structure." U. S. Patent No. 5,200,939 assigned to Matushida Electric Industrial Co., Ltd., issued 6 Apr. 1993.

[30]   H. Sunagawa, T. Suhara, and H. Nishihara, "Optical pickup apparatus for detecting and correcting focusing and tracking errors in detected recorded signals." U. S. Patent No. 5,153,860 assigned to Fuji Photo Film Co., issued 6 Oct. 1992.

[31]   N. Eriksson, M. Hagberg, and A. Larsson, "Highly directional grating outcouplers with tailorable radiation characteristics," *IEEE J. Quantum Electron.*, vol. 32, pp. 1038-1047, 6 June 1996.

[32]   S. Kristjansson, M. Li, N. Eriksson, K. Killius, and A. Larsson, "Circular grating coupled DBR laser with integrated focusing outcoupler," *IEEE Photon. Tech. Lett.*, vol. 9, pp. 416-418, Apr. 1997.

[33]   S. Ura, H. Sunagawa, T. Suhara, and H. Nishihara, "Focusing grating couplers for polarization detection," *J. Lightwave Tech.*, vol. 6, pp. 1028-1033, June 1988.

[34] S. Ura, M. Shinohara, T. Suhara, and h. Nishihara, "Integrated-optic grating-scale-displacement sensor using linearly focusing grating couplers," *IEEE Photon. Techn. Lett.*, vol. 6, pp. 239-241, Feb. 1994.

[35] T. Suhara, T. Taniguchi, M. Uemukai, H. Nishihara, T. Hirata, and S. Iio, "Monolithic integrated-optic position/displacement sensor using waveguide gratings and QW-DFB laser," *IEEE Photon. Lett.*, vol. 7, pp. 1195-1197, Oct. 1995.

[36] T. Suhara, N. Nozaki, and H. Nishihara, "An integrated acoustooptic printer head," in *Proceedings of the Fourth European Conference on Integrated Optics*, vol. 87, pp. 119-122, 1987.

[37] O. Beyer, I. Nee, F. Havermeyer, and K. Buse, "Holographic recording of Bragg gratings for wavelength division multiplexing in doped and partially polymerized poly(methyl methacrylate)," *Appl. Opt.*, vol 42, pp. 30-37, Jan. 2003.

[38] S. Breer and K. Buse, "Wavelength demultiplexing with volume phase holograms in photorefractive lithium niobate," *Appl. Phys. B*, vol. 66, pp. 339-345, 1998.

[39] S. Breer, H. Vogt, I. Nee, and K. Buse, "Low-crosstalk WDM by Bragg diffraction from thermally fixed reflection holograms in lithium niobate," *Electron. Lett.*, vol. 34, pp. 2419-2421, 1999.

[40] G. Meltz, W. W. Morey, and W. H. Glenn, "Formation of Bragg gratings in optical fibers by a transverse holographic method," *Opt. Lett.*, vol 14, pp. 823-825, 1989.

[41] N. Yoshimoto, S. Morino, M. Nakagawa, and K. Ichimura, "Holographic Bragg gratings in a photoresponsive cross-linked polymer-liquid-crystal composite," *Opt. Lett.*, vol. 27, pp. 182-184, 2002.

[42] G. A. Rakuljic and V. Leyva, "Volume holographic narrow-band optical filter," *Opt. Lett.*, vol. 18, pp. 459-461, 1993.

[43] V. Leyva, G. A. Rakuljic, and B. O'Conner, "Narrow bandwidth volume holographic optical filter operating at the Kr transition at 1547.82 nm," *Appl. Phys. Lett.*, vol. 65, pp. 1079-1081.

[44] J. Freeze, *Fabrication of high efficiency diffraction gratings in single-mode d-fibers using a holographic beam interference approach*, Masters

Thesis, Department of Electrical and Computer Engineering, Brigham Young University, 1991.

[45] B. S. Eastwood "Francesco Maria Grimaldi," *Dictionary of Scientific Biography*, Gillispie, Charles. C. ed., 16 vols., vol 5. pp. 543-544, New York: Charles Scribner and Sons, 1972

[46] E. Hecht and A. Zajac, *Optics*, Addison Wesley, Reading, MA, 1975, pp. 329-393.

[47] E. G. Lowen and E. Popov, *Diffraction Gratings and Applications*, Marcel Dekker, New York, 1997, Chapter 3.

[48] E. G. Lowen and E. Popov, *Diffraction Gratings and Applications*, Marcel Dekker, New York, 1997, pp. 2-3.

[49] H.A. Kahlor, "Numerical evaluation of rayleigh hypothesis for analyzing scattering from corrugated gratings – TE polarization," *IEEE Trans. Antennas Propagat.*, vol. AP-24, pp. 884-889, Nov. 1976.

[50] R. Chu and J. A. Kong, "Modal theory of spatially periodic media," *IEEE Trans. Microwave Theory and Tech.*, vol. 25, pp. 18-24, Jan. 1997.

[51] K. Knop, "Rigorous diffraction theory for transmission phase gratings with deep rectangular grooves," *J. Opt. Soc. Amer.*, vol. 68, pp. 1206-1210, Sept. 1978.

[52] L. C. Botten, M. S. Craig, R. C. McPhedran, J. L. Adams, and J. R. Andrewartha, "The dielectric lamellar diffraction grating," *Opt. Acta*, vol. 28, pp. 413-428, Mar. 1981.

[53] L. C. Botten, M. S. Craig, R. C. McPhedran, J. L. Adams, and J. R. Andrewartha, "The finitely conducting lamellar diffraction grating," *Opt. Acta*, vol. 28, pp. 1087-1102, Aug. 1981.

[54] L. C. Botten, M. S. Craig, R. C. McPhedran, J. L. Adams, and J. R. Andrewartha, "Highly conducting lamellar diffraction gratings," *Opt. Acta*, vol. 28, pp. 1103-1106, Aug. 1981.

[55] M. G. Moharam and T. K. Gaylord, "Coupled-wave analysis of reflection gratings," *Appl. Opt.*, vol. 20, pp. 240-244, 15 Jan 1981.

[56]   J. Chandezon, M.T. Dupuis, G. Cornet, and D. Maystre, "Multicoated gratings: A differential formalism applicable in the entire optical region," *J. Opt Soc. Amer.*, vol.72, pp. 839-846, July 1982.

[57]   P. Sheng, R.S. Stepleman, and P.N. Sanda, "Exact eigenfunctions for square-wave gratings: Application to diffraction and surface-plasmon calculations," *Phys. Rev. B*, vol 26, pp. 2907-2916, 15 Sept. 1982.

[58]   M. G. Moharam and T. K. Gaylord, "Diffraction analysis of dielectric surface-relief gratings," *J. Opt. Soc. Amer.*, vol. 72, pp. 1385-1392, Oct. 1982.

[59]   M. G. Moharam and T. K. Gaylord, "Three-dimensional vector coupled-wave analysis of planar-grating diffraction," *J. Opt. Soc. Amer.*, vol. 73, pp. 1105-1112, Sept. 1983.

[60]   T. K. Gaylord and M. G. Moharam, "Analysis and applications of optical diffraction by gratings," *Proc. IEEE*, vol. 73, pp. 894-938, May 1985.

[61]   E. N. Glystis and T. K. Gaylord, "Rigorous three-dimensional dielectric coupled-wave diffraction analysis of single and cascaded anisotropic gratings," *J. Opt. Soc. Amer. A*, vol. 4, pp. 2061-2080, Nov. 1987.

[62]   M. K. Moaveni, "Application of finite differences to the analysis of diffraction gratings embedded in an inhomogeneous and lossy dielectric," *Int. J. Electron. (GB)*, vol. 61, pp. 465-476, Oct. 1986.

[63]   M. G. Moharam and T. K. Gaylord, "Rigorous coupled-wave analysis of metallic surface relief gratings," *J. Opt. Soc. Amer. A*, vol. 3, pp. 1780-1787, Nov. 1986."

[64]   M. K. Moaveni, A. A. Rizvi, and B. A. Kamran, "Plane-wave scattering by gratings of conducting cylinders embedded in an inhomogeneous and lossy dielectric," *J. Opt. Soc. Amer. A*, vol. 5, pp. 832-842, June 1988.

[65]   M. K. Moaveni, "Plane wave diffraction by dielectric gratings finite-difference formulation," *IEEE Trans. Antennas Propagat.*, vol. 37, pp. 1026-1031, Aug. 1989.

[66]   S. D. Gedney and R. Mittra, "Analysis of the electromagnetic scattering by thick gratings using a combined FEM/MM solution," *IEEE Trans. Antennas Propagat.*, vol. 39, pp. 1605-1614, Nov. 1991.

[67]   D. M. Pai and K. A. Awada, "Analysis of dielectric gratings of arbitrary profiles and thicknesses," *J. Opt. Soc. Amer. A*, vol. 8, pp. 755-762, May 1991.

[68]   S. D. Gedney, "A combined FEM/MoM approach to analyze the plane wave diffraction by arbitrary gratings," ," *IEEE Trans. Microwave Theory and Tech.*, vol. 40, pp. 363-370, Feb. 1992.

[69]   L. Li, "Multilayer modal method for diffraction gratings of arbitrary profile, depth, and permittivity," *J. Opt. Soc. Amer. A*. vol. 10, pp. 2581-2591, Dec. 1993.

[70]   L. Li, "A modal analysis of lamellar diffraction gratings in conical mountings," *J. Mod. Opt.*. vol. 40, pp. 553-573, Apr. 1993.

[71]   S. E. Sandstrom, G. Tayev, and R. Petit, "Lossy multistep lamellar gratings in conical diffraction mountings: An exact eigenfunction solution," *J. Electromagnetic Waves Appl.*, vol. 7, pp. 631-649, 1993.

[72]   G. Bao, D. C. Dobson, and J. A. Cox, "Mathematical studies in rigorous grating theory," *J. Opt. Soc. Amer. A*. vol. 12, pp. 1029-1042, May. 1995.

[73]   C. Hafner, "Multiple multipole program computation of periodic structures," *J. Opt. Soc. Amer. A*. vol. 12, pp. 1057-1067, May. 1993.

[74]   M. G. Moharam , D. A. Pommet, E. B. Grann, and T. K. Gaylord, "Formulation for the stable and efficient implementation of the rigorous coupled-wave analysis of binary gratings," *J. Opt. Soc. Amer. A*. vol. 12, pp. 1068-1076, May. 1995.

[75]   M. G. Moharam , D. A. Pommet, E. B. Grann, and T. K. Gaylord, "Stable implementation of the rigorous coupled-wave analysis for surface-relief gratings: Enhanced transmittance matrix approach," *J. Opt. Soc. Amer. A*. vol. 12, pp. 1077-1086, May. 1995.

[76]   R. H. Morf, "Exponentially convergent and numerically efficient solution of Maxwell's equations for lamellar gratings," ," *J. Opt. Soc. Amer. A*. vol. 12, pp. 1043-1056, May. 1995.

[77]   S. Peng and G. M. Morris, "Efficient implementation of rigorous coupled-wave analysis for surface-relief gratings," ," *J. Opt. Soc. Amer. A*. vol. 12, pp. 1087-1096, May. 1995.

[78] M. G. Moharam and T. K. Gaylord, "Diffraction characteristics of photoresist surface-relief gratings," *Appl. Opt.*, vol. 23, pp. 3214-3220, Sept. 1984.

[79] M. G. Moharam, "Coupled-wave analysis of two-dimensional dielectric gratings," *Proc. IEEE*, vol. 883, pp. 8-11, 1988.

[80] H. Nishihara, M. Haruna and T. Suhara, *Optical Integrated Circuits*, McGraw Hill, New York, 1985, pp. 88-90.

[81] J. Harris, R. K. Winn, and D. G. Dalgoutte, "Theory and design of periodic couplers, *Appl. Opt.*, vol. 11, pp. 2234-2241, Oct. 1972.

[82] S. M. Schultz, E. N. Glytsis, and T. Gaylord, "Design of a high-efficiency volume grating coupler for line focusing," *Appl. Opt.*, vol. 37, pp. 2278-2287. April 1998.

[83] H. Tanaka, T. Kobayashi, T. Saitoh, Y. Suzuki and Shigeru Kawai, "Design Technique of Crossed Gratings for Beam Couplers in Large-Core Optical Fibers," *Jpn. J. Appl. Phys.*, vol. 41, pp. 4817–4820, July 2002

[84] M. Oh, S. Ura, T. Suhara, and H. Nishihara, "Integrated-optic focal-spot intensity modulator using electrooptic polymer waveguide," *J. Lightwave Tech.*, vol. 12, pp. 1569-1576, Sept. 1994.

[85] N. Eriksson, M. Hagberg, and A. Larsson, "Highly efficient grating-coupled surface emitters with single outcoupling elements," *IEEE Phot. Lett.*, vol. 7, pp. 1394-1396, 12 Dec 1995.

[86] A. Alphones, "Double grating coupler on a grounded dielectric slab waveguide," *Opt. Commun.*, vol. 92, pp. 35-39, 15 Aug. 1992.

[87] I. A. Avrutskii, A. S. Svakhin, V. A. Sychugov, and O. Parriaus, "High – efficiency single-order waveguide grating coupler," *Appl. Opt.,* vol. 15, pp. 1446-1448, Dec. 1990.

[88] J. C. Brazas, L. Li, and A. L Mckeon, "High-efficiency input coupling into optical waveguides using gratings with double-surface corrugation," *Appl. Opot.*, vol. 34, pp. 604-609, Feb. 1995.

[89] M. Hagberg, N. Eriksson, and A. Larsson, "High efficiency surface emitting lasers using blazed grating outcouplers," *IEEE J. Quantum Electron.*, vol. 32, pp. 1596-1605, Sept 1996.

[90]   T. Liao, S. Sheard, M. Li, J. Zhu, and P. Prewett, "High-efficiency focusing waveguide grating coupler with parrallelogramic groove profiles," *J. Lightwave Tech.*, vol. 15, pp. 1142-1148, July 1997.

[91]   M. Neviere, "The homogeneous problem," in *Electromagnetic Theory of Gratings* (R. Petit, ed.), ch 5, pp. 123-157, Berlin: Springer-Verlag, 1980.

[92]   T. Tamir, S. T. Pengm and H. L. Bertoni, "Theory of periodic dielectric waveguides," *IEEE Trans. Microwave Theory Tech.*, vol. 73, pp. 894-938, 1985.

[93]   T. Tamir, and S. T. Peng, "Analysis and design of grating couplers," *IEEE J. Quantum Electron.*, vol. 22, pp. 544-550, 1986.

[94]   G. Hadjicostas, J. Butler, G. Evans, N. Carlson, and R. Amantea, "A numerical investigation of wave interactions in dielectric waveguides with periodic surface corrugations," *IEEE J. Quantum Electron.*, vol. 26, pp. 893-902, 1990.

[95]   T. Fujita, H. Nishihara and J. Kozoma: "Blazed grating Fresnel lenses fabricated by e-beam lithography," *Opt. Lett.*, vol. 7, pp. 578-580, 1982.

[96]   S. Ogata, M. Tada, and M. Yoneda: "Electron-beam writing system and its application to large and high density diffractive optical elements," *Appl. Opt.*, vol. 33, pp. 2032-2038, 1994.

[97]   T. Shiono and H. Ogawa: "Diffraction-limited blazed reflection diffractive microlenses for oblique incidence fabricated by electron-beam lithography," *Appl. Opt.*, vol. 30, pp 3643-3549, 1983.

[98]   Y. Handa, T. Suhara, H. Nishihara, and J. Koyama, "Microgratings for high-efficiency guided-beam deflection fabricated by electron-beam direct-writing techniques," *Appl. Opt.*, vol 19, pp. 2842-2847, 1980.

[99]   S. M. Shank, M. Skvarla, F. T. Chen, H. G. Craighead, P. Cook, R. Bussjager, F. Hass, and D. A. Hone, "Fabrication of multi-level phase gratings using focused ion beam milling and electron beam lithography," Tech. Digest Series Opt. Soc. Am., vol 11, *Diffractive Optics: Design Fabricatio , and Applications*, Rochester, pp. 302-305, 1994.

[100] G. R. Harrison, "Production of diffraction gratings: I. Development of the ruling art," *J. Opt. Soc. Amer.*, vol. 39, pp. 413-426, 1949.

[101] T. Harada, S. Moriyama, and T. Kita, "Mechanically ruled stigmatic concave gratings," *Jpn. J. Appl. Phys.*, vol 14, suppl. 14-1, pp. 174-179, 1974.

[102] E. G. Loewen, R. S. Wiley, and G. Portas, "Large diffraction gratings ruling engine with nanometer digital control system," *SPIE*, vol 815, pp. 88-95, 1987.

[103] R. Bartlett and P. C. Wildy: "Diffraction grating ruling engine with piezo-electric drive," *J. Appl. Opt.*, vol. 14, pp. 1-3, 1975.

[104] T. Kita and T. Harada: "Ruling engine using piezo electric device for large and high groove density gratings," *J. Appl. Opt.*, vol. 21, pp. 1399-1406, 1992.

[105] K. Hill, B. Malo, F. Bilodeay, D. Johnson, and J. Albert, "Bragg gratings in monomode photosensitive optical fiber by UV exposure through a phase mask," *Appl. Phys. Lett.*, vol 62, pp. 1035-1037, 1993.

[106] M. Okai, S. Tsuji, N. Chinone, and T. Harada, "Novel method to fabricate corrugation for a $\lambda/4$ shifted distributed feedback laser using a grating photomask," *Appl. Phys. Lett.*, vol 45, pp. 415-417, 1989.

[107] J. M. Verdiell, T. L. Koch, D. M. Tennant, R. P. Gnall, K. Feder, M. G. Young, B. I. Miller, U. Koren, M. A. Newkirk, and B. Tell, "Single step contact printing of Bragg gratings using a conventional incoherent source and a phase mask: Application to multi-wavelength BBR lase array," *Proc. 6th Europ. Conf. Integr. Opt.*, P. Roth, ed., Neuchatel, 1993, pp. 4.8-4.9.

[108] D. M. Tennant, K. F. Dreyer, K. Feder, R. P. Gnall, T. L. Koch, U. Koren, B. I. Miller, C. Vartuli, and M. G. Young, "Advances in near field holographic grating mask technology," *J. Vac. Sci. Technol. B*, vol. 12, pp. 3689-3694, Nov/Dec 1996.

[109] C. H. Lin, Z. H. Zhu, and Y. H. Lo, "New grating fabrication technology for optoelectronic devices: Cascated self-induced holography," *Appl. Phys. Lett.*, vol. 67, pp. 3072-3074, Nov 1995.

[110] C. H. Lin, S. H. Zhu, Y. Qian, and Y. H. Lo, "Cascade Self-Induced Holography: A New Grating Fabrication Technology for DFB/DBR Lasers and WDM Laser Arrays," *IEE Journal of Quant. Electr.*, vol. 32, pp. 1752-1759, Oct. 1996.

[111] P. I. Jensen, and A. Sudbo, "Bragg gratings for 1.55 µm wavelength fabricated on semiconductor material by grating-period doubling using a phase mask," *IEEE Photon. Lett.*, vol. 7, pp. 783-785, July 1995.

[112] L. Mashev, and S. Tonchev, "Formation of holographic diffraction gratings in photoresist," *Appl. Phys A.*, vol 26, pp. 143-149, 1981.

[113] L. Mashev and S. Tonchev, "Formation of blazed holographic gratings," *Appl. Phys. B*, vol. 28, pp. 349-353, 1982.

[114] G. Schmahl, "Holographically made diffraction gratings for the visible, UV, and soft X-ray region," *J. Spectr. Soc. Jpn.*, vol 23, suppl. 1, 3-11, 1974.

[115] S. Johansson, L. E. Nilsson, K. Beidermann, and K. Klevby, "Holographic diffraction gratings with asymmetrical groove profiles," *Proc. Conf. Appl. Of Holography and Opt. Data Processing,* Jerusalem, 1976.

[116] S. Lindau, "The groove profile formation of holographic gratings," *Opt. Acta*, vol. 29, pp. 1371-1381, 1982.

[117] R. A. Bartolini "Characteristics of relief phase holograms recorded in photoresist," *Appl. Opt.*, vol. 13, pp. 129-139, 1974.

[118] M. J. Beesley and J. G. Castledine, "The use of photoresist as holographic recording medium," *Appl. Opt.*, vol. 9, pp. 2720-2724, 1970.

[119] P. Lehmann, "Theory of blazed holographic gratings," *J. Mod. Opt.*, vol. 36, pp. 1471-1487, 1989.

[120] U. Unrau and R. Nietz, "Quick precision alignment of interferometric equipment," *J. Phys. E. Sci. Instrum.*, vol. 13, pp. 608-610, 1980.

[121] L. Wosinski and M. Breidne, "Large holographic diffraction gratings made by multiple exposure technique," *Research in Optics, Tech. Report of The Royal Inst. of Technology*, vol 210, pp. 10-11, Stockholm, 1988.